Jules Hazeleger, s1248936

03-11-2017

THE HYDRAULIC AND MORPHOLOGICAL EFFECTS OF THE ISLE GROYNE

A *numerical study in Delft3D on the effects of an altered groyne design on the magnitude and orientation of groyne flames*

Royal HaskoningDHV
Enhancing Society Together

UNIVERSITY OF TWENTE.

THE HYDRAULIC AND MORPHOLOGICAL EFFECTS OF THE ISLE GROYNE

A numerical study in Delft3D on the effects of an altered groyne design on the magnitude and orientation of groyne flames

Master Thesis

Jules C. Hazeleger, November 2017

Graduation Committee:

University of Twente	dr. ir. Bart Vermeulen
	dr. ir. Pieter Roos
Royal HaskoningDHV	ir. Wiebe de Jong
Rijkswaterstaat	ir. Arjan Sieben

Abstract

This research focuses on the effects of the isle groyne on the hydrodynamics around groynes and on the magnitude and orientation of groyne-induced accretion of the bed – groyne flames – in comparison to the current, lowered groynes present in the Waal.

The Waal is of high importance to the inland water transport in the Netherlands. The river is however stretched to its limits. Continuous dredging takes place to maintain sufficient water depths in the navigation channel. One of the reasons for these dredging activities is the existence of groyne flames alongside the groyne fields. The convergence and divergence of the flow around groynes, the formation of turbulence along the boundary between the main flow and the groyne fields, as well as the formation of coherent turbulent structures near the groyne tip induce a pattern of scour near the tip of the groyne and downstream sedimentation: the groyne flame. The isle groyne is designed to reduce the negative impact of these groyne flames on the quality of the navigation channel. The isle groyne is an alternative to the current groynes in the river Waal. A couple of meters away from the tip of the groyne, the structure is lowered, creating an inlet behind an elongated groyne head and generating the illusion that the elongated head of the groyne is an isle during several discharge regimes.

To assess the effect of this isle groyne, the numerical model Delft3D-FLOW is used. On a fine grid, using a schematized representation of the Waal with a flat bed and sloping, asymmetric groyne fields, the flow and sediment transport processes are calculated under constant discharge conditions. Horizontal Large Eddy Simulation is used to determine the horizontal turbulence around the groynes.

The results show that the isle groyne could significantly alter the flow pattern within the groyne field during low discharge conditions as it may disrupt the formation of a primary eddy. The flow through the inlet of the isle groyne further leads to slightly lower flow velocities in the main channel. The different flow pattern around the isle groyne has no significant effect on the velocity gradients between the accelerated (converged) and decelerated (diverged) flow in the main channel. Furthermore, the isle groyne changes the turbulent motion around groynes during low discharge conditions. The vorticity at the downstream end of the head of the isle groyne and along the isle groyne's inlet seems to increase. In contrast, turbulence decreases at the upstream side of the head and further downstream the shear zone between the groyne field and the main flow. During high discharge conditions, the hydrodynamics around both groynes are more alike. The hydrodynamic changes do not cause significant morphological changes. Only minor differences are present in the magnitude of the groyne flame; its height has increased close to the groyne field and is slightly reduced further away from the groyne field. No significant changes are present in the transverse location of the groyne flame.

Despite several model uncertainties and shortcomings it may be concluded that the isle groyne does not alter the groyne flames in the Waal significantly compared to the current, lowered groynes. On the basis of this model study, it is not advised to implement these structures in the Waal on a large-scale as a mean to decrease the impact of groyne flames on the navigational quality. Further research is recommended to confirm this conclusion and to investigate other benefits of the isle groyne.

Table of Contents

1. Introduction

The Waal is a heavily regulated river in the Netherlands which bifurcates from the Niederrhein at Pannerden in the Eastern part of the country. Being the main distributary of the river Rhine – transporting two-thirds of the total discharge coming in from Germany – the river is an important fairway for inland water transport. More than 50% of the goods arriving in the Rotterdam harbour is carried by ship to Germany over the Rhine branches, with the Waal as the most significant facilitator (Havinga, Taal, Smedes, Klaassen, Douben, & Sloff, 2006). Over the past centuries, several measures have been taken both to improve the navigational quality of the river Waal and to meet the high flood standards in the Netherlands. The construction of circa 700 groynes in the late 19th century has been one of the early regulations (Yossef & Klaassen, 2002); confinement of the river flow allowed for large amounts of cargo transport over the river Waal throughout the whole year.

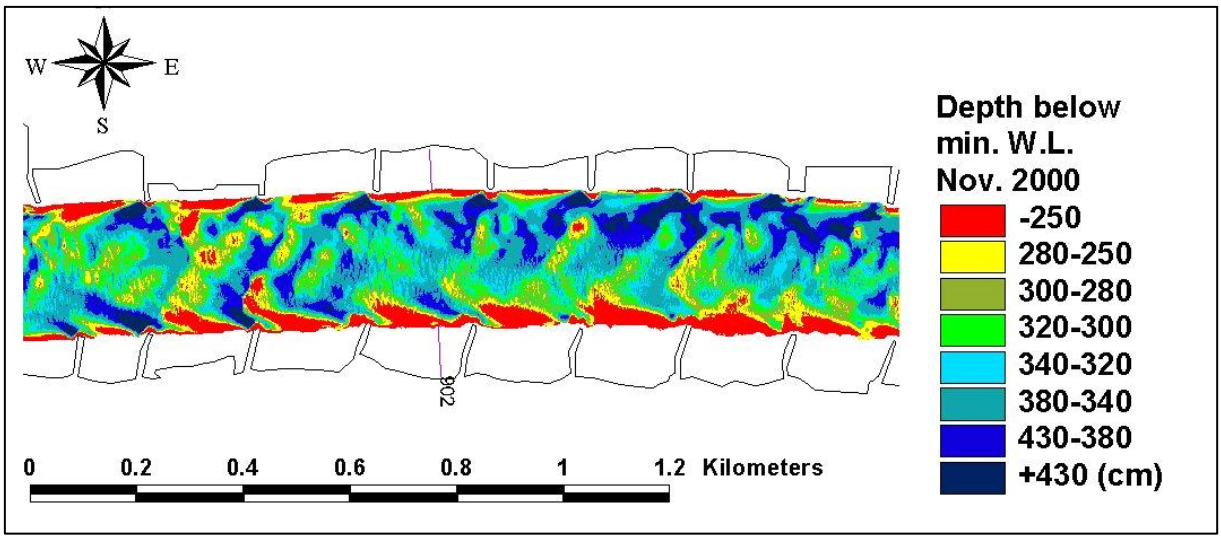

Figure 1: Bed Topography near Druten indicating the presence of groyne flames (red patches) (Yossef, Jagers, Mosselman, & Sieben, 2007)

The navigation of the river Waal is however stretched to its limits. The relatively narrow and shallow river is one of the most busy waterways of Western Europe and plenty of effort is put in the maintenance of a sufficient minimum water depth in the navigation channel (Kisoensingh, 2015). Continuous dredging operations are executed along the Waal to satisfy the minimum guaranteed water depth of 2.8 m and the average guaranteed depth of 4.0 m during OLR-conditions (Dutch: Overeengekomen Laagste Rivierstand) (Kisoensingh, 2015). These activities not only cost the Dutch government agency Rijkswaterstaat several millions a year, they also hamper the navigation by the partial blocking of the navigation channel by dredging vessels.

Despite its function of enabling continuous cargo transport over the river Waal, the groynes create side effects which can pose a threat to the navigation and may create a necessity of dredging. The convergence and divergence of the flow near groynes as well as the turbulent flow structure generated by the obstructive nature of the groyne, induce a pattern of erosion and sedimentation (Klaassen & Sloff, 2000). An erosion hole is formed in the direct vicinity of the groyne head whereas a local accumulation of sand, i.e. the groyne flame, is formed downstream of the erosion hole (Figure 1). The

importance of these groyne flames on the occurrence of shallow areas within the navigation channel is indicated by the locations at which dredging operations took place along the river Waal. At a relatively straight river stretch near Dodewaard, an evident need for dredging operations is present on the far-right side of the channel (Figure 2) where the aforementioned scourholes and groyne flames dominate the morphological pattern. Van Heereveld (2006) further highlighted that this river section contained the majority of locations which were identified as having a depth below the guaranteed minimum depth of 2.8 metres between 1999 and 2001.

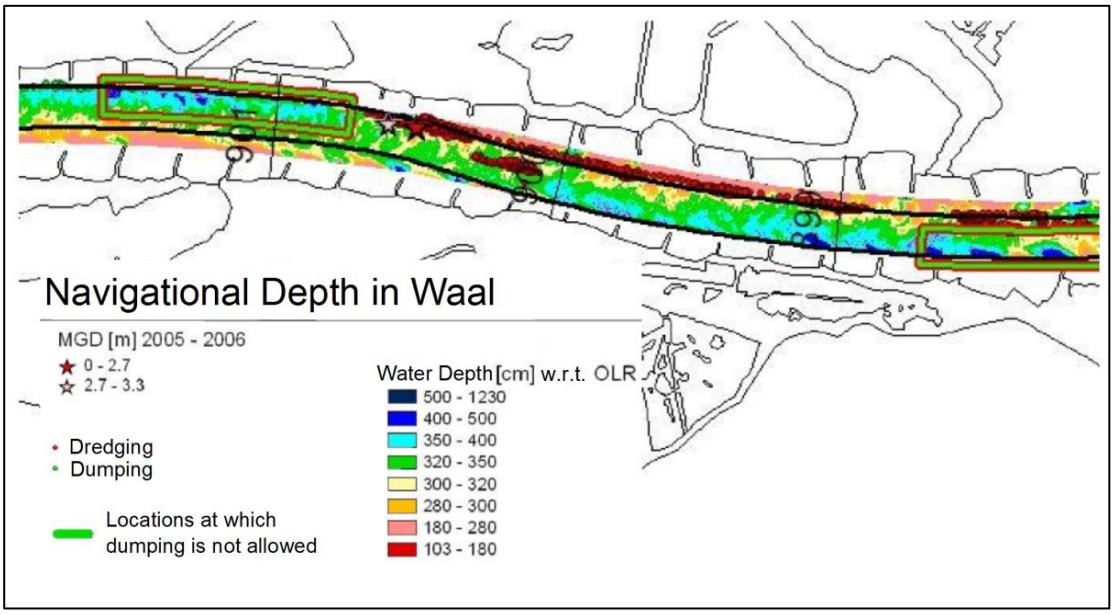

Figure 2: Planview of the navigational depth of the river Waal near Dodewaard including the locations at which dredging operations have taken place between 2005 and 2006. The far-right side of the channel shows a big need for dredging

A design contest organized by Rijkswaterstaat in 2006 triggered Royal Haskoning in designing the isle groyne (Figure 3). The new groyne design may mitigate the aforementioned problems concerning the reduced navigational depth due to groyne flames. Within the design of the isle groyne, the ordinary groyne is modified by creating an inlet just behind the groyne head. In addition to that, the groyne head is elongated in downstream direction. The isle groyne is expected to favour the morphology in the vicinity of groynes as a result of its likely effects on the hydrodynamics around these structures. The groyne is designed to minimize the generation of turbulent structures by improving the stream guidance along the elongated groyne head and reducing the deflection of flow through the construction of the notch. The groyne is further expected to decrease the pattern of convergence and divergence. This is achieved by allowing the flow to pass the groyne through the inlet and preventing the flow from intruding into the groyne field by elongating the head. These hydrodynamic effects are considered to reduce the degradation and accretion around groynes and thus to favour the morphological conditions in the river Waal (Heereveld, 2006; Consortium Kribben, 2006). The isle groyne is thought to have additional benefits. The partial prevention of flow intrusion into the groyne field by the elongated groyne head and the additional inflow of water through the notch are expected to lead to a calmer flow pattern in the groyne fields, especially during the passage of ships. This may

result in reduced erosion of the groyne fields and an increase of ecological and recreational potential. Furthermore, the construction of the inlet causes increased flow conveyance capacity and a consequential decrease of maximum water levels (Heereveld, 2006). These effects are however of hypothetical nature since no elaborate research has been performed on the hydraulic and morphological effects of the isle groyne.

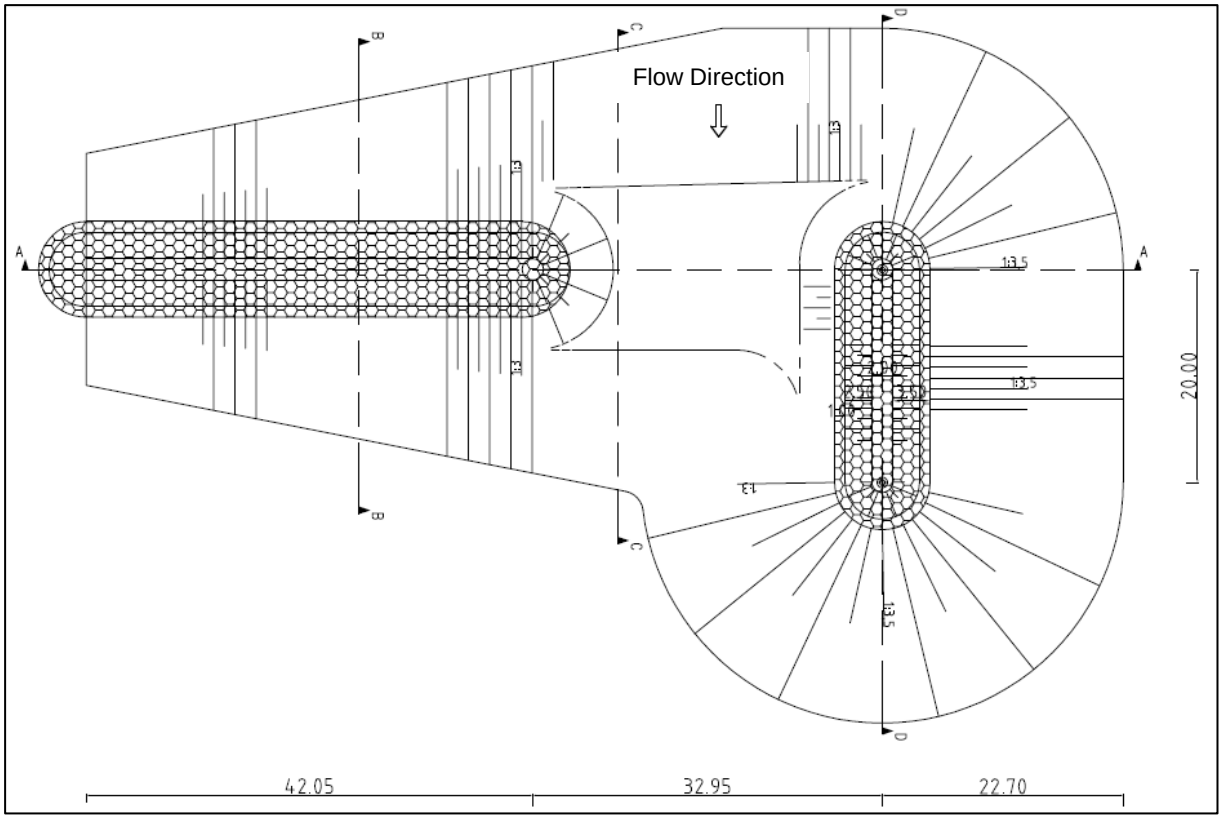

Figure 3: Design of the isle groyne **(Heereveld, 2006)**

A preliminary research by Van Heereveld (2006) employed a one-dimensional SOBEK-model to conclude on heightened average bed levels due to the increased cross-sectional area, reduced velocities during the majority of discharges and decreased maximum water levels. The evolution of groyne flames is however influenced by complex and turbulent flow structures which can not be captured within a one-dimensional model. No conclusion could thus be derived on the effects of the isle groyne on groyne flames based on this preliminary research.

In fact, research which evaluates on the evolution of groyne flames is scarce. Yossef and Klaassen (2002) and Yossef (2005) performed numerical calculations in Delft3D to conclude on the model necessities to reproduce groyne flames using Delft3D. They found that a numerical model is able to reproduce groyne flames in case it is able to resolve the large horizontal turbulent motions near the groyne tips, i.e. dynamic eddies. Talstra (2011) presented results on the morphological evolution around groynes that are provided with a pile sheet in front of the groyne head. The research yielded favourable results for the reduction of the magnitude of groyne flames when the pile sheet was aligned perpendicular to the groyne.

To the best knowledge of the author, other scientific researches that focused on the effects of groynes on hydro- and morphodynamics did not reproduce groyne flames either numerically or in flume experiments. However, research on the hydrodynamics around groyne field is performed more often (e.g. Uijttewaal, Lehmann and Van Mazijk (2001), Hinterberger, Fröhlich and Rodi (2007) and Yossef and De Vriend (2011)). Uijttewaal et al. (2001) provided additional insight in the hydrodynamics contributing to the formation of groyne flames by performing flume experiments on the turbulent motions and velocity patterns which govern the exchange of sediment between the main flow and groyne field. Hinterberger et al. (2007) performed a study on the applicability of several turbulence model to reproduce the hydrodynamic characteristics around groyne fields. Yossef and De Vriend (2011) carried out flume experiments on the hydrodynamics around groynes and evaluated on differences between submerged and emerged conditions.

Numerous other researches which discuss the influence of groynes on the hydrodynamics and morphology are present. These however mainly focus on the effects of a single groyne or transverse bluff body (Saberi & Galoie, 2017; Li, Lang, & Ning, 2013; Ouillon & Dartus, 1997; Yazdi, Sarkardeh, Azamathulla, & Ghani, 2010; Safarzadeh, Neyshabouri, & Zarrati, 2016; Karami, Basser, Ardeshir, & Hosseini, 2014; Koken & Constantinescu, 2008; Kang, Yeo, Kim, & Ji, 2011). Whenever morphological processes were included in the researches, focus was applied on the evolution of the scour holes near the groyne head (Kang et al., 2011, Karami et al., 2014, Li et al., 2013). Although these provide valuable information on the turbulent motions and flow confinement around groynes, their results are less applicable to derive conclusions on the evolution of groyne flames in the river Waal.

No research has thus been conducted on the hydraulic and morphological effects of structures in the form of the isle groyne. Also, few researches have been conducted on the effects of a series of current groynes, certainly on sedimentation patterns, let alone within the specific circumstances present in the Waal. To assess the applicability of the isle groyne as a measure to mitigate the negative effects of groyne flames on the inland water transport over the Waal, a thorough understanding of the hydraulic and morphological effects around the isle groyne in comparison with current groynes is required.

1.1. Goal and Research Question

The ***goal*** of this research is therefore…:

"to determine the effects of the isle groyne on groyne flames in the river Waal in comparison with the current groynes."

In order to determine the effects of the isle groyne on groyne flames, insight in the hydraulic effects is necessary to be able to understand the morphological effects. The research question is therefore twofold:

1. What are the effects of the isle groyne on the hydrodynamics in the river Waal in comparison with the current groynes?

a. What are the effects of the isle groyne on the flow and velocity pattern in the river Waal in comparison with the current groynes?
b. What are the effects of the isle groyne on turbulent motions in the river Waal in comparison with the current groynes?

2. What are the effects of the isle groyne on groyne flames in the river Waal in comparison with the current groynes?

To answer these questions, a numerical study is performed using Delft3D-FLOW. Delft3D-FLOW is a module within the computer software suite Delft3D. It is capable of both calculating two- and three-dimensional non-steady flow and transport phenomena and resolving the horizontal turbulent motions. Hydrodynamic and morphological characteristics are assessed for two cases of the river Waal: the one being the schematized representation of the river Waal with current groynes, the other with isle groynes. Apart from the novelty of assessing the effects of the isle groyne, this research is unique in the sense that only very few other researches have numerically assessed the effects of groynes on groyne flames and its hydrodynamic effects around groyne fields in this detail.

1.2. Reading Guide

This report will first elaborate on some theoretical background information necessary to understand the methodology, results and conclusions of the research. The chapter includes general information on the morphology of the river Waal and the design of the current groynes and isle groynes (Sector 2.1) as well as an elaboration of the hydraulic (Sector 2.2) and morphological (Sector 2.3) effects of both types of groynes. The effects of the isle groyne include hypotheses as the present research should provide further insight on this subject. Chapter 2 further includes information on the way flow and sediment transport phenomena are modelled in Delft3D-FLOW (Sector 2.4).

The report then discusses the methodology in chapter 3, which outlines the approach of the research and the most important steps to be taken. Chapter 4 describes the set-up of the numerical model. Chapter 5 and 6 highlight the most important results of the research. Chapter 5 focuses on the hydrodynamic effects of the current groyne and isle groyne (research question 1) whereas Chapter 6 concentrates on the morphological effects (research question 2). Finally, Chapter 7 – 9 contain a discussion of the results, a conclusion on the findings and a set of recommendations.

2. Theoretical Framework

Before any methodology or result is presented, it is necessary to obtain the relevant knowledge to understand and interpret the results of this study. This chapter first highlights the bathymetric characteristics of the Waal and the design characteristics of both groyne types (Section 2.1). It then discusses the hydraulic and morphological effects of both the current and isle groyne in, respectively, Section 2.2 and Section 2.3. The effects of the latter groyne type include hypotheses since the present research should provide further insight on this topic. Lastly, the chapter includes information on the numerical flow and sediment transport equations used by Delft3D-FLOW to model the hydrodynamic and morphological pattern around groynes (Section 2.4).

2.1. Characteristics of the Waal and the Groynes

A basic understanding of the characteristics of the river Waal, its current groynes and the isle groynes is necessary to understand the hydrodynamic and morphological impact of both types of groynes and the choices made within this research. Subsequently, this section addresses the main characteristics of the Waal (Section 2.1.1.), the design of the current groyne (Section 2.1.2.) and the design of the isle groyne (Section 2.1.3.). The characteristics presented apply to the situation around the river stretch near the village of Dodewaard (from river kilometre 898 – 901, see Figure 4). Preliminary research conducted by Royal Haskoning (Heereveld, 2006) highlighted this location as being interesting for the implementation of the isle groyne given the combination of a relatively straight part of the river and necessity of dredging activities near the side of the navigation channel. This indicated the presence of groyne flames.

2.1.1. Characteristics of the Waal near Dodewaard

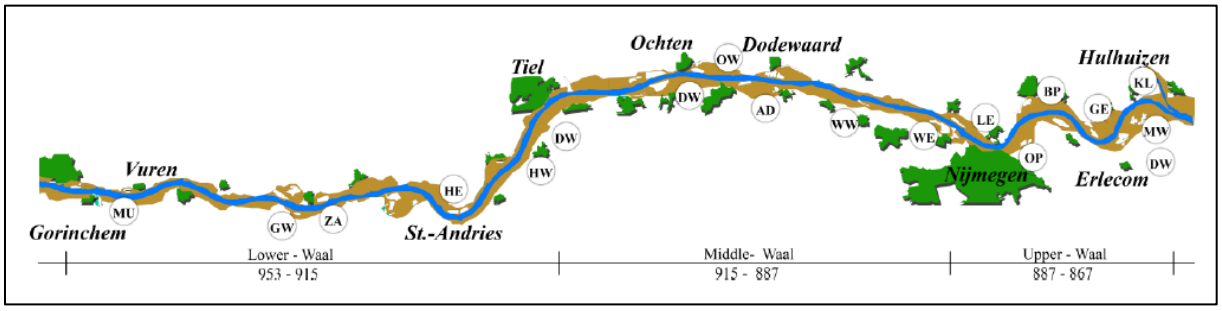

Figure 4: Overview of the river Waal and the location of Dodewaard (Kisoensingh, 2015)

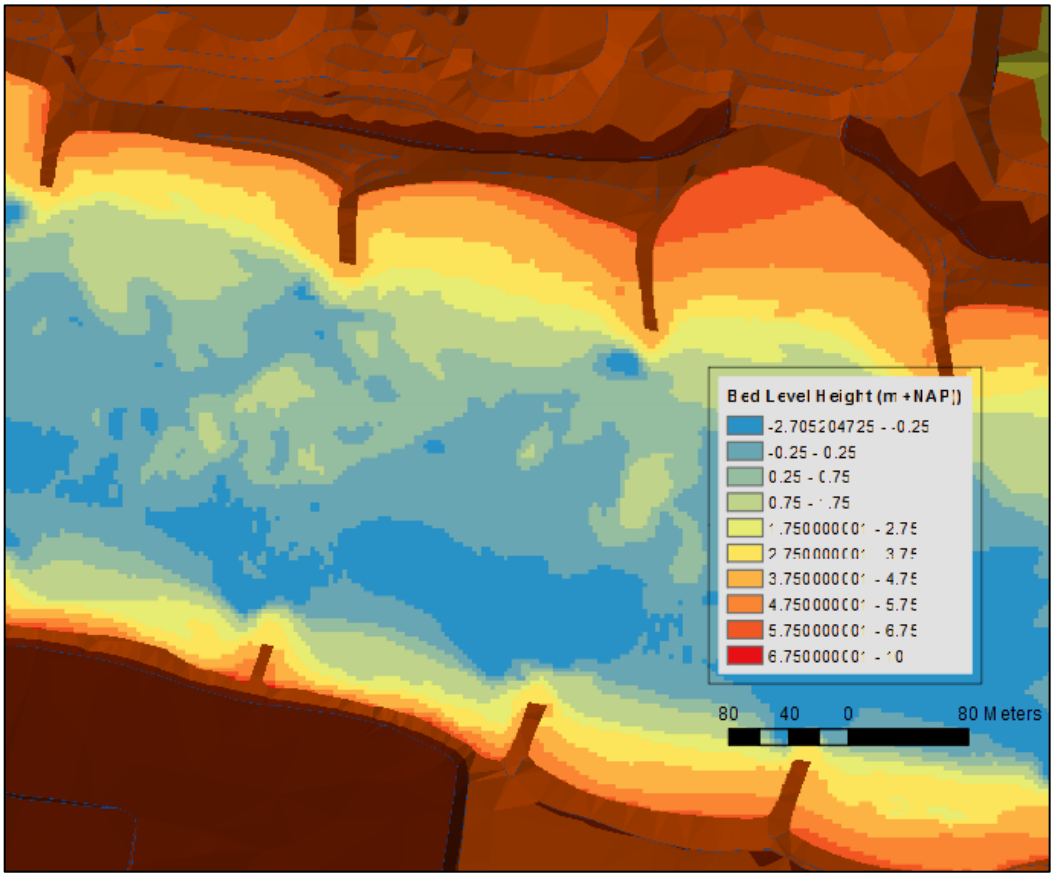

Figure 6: Bed Level at a river stretch near Dodewaard. The average bed level is circa 0 m+NAP. The groyne fields differ in size and shape and have a characteristic bell-shaped form. Scour holes are present near the groyne tip. Downstream of the scour holes, especially on the right side of the river, groyne flames are present.

The village of Dodewaard is located in the Middle Waal, circa 20 kilometres West of Nijmegen. The Middle Waal is characterized by relatively few meanders and a non-stationary river bed in the main channel with groyne fields on either side (Kisoensingh, 2015). This non-stationary bed includes dunes and ripples as well as groyne flames. Around Dodewaard, these bed features are superimposed on an average bed level in the centre of the circa 200 metres wide main channel of circa 0m +NAP (Figure 6). The bed has a longitudinal slope of 10^{-4} m^{-1} and a slight inclination towards the side of the fairway. At the sides, erosion holes and groyne flames create a pattern of subsequent scour and accumulation of sediment on both sides of the river which extends to heights, respectively depths, of more than 1 meter (Figure 5). Next to the pattern of groyne flames and erosion holes, numerous groynes create the iconic repetitive planview of adjacent groyne fields which differ in size and shape.

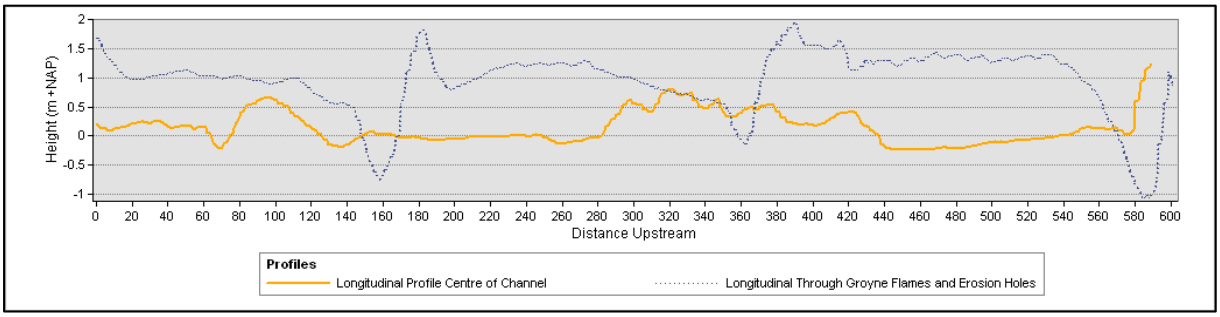

Figure 5: Longitudinal Profiles within centreline of the main channel and along the sides of the main channel. Scour holes and groyne flames cause significant decreases, respectively increases of the bed level

The groyne fields slope upwards towards the river's embankments. Along the normal line – the imaginary line connecting two adjacent groyne heads – these fields have a rather steep gradient. Further towards the embankment, the slope is weaker at circa 1:25. These gradients are however not uniform over the entire groyne field. The bed of the groyne fields is non-uniform and asymmetric. The down- and upstream ends of groyne fields show some differences; the main channel intrudes further into the groyne field at the downstream side. This gives the fields their bell-shaped/triangular form (Figure 6).

The bathymetry of the river Waal is thus far from uniform. Its geometric characteristics can – on average – best be represented by the values in Table 1

Table 1: Representative dimensions of an average river stretch of the Waal. Values obtained from multibeam measurements and from Yossef (2002)

	Measured
Width in between two opposing groyne heads	220 m
Height of the bed	0 m +NAP
Slope of the bed	10^{-4}
Distance in between two adjacent groynes	200 m
Width of a groyne field	60 m
Average transverse slope of the groyne fields	1:22

2.1.2. Design of the current groyne

The groynes present in the Waal separate the aforementioned groyne fields. Originally constructed to prevent the embankments from eroding (Appendix I), the groynes now serve several goals. As mentioned in the introduction, the groynes serve as a mean to maintain sufficient water depth in the navigation channel by increasing the efficiency of the sediment transport. Furthermore – as groynes constrict the river, prevent the river from meandering and increase the average stream velocities – they serve as a measure to decrease flooding probabilities. The structured constriction of the river by

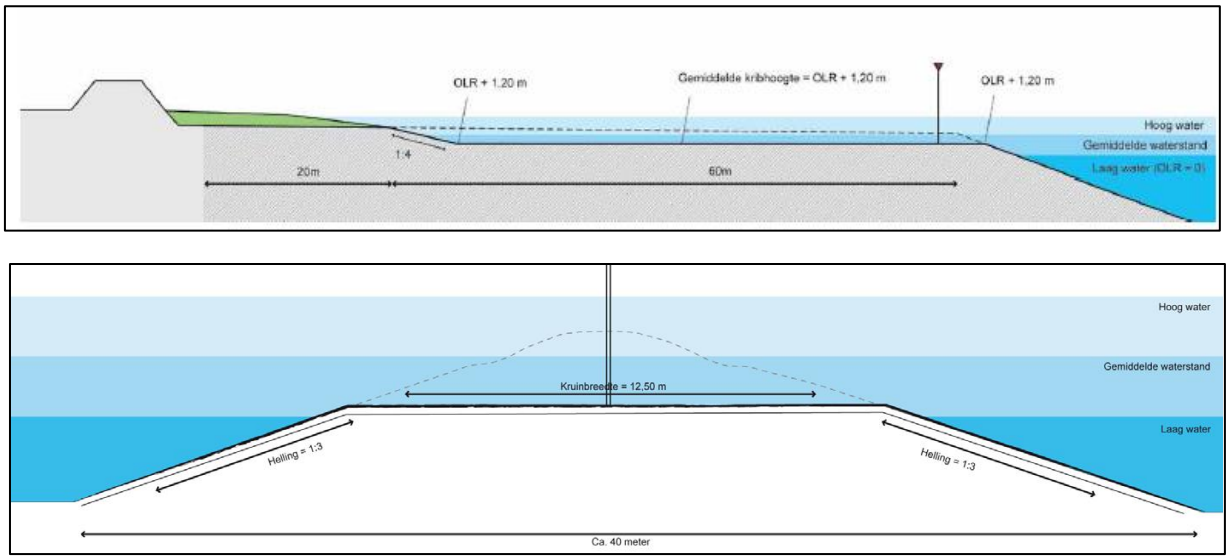

Figure 7: Design of the lowered groynes. The crest is lowered to a height of 5.2 metres above the river bed. (Schuurman, Nagtegaal, & Karelse, 2010)

groynes further prevents the formation of ice dams which used to threaten the flood safety in the Netherlands when only few groynes were present (Yossef, 2002).

The groynes near Dodewaard were first designed with a crest level of circa 6.5 m +NAP. Autonomous subsidence of the river bed however caused the groynes to be relatively higher than initially intended and necessary (Schuurman, Nagtegaal, & Karelse, 2010). To increase the flow conveyance capacity, the groynes were lowered within the Room for the River program (Klop, 2016). This program adopted the idea of lowering water levels rather than heightening levees to protect the land from flooding, hence the groyne lowering. The lowered groynes have a height of circa 5.2 meters at their head which is 1.2 m above OLR (Dutch: Overeengekomen Laagste Rivierstand). The OLR represents the lowest water height at which a minimum water depth is guaranteed by the agency Rijkswaterstaat. This water level corresponds to a discharge of 1020 m³/s at Lobith (Busnelli, Schuurman, Sieben, Wal, & Hector, 2011). The lowered groynes have a small incline of the crest (1:100) from the tip of the groyne to its root. They have a flat crest with a width of 12.5 meters and their slopes have, as can be seen in Figure 7, a gradient of 1:3 (Schuurman, Nagtegaal, & Karelse, 2010).

The current, lowered groynes are emerged during the majority of the year; the crest of the groyne is below the height corresponding to the average discharge in the Waal (Schuurman, Nagtegaal, & Karelse, 2010). The discharge hydrograph of the Waal is characterized by irregular high floods during winter, spring and fall. Periods of low flow and occasional small floods dominate the discharge pattern during summer times (Havinga, Taal, Smedes, Klaassen, Douben, & Sloff, 2006). The groynes are thus mostly emerged during the summer.

2.1.3. Design of the isle groyne

The proposed design of the isle groyne was, as it was designed before the groyne-lowering-projects in the Room for the River program, thought of as an alternative for the prior Waal-groynes with crests at circa 6.5 m +NAP (Figure 3). The trapezoidal inlet was lowered to a level corresponding to the OLR (4m +NAP at Dodewaard) over a width of – including its slopes - circa 32 meters. This would increase the cross-sectional profile of the river with 60 m² per groyne. The groyne's head was extended over a length of 20 meters in downstream direction which gives the groyne a characteristic L-shape. A further change opted for in the initial design of the isle groyne is the gradient of the slope on the channel-side of the groyne. The steepness of the slope was reduced to 1:3.5 compared to 1:3 for the ordinary groynes. The gradients on the down- and upstream sides of the groynes are maintained at 1:3 whereas the gradient of the slope of the trapezoidal inlet is designed at 1:2.5 (Heereveld, 2006).

2.2. Hydraulic effects of groynes

While the groynes fulfil their role in minimizing bank erosion and maintaining channel navigability, the main flow is funnelled through the navigation channel, diverting the flow away from the banks, increasing the mean velocity in the centre of the channel and improving the sediment transport efficiency (McCoy, Constantinescu, & Weber, 2008). In doing so, a complex pattern of two-dimensional and three-dimensional flow structures arises in the vicinity of groynes.

The hydrodynamics directly influence the morphology. To evaluate the impact of the isle groyne on the location and magnitude of groyne flames it is thus important to obtain a thorough understanding of the hydrodynamics around the current and isle groyne and how these contribute to the pattern of erosion and sedimentation in the vicinity of groynes. This section therefore describes the hydraulic effects of the current groynes and the expected impact of the isle groyne.

The effects discussed in this section focus on a series of representative groynes in the Waal of which the measures are presented in Table 1. Hydraulic consequences due to e.g. the groyne permeability, the angle of repose and building material are not discussed. Focus is applied to the situation of emerged groynes with a water level just below the crest of the groyne. As is later highlighted in section 2.3, it is during these circumstances that the groyne flames pose the biggest threat to the navigational quality of the river. Differences in hydrodynamics between the emerged and submerged situation are shortly addressed if applicable.

To structure the discussion of the different flow structures, this chapter is subdivided in two paragraphs. The first describes the time-averaged two-dimensional flow pattern distinguished around a groyne and its adjacent groyne field, the second discusses the turbulent structures induced by groynes.

2.2.1. Time-averaged two-dimensional flow pattern

Groynes confine the main flow as they block a part of the river's channel and thereby generate a pattern of convergence and divergence. This results in locations of high mean flow velocity in between two opposing groynes and low(er) flow velocity where the stream passes a groyne field (Yossef, Jagers, Mosselman, & Sieben, 2007). The flow can accelerate to velocities up to 1.5 times the values in the unaffected approaching flow (Zhang & Nakagawa, 2008). The acceleration and deceleration of the main flow is less severe in the presence of a series of groynes. Stable eddies within the groyne field partly prevent the flow from intruding into the groyne field, mitigate the flow divergence and convergence and increase the velocity and sediment transport efficiency in the main channel (Yossef, 2005). These stable eddies are formed during low discharges when the groynes in the Waal are emerged. The groyne fields do then not contribute to the flow conveyance capacity of the river and show the distinct hydrodynamic patterns as presented in Figure 8.

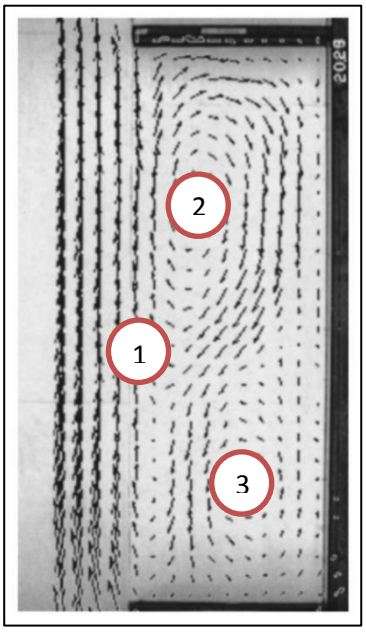

Figure 8: The hydrodynamics within a groyne field. A primary (1) and secondary (2) eddy are formed. The flow from the primary eddy is launched in the main channel (3) (Uijttewaal, Lehmann, & Mazijk, 2001)

The large stable eddies differ in size, location and number based on the ratio between the spacing (L) and width (W) of the groyne field (Figure 9). In the Waal, this ratio (L/W) is approximately 3, resulting in a situation in which two eddies – rotating in opposite directions – are formed in the groyne field (Yossef, 2005) (Point 2 and 3 in Figure 8). The largest eddy covers the downstream two-third of the embayment and

rotates in clockwise-direction (observed from the stream) at a velocity of circa 30-40% of the velocities of the main flow (Yossef & Klaassen, 2002). Upstream of this eddy, near the root of the spur dike, an anti-clockwise rotating eddy will form which is induced by the primary eddy. The stream pattern shows close comparison with type 3 in Figure 9.

In case of higher aspect ratios (i.e. relatively large spacing in between two adjacent groynes), the large eddy diminishes and enables the flow to intrude further into the groyne field. A smaller aspect ratio on the other hand may result in the diminishment of the smaller, anti-clockwise rotating eddy (Figure 9).

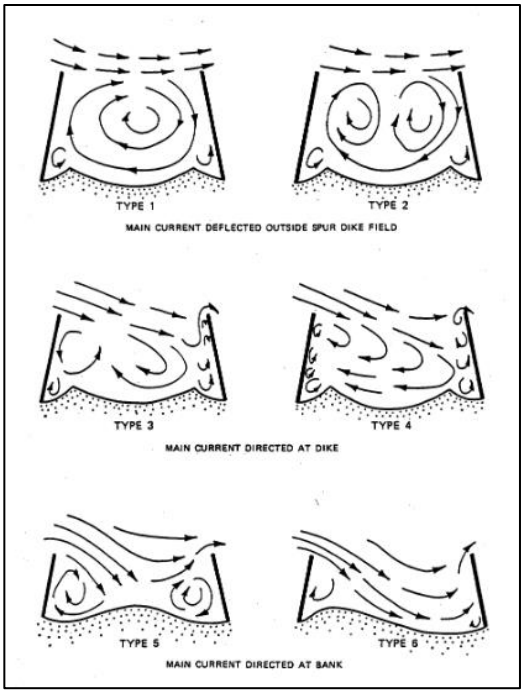

Figure 9: The dependency of the aspect ratio of groyne fields on the formation of stable eddies in the groyne fields (Klingeman, Kehe, & Owusu, 1984)

Although the primary eddy significantly contributes to the mitigation of the divergence of the flow by preventing the inflow of water into the groyne field, it, contrarily, slightly enhances the acceleration of the main flow. At the location where the primary eddy is reattached to the main channel, the flow is directed towards the channel's centreline and 'launched' into the main flow (Point 1 in Figure 8) (Talstra, 2011). This causes flow contraction. The location of this 'launch' may vary over time as the primary eddy is found to change in size and position (Uijttewaal, Lehmann, & Mazijk, 2001); the eddy oscillates back and forth within the groyne field. This effect – i.e. the 'breathing' of the primary eddy (Talstra, 2011) – is induced by the formation and migration of dynamic eddies at the groyne's tip. These eddies are further discussed in Section 2.2.2.1.

The primary and secondary eddy are not present during all discharge conditions. In contrast to low discharge conditions, groyne fields contribute to the flow conveyance capacity of the river in case the groynes are (completely) submerged. Although this region can still be characterized as a low flow region, the primary and secondary eddy will disappear. In the rare case of water levels just slightly above the crest of the groyne, highly three-dimensional flow structures may arise which are difficult to get a grasp on in numerical models. During these circumstances, the groynes might act as if they were being a dam, blocking the flow and causing a sudden drop of water level on the downstream side of the structure causing the slope of the water in the groyne field to be small compared to the average slope of the river (Yossef, 2005). This situation might lead to high flow velocities over the top of the groyne, consequential erosion just downstream of the structure and to the disappearance of the secondary anti-clockwise rotating eddy (Yossef, 2002). During very low discharge conditions – further below the groyne's crest – the water level decrease might result in a smaller primary eddy and a bigger secondary eddy (Talstra, 2011).

Expected effects of the isle groyne

The inlet of the isle groyne increases the flow conveyance capacity of the river and thus decreases the mean velocities in the main channel (Heereveld, 2006). The inlet is further thought to reduce the convergence and divergence of the flow. This idea originates from two expected effects. Firstly, the flow – opposing the groyne at its upstream side – is not forced to find its way through the narrowed river cross-section in between two groynes. Secondly, the elongated groyne head should be able to partly prevent the flow from intruding far into the groyne field. The latter effect could possibly be reduced by the portion of the flow which is bypassed through the notch. The flow – if strong enough – could penetrate into the large stable eddy within the groyne field and disturb its formation (Henning & Hentschel, 2013). As this stable eddy prevents the main flow from intruding into the groyne field (Yossef, 2005), disturbance of its formation might have undesired side-effects on the convergence-divergence pattern.

2.2.2. Turbulent structures around groynes

The obstructive nature of the groynes, the consequential need of the flow to bend around the groyne's head and the velocity differences between the main flow and the groyne field create a pattern of complex two- and three-dimensional turbulent flow structures.

Turbulence is generated in case of relative internal motion or when a fluid passes a solid surface (Robert, 2003). The velocity difference along the boundary between the faster and slower moving bodies creates a frictional force which retards the relative motion (Anderson, 2011); a logarithmic boundary layer is formed. In turbulent flows, the velocity differences in the boundary layer cause flow instabilities; a turbulent flow is generated as fluid particles move in irregular paths and flows with different velocities are injected into adjacent portions of the flow. Eddies – "swirls of fluid with highly irregular shapes and a wide range of sizes" (Robert, 2003) – and vortices – "a solid body-like rotation of the fluid" (Robert, 2003) – are formed. The interference of adjacent layers causes local velocity fluctuations and flow properties to be spread out over the flow (Anderson, 2011). Consequentially, turbulence can alter the morphological processes and are thus important to discuss in this chapter. For example, 'sweep' – the injection of faster moving fluid with high energy into the bottom layers of the flow – results in a local increase of velocity gradients and bed shear stresses near the bed and enhances the entrainment of sediment. 'Ejection' – the movement of a fluid particle with relatively low velocity to a location further away from the bed – enhances the capability of the flow to keep sediment in motion (Robert, 2003).

Eddies and vortices are both present in the vicinity of groynes and influence the bathymetry. These turbulent flow structures are discussed in this section. Subsequently the turbulent flow in the mixing zone between the groyne field and the main flow as well as the dynamic eddies within this mixing layer (§2.2.2.1) and the horseshoe vortex (§2.2.2.2.) are addressed.

2.2.2.1. Mixing zone

The mixing zone, or (detached) shear layer, is a zone of dynamic flow and large velocity gradients (Yossef, 2002). This zone emerges at the tip of the groyne where flow separation takes place; the main flow is not capable of following the course of the groyne, resulting in an area of low/no downstream velocity directly adjacent to the main flow. The flow velocity gradients give rise to high mixing along the boundary of the two areas: hence, the mixing zone (Robert, 2003). This zone elongates downstream along the normal line between the groyne field and the main flow zone where differences in flow velocities also lead to strong gradients, mixing and thus to turbulent flow features. Further downstream, the turbulence intensity is decreased as the velocity gradients in the mixing layer decrease.

Whenever groynes are fully submerged, the increased flow conveyance capacity of the groyne field results in smaller velocity gradients within the mixing zone. This leads to reduced turbulence intensity. In case of only slight submergence, the velocity gradients remain large as the groyne fields just barely contribute to the flow conveyance capacity (Yossef & Vriend, 2011). Since the formation of a primary and secondary eddy is disturbed during these conditions, the large velocity gradients are present along the entire normal line between two adjacent groyne fields. This leads to strong turbulence in a well-developed mixing layer with a constant width (Figure 10). Furthermore, the detached shear layer is thought to be more parallel to the groyne field during periods of higher discharge since the flow is to fewer extent converged and diverged as it passes the groynes and adjacent groyne fields (Heereveld, 2006).

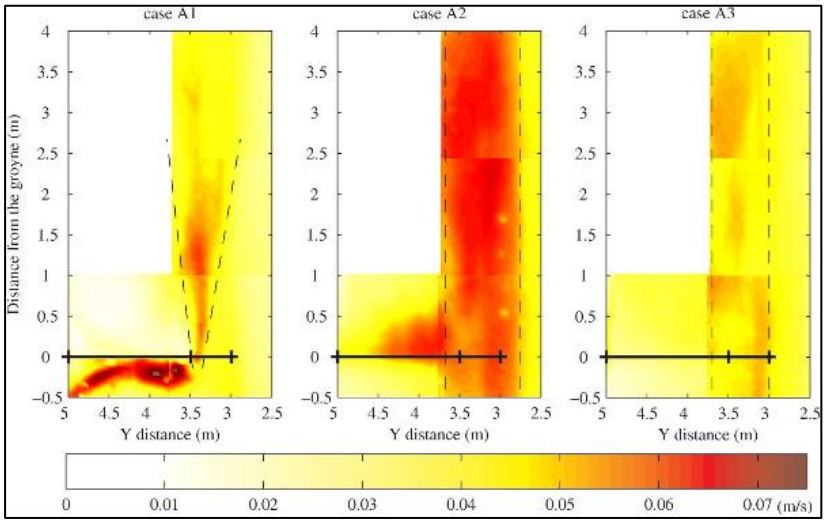

Figure 10: Turbulence intensity along groyne fields. Case A1 represents the situation in which the groynes are emerged, A2 the situation with a water level just above the crest of the groyne, A3 the situation with water levels high above the crest of the groyne (Yossef, 2011).

Detached Shear Layer

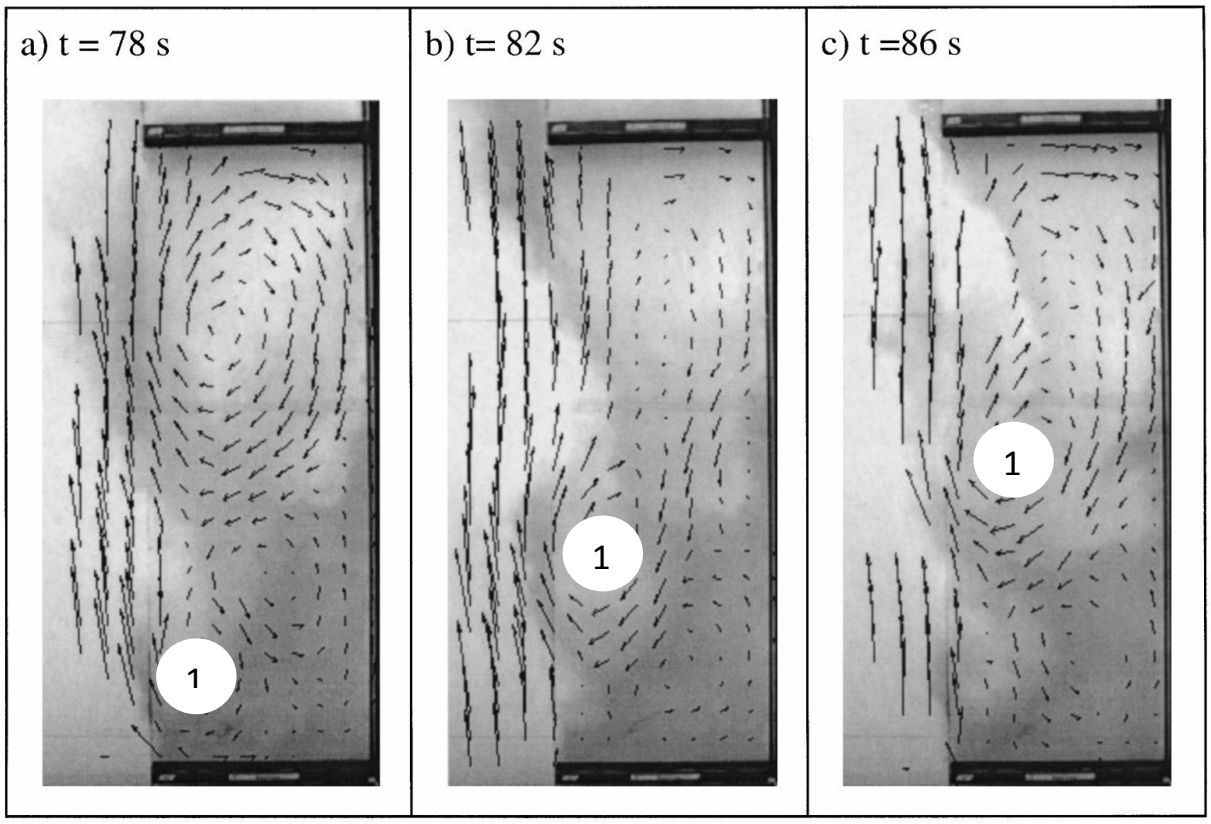

Figure 11: Snapshots of the flow pattern in groyne fields. Dynamic eddies (Points 1) are formed, migrate downstream and merge with the primary eddy **(Uijttewaal, Lehmann, & Mazijk, 2001)**

The flow separation at the tip of the groyne and consequential high velocity gradients give rise to the formation of eddies (Robert, 2003). These eddies are quasi-2D, meaning that their structure extends almost uniformly over the full water depth. They are dynamic and propagate downstream (points 1 in Figure 11) with a velocity slightly higher than the mean stream velocity (1.5%) along the fully turbulent detached shear layer (Yossef, 2002; Zhang & Nakagawa, 2008). The dynamic eddies are further amplified by the secondary eddy in the groyne field which – due to its anti-clockwise rotation and consecutive negative flow velocities near the main flow – induce even larger velocity gradients. Talstra (2011) mentioned the importance of this secondary eddy on the formation of the dynamic eddies. Koken and Constantinescu (2008) found that, as the dynamic eddies propagate, they may merge and create an increase of turbulent kinetic energy (the kinetic energy associated with eddies in turbulent flow). The dynamic eddies further interact with the primary eddy, which cause the primary eddy to show the oscillation described in section 2.2.1. and depicted in Figure 11.

These turbulent dynamic eddies create a local increase of bed shear stresses, mainly in the upstream part of the detached shear layer. Also further downstream, some patches of high turbulence can be present, likely originating from the increase of turbulent kinetic energy created during the merge of two dynamic eddies (Koken & Constantinescu, 2008).

The formation of dynamic eddies is, as for the primary and secondary eddy, disturbed when the groynes are submerged.

Expected effects of the isle groyne

The dynamic eddies in the detached shear layer could be weakened. The reduced accelerations around the tip of the groyne might result in a better streamlining and enlarged capability of the flow to follow the geometry of the groyne; flow separation might be reduced/absent (Heereveld, 2006). Furthermore, the flow through the inlet, propagating downstream parallel to the main flow, could reduce the velocity gradients between the main channel and the groyne field. It creates a zone of positive rather than negative (secondary eddy) flow velocities adjacent to the main channel. The turbulence in the detached shear layer is also thought to reduce because of the possible reduction of flow separation at the head of the groyne.

The upstream part of the mixing zone could also be displaced in comparison to its location near the normal groyne. The construction of the inlet leads to reduced convergence of the flow which may cause the upstream part of the detached shear layer to be moved in a position more parallel to the groyne field (Heereveld, 2006). As mentioned in Section 2.2.1., the isle groyne may lead to increased divergence due to the dissipation of the large primary eddy or decreased divergence due to the streamlining by the elongated groyne head. Depending on the governing effect, the downstream end of the detached shear layer might propagate to larger or smaller extent parallel to the normal line in between two adjacent groynes.

2.2.2.2. Horseshoe vortex

Just upstream of the emerged groyne, the water piles up as a result of the blockage of the flow. This results in a bow wave at the water surface and a downflow along the sidewall of the groyne (Safarzadeh, Neyshabouri, & Zarrati, 2016). The set-up of water further results in an increase of the static water pressure. The resulting positive gradient of the static water pressure in the direction of the flow is referred to as an adverse pressure gradient. Meanwhile, the vertical velocity distribution of the incoming flow can, as in most river situations, be represented by a logarithmic profile. This results in low flow velocities near the bottom of the river. This slowly moving fluid further decelerates due to the higher pressure which results in a standstill of the flow near the bottom or even in a reversed flow (Anderson, 2011). Interaction between this slowly moving bottom layer and the faster moving layers on top causes the formation of a horizontally rotating vortex: the horseshoe vortex (Safarzadeh, Neyshabouri, & Zarrati, 2016). The vortex is first located

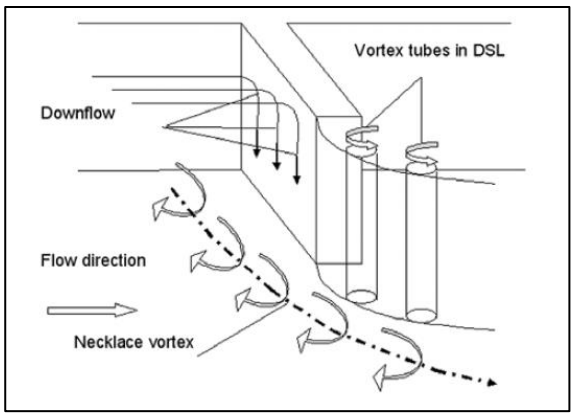

Figure 12: A horseshoe vortex (necklace vortex in this figure) is formed on the upstream side of the groyne (Koken & Constantinescu, 2008)

parallel to the groyne and then folds and accelerates around the groyne's head (Koken & Constantinescu, 2008) (Figure 13).

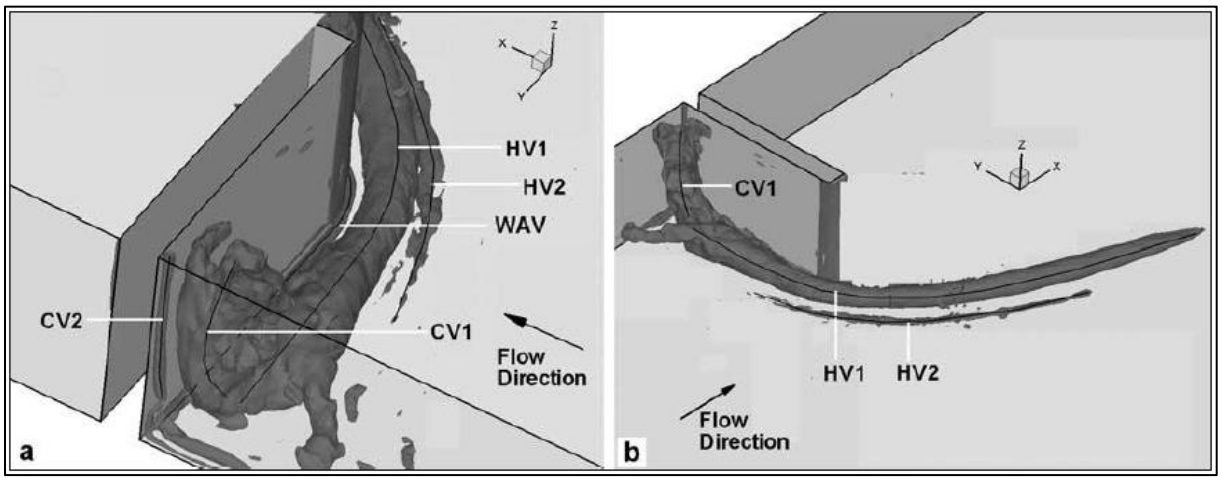

Figure 13: The coherent horseshoe vortex structure (HV1), first located parallel to the groyne, and the corner vortex (CV1) (Koken & Constantinescu, 2008)

As the horseshoe vortex accelerates around the groyne, it increases the bed shear stresses, entraining large amounts of sediment. Further downstream, the bed shear stresses reduce. However, also here, patches of flow with high vorticity which are shed from the horseshoe vortex create local higher bed shear stresses (Koken & Constantinescu, 2008).

It should be mentioned that it is questioned to which extent the horseshoe vortex is formed along the series of groynes present in the Waal. Talstra (2011) and Van Heereveld (2006) both mention the horseshoe vortex in their discussion on the hydrodynamics around groynes and mention their importance on the scour around the groyne tip. However, the relatively smooth slope of the groyne might decrease the adverse pressure gradient upstream of groynes. Furthermore, the flow inside groyne fields is only directed towards the river's centreline near the tip of the groyne, in contrast to the case presented in Figure 11. This possibly reduces the size of the vortex. Lastly, the formation of the corner vortex (Figure 13) which amplifies the horseshoe vortex is hampered by the presence of multiple groynes and sloping groyne fields. The large horizontal velocity gradients between the river's embankment and the approaching main flow are absent in the case of a series of sloping groyne fields.

In case the groynes are submerged, the increased ability of the flow to pass the groyne weakens the adverse pressure gradient and consequentially the horseshoe vortex.

Expected effects of the isle groyne

The horseshoe vortex is thought to weaken in comparison with the normal groyne. The inlet reduces the obstruction of the flow, consecutively weakens the adverse pressure gradient and thus the formation of the horseshoe vortex. It is furthermore expected that the elongated groyne head results in the horseshoe vortex to stick to the head of the groyne (Heereveld, 2006). This decreases both the

angle of deflection of the vortex and its strength; the induced friction along the turbulent coherent structure and the groyne decreases the turbulent kinetic energy of the horseshoe vortex.

2.3. Morphological Effects of Groynes

Flow accelerations and turbulent features locally increase bed shear stresses and enhance the mobility of sediment which induces erosion of the bed. Subsequent deposition occurs when bed shear stresses decrease again. The hydrodynamic processes caused by the obstructive nature of the emerged groyne results in a variety of bed forms among which the degradation of the main channel, uni-dimensional waves between groynes, groyne flames and scour holes (Yossef, Jagers, Mosselman, & Sieben, 2007).

The groynes confine the main channel, resulting in higher flow velocities. Higher velocities lead to increased erosion and thus to the degradation of the main channel. This degradation is not uniformly distributed along the entire Waal. As the flow converges and diverges during its passage along the groynes and groyne fields, the flow accelerates and decelerates, forming a pattern of uni-dimensional bed waves with the length of the spacing between two adjacent groynes and having their peak alongside the groyne fields (Yossef, Jagers, Mosselman, & Sieben, 2007).

These uni-dimensional waves are superimposed on a pattern of scour holes and groyne flames; two morphological features which require additional attention. Attention which is given in the following sections.

2.3.1. Groyne Flame

The groyne flame, referred to in several occasions in this report, is a large patch of sedimentation alongside the groyne field. The local shoal, which fluctuates in size with varying discharge, can reach lengths and widths of, respectively, 60 by 40 meters (Figure 14) and has a mean height of 75 centimetres above the average bed level (Klaassen & Sloff, 2000; Heereveld, 2006). Slightly higher values can be found in the multibeam measurements presented in Figure 5. The driving mechanisms behind the formation of groyne flames are the dynamic eddies present in the detached shear layer (Yossef, Jagers, Mosselman, & Sieben, 2007). These eddies entrain sediment, transport the sand downstream and, as the eddies disperse, drop the sediment to form the groyne flame. Furthermore, the pattern of divergence and convergence is important for the formation of groyne flames. Additional sediment is provided to the groyne flames in times of low flows as navigation

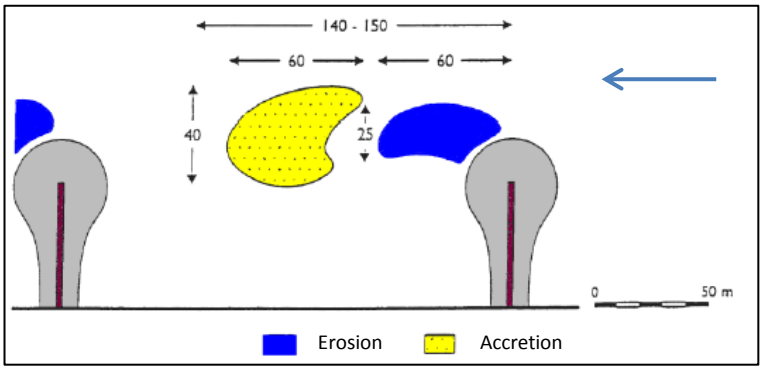

Figure 14: The pattern of the scour hole (ontgronding) and adjacent groyne flame (aanzanding) with their approximate dimensions (in m) **(Klaassen & Sloff, 2000)**

induced currents cause a return flow from the groyne fields into the main channel, delivering an additional sediment inflow along its way. The exact contribution of this flow to the magnitude of the groyne flame is unknown (Yossef, 2002). Furthermore, Klop (2016) found that the height of the groyne flame is related to the depth of the upstream scour hole. This indicates an indirect effect of the factors governing the formation of these scour holes (§2.3.2.) on the formation of groyne flames.

Groyne flames differ significantly from one another, both in time and space. The parameters affecting the hydrodynamics, i.e. the dynamic eddies and con-/divergence of flow, influence the magnitude and shape of groyne flames. Hampered formation of dynamic eddies leads to a lower equilibrium magnitude of groyne flames (Yossef, 2002). For example, increased water depth – leading to the submergence of groynes – would decrease the height of groyne flames. Similar effects are visible for lower flow velocities and a more streamlined groyne head; the reduced obstructive nature of the groyne improves the smoothness of the confinement of the flow, decreases the deflection of the stream and the strength of the dynamic eddies. Reduced convergence of the flow leads to the displacement of the detached shear layer. This positively affects the location of the groyne flame; a more parallel orientation of the groyne flame reduces the amount of local shallow areas in the navigation channel.

A change of some of the aforementioned parameters may lead to a change of the equilibrium height of groyne flames. It takes time for groyne flames to reach this new equilibrium. During this time of adaptation, the groyne flames show dissimilarities with one another. As time proceeds, groyne flames become more alike. Also, groyne flames might show two apexes in the initial phases of their development. This feature fades away with time as well (Yossef & Klaassen, 2002).

Expected effects of the isle groyne

The groyne flame is thought to be reduced in size (Figure 15). The dominant hydrodynamic force in the formation of this morphological feature – the dynamic eddies in the detached shear layer – are expected to be weakened (§2.2.). Also, the groyne flame is thought to be located more parallel to the groyne field due to the displaced detached shear layer (Heereveld, 2006). The combination of both effects could decrease the negative impact of groyne flames on the navigational quality of the river Waal (Figure 15).

Additional beneficial effects on the height of groyne flames might result from a reduced sediment inflow from the groyne fields. The elongated groyne head partly prevents navigation-induced waves to influence the sediment exchange between the groyne field and the main channel (Heereveld, 2006). This effect is further amplified by the inlet; during the passage of a ship in times of low discharge, the inlet provides additional water inflow preventing both a sudden drop of water level due to the ship-induced water movement and the consecutive erosion from the groyne fields.

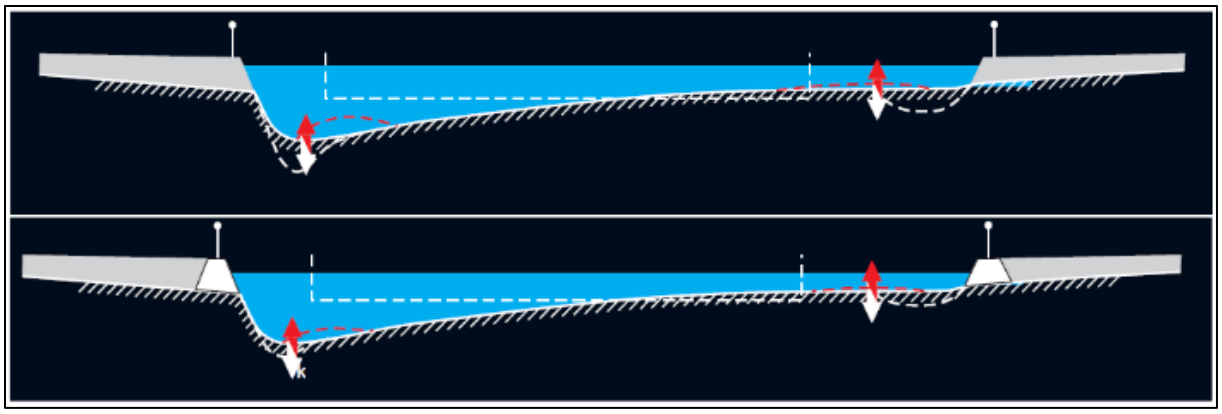

Figure 15: The expected effect of the isle groyne on groyne flames: a decrease in height and a transverse shift towards the channel's embankments. The current situation is placed in the top figure, the situation with the isle groyne in the bottom figure (Consortium Kribben, 2006)

2.3.2. Scour hole

At the groyne's head, a relatively deep scour hole is developed. Driving mechanisms behind this formation are the dynamic eddies which are shed from the groyne tip, the acceleration of the flow around the groyne tip and, most importantly, the horseshoe vortex (Klaassen & Sloff, 2000; Koken & Constantinescu, 2008). According to Verheij (1997) these scour holes can reach depths of up to 4-6 meters below the average river bed, causing serious issues concerning the structural stability of the groynes. The depth of these scour holes however depend on several parameters, resulting in lower scour holes around the groynes in the Waal.

As for the groyne flame, parameters affecting the hydrodynamics around groynes can influence the depth of scour holes. Lower flow velocities as well as better streamlining of, and stream guidance by the groyne decrease the strength of the horseshoe vortex and the magnitude of the flow acceleration (Heereveld, 2006). This leads to a reduced size of the scour hole. Multibeam measurements of the Waal further show that higher water depths and consequential submergence of the groynes have similar effects; scour holes are lower after the winter season when discharges are highest (Klop, 2016). There is however some dispute on this issue as Verheij (1997) highlights the positive effect of increased water levels on the depth of scour holes. According to him, deepest scour occurs when the groynes are submerged.

Expected effects of the isle groyne

The scour holes are expected to be reduced in size by the isle groyne due to the mitigation of the hydrodynamic forces responsible for the development of the erosion. Both the horseshoe vortex and the acceleration around the groyne tip are thought to reduce (§2.2.1. and §2.2.2.2.)

2.4. Numerical modelling of flow and sediment transport with Delft3D-FLOW

To determine the hydrodynamic and morphological effects of the isle groyne, the hydraulic and morphological phenomena described in section 2.2 and 2.3 are numerically modelled with Delft3D-FLOW. Delft3D-FLOW is a module within Delft3D, a computer software suite used for a multi-disciplinary approach of three-dimensional computations of riverine and coastal areas. The module Delft3D-FLOW accounts for the two- and three-dimensional hydrodynamic and morphological numerical modelling of non-steady flow and transport phenomena within Delft3D (Deltares, 2014). It forms the basis for other modules within Delft3D (e.g. for waves, water quality and ecology). In order to be able to interpret the outcomes of this research correctly, it is important to know the calculations and formulae which govern these outcomes. This section introduces the most important formulae and equations used to resemble the hydraulic and morphological effects described in section 2.2 and 2.3. The Delft3D-FLOW Manual has been the source for these formulae. For a full explanation of the description of Delft3D, one is referred to this manual. The subjects to be discussed are:

1. The Navier-Stokes equations
2. Turbulence in Delft3D-FLOW: Horizontal Large Eddy Simulation
3. The sediment transport equations and morphological updating

2.4.1. Navier-Stokes Equations

The rudimentary equations underlying the way Delft3D-FLOW solves the flow phenomena in the vicinity of groynes are the well-known mass and momentum equations. The momentum equations – stating that the change in momentum of a revised element is in equilibrium with the external forces acting on this element – are represented by the Navier-Stokes equations.

Solving these equations for turbulent riverine applications requires the use of several assumptions:

- Delft3D-FLOW assumes shallow water in which vertical accelerations due to buoyancy effects and due to variations in the bottom topography are negligible (Deltares, 2014). This results in the reduction of the momentum equation in z-direction to the hydrostatic pressure equation.
- Delft3D-FLOW uses Reynolds Averaging. This refers to the fact that the set of momentum equations are time-averaged over small turbulent time-scales – far smaller than the computational time-step applied in Delft3D-FLOW – to ease the numerical calculations. Time-averaging occurs through decomposition of instantaneous velocities in an average and a fluctuating component, giving an equation of motion for the average (RANS) and fluctuating quantities (Nieuwstadt, Boersma, & Westerweel, 2016).
- It is assumed that the transfer of momentum caused by the presence of turbulence can be modelled by a viscosity term: the eddy viscosity (Deltares, 2014). This is known as the Boussinesq approximation.
- The external forces that should be in equilibrium with the change in momentum can be applied by a combination of factors. The formulae in Delft3D-FLOW take account of the forces due to

spatial variations in water pressure, the gravitational force, the Coriolis force and the forces due to turbulence (Deltares, 2014).

Under these assumptions, the momentum equations are given by:

$$\frac{\partial u}{\partial t} + u\frac{\partial u}{\partial x} + v\frac{\partial u}{\partial y} + w\frac{\partial u}{\partial z} = -\frac{1}{\rho_0}P_x + F_x + \frac{\partial}{\partial z}\left(\nu_V \frac{\partial u}{\partial z}\right) + fv \quad (1)$$

$$\frac{\partial v}{\partial t} + u\frac{\partial v}{\partial x} + v\frac{\partial v}{\partial y} + w\frac{\partial v}{\partial z} = -\frac{1}{\rho_0}P_y + F_y + \frac{\partial}{\partial z}\left(\nu_V \frac{\partial v}{\partial z}\right) + fu \quad (2)$$

$$\frac{\partial P}{\partial z} = -\rho g \quad (3)$$

u/v/w *Velocity in x/y/z-direction [m/s]*
$P_{X/y}$ *Pressure gradients in x/y-direction [kg/(m²s²)]*
p *Pressure [kg/m²]*
ρ *Density of fluid [kg/m³]*
g *Gravitational acceleration [m/s²]*
$F_{X/y}$ *Divergence of horizontal Reynold's stresses in x/y-direction [kg/(ms²)]*
f *Coriolis parameter [s⁻¹]*
ν_v *Vertical eddy viscosity [m²/s]*

P_x and P_y represent the pressure gradients. These are – considering constant density of the water – composed of the change in atmospheric and hydrostatic pressure. F_x and F_y are the terms for the divergence of the horizontal Reynold's stresses. These stresses account for the turbulent fluctuations in a fluid and can be represented by viscosity terms; the turbulent exchange of momentum through adjacent layers of a fluid with different properties acts as if it were a viscous force (Nieuwstadt, Boersma, & Westerweel, 2016). The forces F_x and F_y can be computed through the use of the following formulae (Deltares, 2014).

$$F_x = \frac{\partial}{\partial x}\left(2\nu_H \frac{\partial u}{\partial x}\right) + \frac{\partial}{\partial y}\left(\nu_H \left(\frac{\partial u}{\partial y} + \frac{\partial v}{\partial x}\right)\right) \quad (4)$$

$$F_y = \frac{\partial}{\partial y}\left(2\nu_H \frac{\partial v}{\partial y}\right) + \frac{\partial}{\partial x}\left(\nu_H \left(\frac{\partial u}{\partial y} + \frac{\partial v}{\partial x}\right)\right) \quad (5)$$

ν_H *Horizontal eddy viscosity [m²/s]*

These equations are solved in a three-dimensional domain with the use of the σ-grid. This grid consists of a user-defined number of layers in between two flexible σ-planes which follow the bottom geometry on the one side and the water surface on the other, meaning that the thickness of a layer is dependent on the local water depth (Deltares, 2014). Contrarily the Z-grid uses vertical layers of constant thickness (Figure 16).

N.B. The use of a Z-grid would allow the introduction of non-hydrostatic pressure gradients. However, this grid type has not been tested in combination with the use of Horizontal Large Eddy Simulation. Horizontal Large Eddy Simulation is found to be highly valuable to model groyne flames (§2.4.2.1.). A small test has shown that the use of a Z-grid does give qualitatively different results for the horizontal

eddy viscosity v_H. As the Horizontal Large Eddy Simulation has been tested in combination with the σ-grid, it is assumed that the results using the Z-grid are incorrect and that it is thus not desired to use in the calculations for the turbulence around groynes.

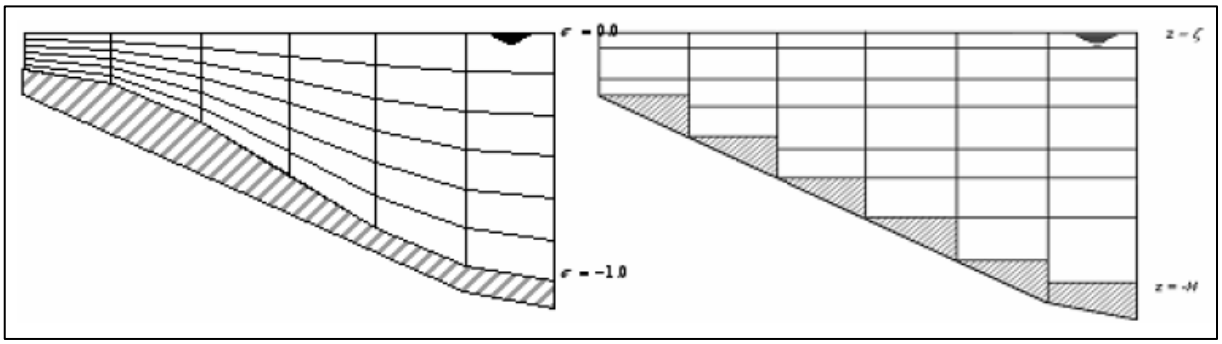

Figure 16: Example of a sigma and a Z-grid **(Deltares, 2014)**

2.4.2. Turbulence in Delft3D-FLOW: Horizontal Large Eddy Simulation

As introduced in section 2.4.1. the Navier-Stokes equations are split up into a mean and a fluctuating component. This leads to the Reynold's Averaged Navier Stokes equations in which the turbulent flow phenomena are described by the Reynold's stresses. The term expressing these stresses is however nonlinear which results in the Navier-Stokes equations to be instable. This is referred to as the closure problem (Nieuwstadt, Boersma, & Westerweel, 2016). Further explanation on this topic can be found in Appendix III. To overcome the closure problem, several closure models have been developed which model the Reynolds stresses solely as a function of the mean component of the flow.

In this research, the k-epsilon closure model has been applied to calculate the vertical eddy viscosity which governs the viscous stresses from 3D-turbulence. Explanation on the k-epsilon closure model is found in Appendix IV. The method of Horizontal Large Eddy Simulation (HLES) has been applied to grasp the contribution of horizontal turbulent motions.

The turbulence models contribute to the momentum equations according to (Deltares, 2014):

$$\nu_H = \nu_{SGS} + \nu_V + \nu_H^{back} \tag{6}$$

$$\nu_V = \nu_{mol} + \max(\nu_{3D}, \nu_v^{back}) \tag{7}$$

v_{SGS} *Horizontal Eddy Viscosity due to sub-grid scale (SGS) turbulence (with HLES) [m²/s]*

v_H^{Back} *Background horizontal eddy viscosity, user-defined [m²/s]*

v_{mol} *Kinematic viscosity of water [m²/s]*

v_{3D} *Three-dimensional eddy viscosity, determind by the k-ε closure model [m²/s]*

v_V^{Back} *Background vertical eddy viscosity, user-defined [m²/s]*

2.4.2.1. Horizontal Large Eddy Simulation

The ability of Delft3D-FLOW to model the horizontal turbulent motions with the use of Horizontal Large Eddy Simulation, is one of its great advantages over other numerical models. Correct representation of the quasi two-dimensional dynamic eddies which are shed from the groyne tip is proven to be essential for the representation of groyne flames (Yossef, 2005). Usually, horizontal turbulent eddies are not resolved. A constant horizontal eddy viscosity and diffusivity are then used which is an unsatisfactory reproduction of the actual turbulent flow (Liek, 2000). Yossef (2005) found that Horizontal Large Eddy Simulation (HLES) is capable of modelling these turbulent features. It should be mentioned that vertical turbulent motions, e.g. the horseshoe vortex, can not be captured by HLES.

HLES uses a method of decomposing the turbulent motions in larger and smaller scale eddies. The large-scale eddies are directly resolved by the Navier-Stokes equations whereas the contribution of smaller scale eddies to the flow is modelled using a subgrid-scale closure model (Liek, 2000). HLES can thus be seen as a 'hybrid' form in between direct numerical simulation (DNS) – which solves all turbulent scales (Appendix II) with the Navier-Stokes equations – and a closure model like the k-ε model (Sodja & Podgornik, 2007). The separation of the large- and small-scale eddies offers great advantage over both DNS and ordinary closure models like the k-ε model.

As can be found in Appendix II, small scale turbulent motions have a universal form and are independent of the geometric characteristics of the mean flow (Nieuwstadt, Boersma, & Westerweel, 2016). It is therefore thought that small scale motions are more easily captured by a closure model than large-scale motions. Within HLES, these large-scale motions are solved on the numerical grid via the RANS-equations (Liek, 2000), giving more reliable results for the horizontal turbulent motions than the k-ε closure model. Modelling the small-scale turbulent motions with a closure model offers significant advantages for the computational time compared to DNS. A disadvantage of the HLES over the k-ε closure model is that sufficiently small spatial steps and accompanying temporal steps should be applied in the numerical model to be able to directly model the large-scale motions on the numerical grid.

The contribution of the small scale eddies to the large scale motions is determined via the subgrid-scale eddy viscosity calculated by (Deltares, 2014):

$$\nu_{SGS} = \frac{1}{k_s^2}\left(\sqrt{(\gamma\sigma_T S^*)^2 + B^2} - B\right) \tag{8}$$

- S^* *Sum of strain rates [s^{-1}]*
- B *Effect of bottom friction [s^{-1}]*
- k_s *Wave number of wave length below which the equation is designed to represent the effect of SGS-turbulence [m^{-1}]*
- σ^T *Turbulent Prandtl-Schmidt number [-]*
- γ *Parameter representing the influence of the slope in the log-log spectrum of the turbulent kinetic energy density [-]*

$(S^*)^2$ represents the sum of strain rates squared and is determined by:

$$(S^*)^2 = 2\left(\frac{\partial u^*}{\partial x}\right)^2 + 2\left(\frac{\partial v^*}{\partial y}\right)^2 + \left(\frac{\partial u^*}{\partial y}\right)^2 + \left(\frac{\partial v^*}{\partial x}\right)^2 + 2\frac{\partial u^*}{\partial y}\frac{\partial v^*}{\partial x} \quad (9)$$

*u** *Fluctuation of the velocity in x-direction [m/s]*

*v** *Fluctuation of the velocity in y-direction [m/s]*

*w** *Fluctuation of the velocity in z-direction [m/s]*

In equation 9, the star-denoted velocity terms represent fluctuating flow variables which are defined through a high-pass filtering operation defined in equations 10 and 11. A filtering operation is necessary to filter steady spatial variations from variations due to turbulent motions.

$$\psi^* = \psi_{n+1} - \bar{\psi}^t_{n+1} \quad (10)$$

$$\bar{\psi}^t_{n+1} = \left(1 - \exp\left(-\frac{\Delta t}{\tau}\right)\right)\psi_{n+1} + \exp\left(-\frac{\Delta t}{\tau}\right)\bar{\psi}^t_n \quad (11)$$

τ *Relaxation time [s]*

ψ^* *Fluctuation of the velocity in any direction [m/s]*

The effect of bottom friction on ν_{SGS} is given by:

$$B = \frac{3g|\vec{U}|}{4HC^2} \quad (12)$$

g *Gravitational acceleration [m/s²]*

U *Flow velocity [m/s]*

C *Chézy-coefficient [m$^{1/2}$/s]*

H *Water depth [m]*

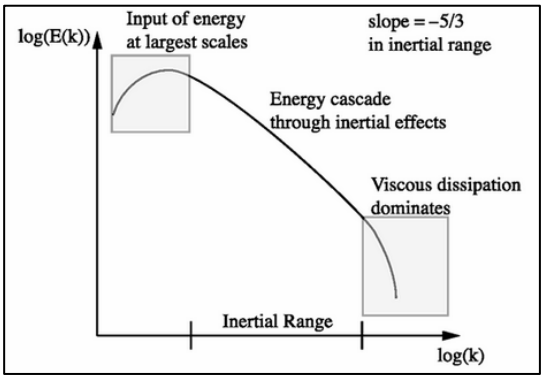

Figure 17: The turbulent kinetic energy contained by the different turbulent scales. The slope of the decrease of energy in a log-log-spectrum is -5/3 (Berselli, Illiescu, & Layton, 2006)

The parameter γ in Eq. 8 can be calculated by the means of equation 13. The governing term in this formula is the slope α in the log-log spectrum of the energy density E(k). This is the gradient of the logarithmic graph of the turbulent kinetic energy density (E) over the wave number of the turbulent eddies (k) within the inertial subrange of the turbulent scales (Figure 17). The gradient represents the dissipation of turbulent kinetic energy into heat, a process which only occurs at small turbulent scales, i.e. small wave numbers (Appendix II).

$$\gamma = 0.844\sqrt{\frac{1-\alpha^{-2}}{2n_D}} \quad (13)$$

α *Slope in log-log spectrum of the energy density [-]*

n_D *Indication of the dimensionality of the turbulence (2 or 3) [-]*

Lastly, k_s represents the wave number of the wave length below which the equation for the subgrid-scale eddy viscosity is designed to represent the influence of the subgrid-turbulence on the base flow.

$$k_s = \frac{\pi f_{lp}}{\Delta} \tag{14}$$

k_s *Wave number [m^{-1}]*

f_{lp} *Spatial low-pass filter coefficient [-]*

2.4.2.2. Sediment Transport and Morphology

The flow of water, if strong enough to initiate motion, mobilizes sediment and causes erosion and deposition. The resulting change in the topography in turn affects the flow field, which influences the sediment transport: the morphological loop. This process is incorporated in Delft3D-FLOW (Figure 18), which gives the model another advantage over many other models. The influence of the flow field on the time-varying sediment transport and consequential morphological change is presented in the current section.

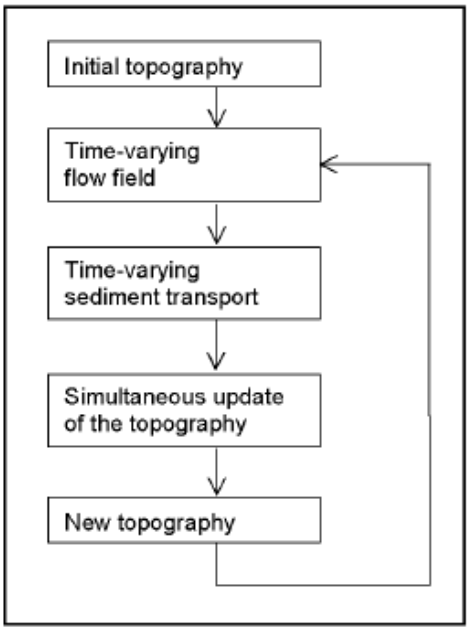

Figure 18: The morphological loop in Delft3D-FLOW **(Rupprecht, 2004)**

The drivers of morphological change

Delft3D-FLOW`is able to distinguish two modes of sediment transport which interact with the bed: bed load transport and suspended load transport. The former refers to the sediment which slides or rolls over the riverbed or which is in either uninterrupted or interrupted saltation. This type of transport propagates at velocities considerably lower than the flow velocity. Suspended sediment transport is in less contact with the river bed and moves at higher velocities. One distinguishes between the two modes based on, among other, the assumption that particles that can be maintained in suspension by the upward forces of turbulence are defined as being in suspension (Robert, 2003).

Many researchers have composed standard sediment transport formulations to determine the bed load transport and suspended sediment transport of non-cohesive sediment (e.g. the formulae of Van Rijn, Meyer-Peter-Muller and Engelund-Hansen). It depends on the user which sediment transport formulation to use and whether Delft3D-FLOW consequentially distinguishes between the two modes of transport or merely calculates a total sediment transport. This research uses the total sediment transport formulations of Engelund-Hansen. The total sediment transport is treated as if it were bed load transport (Deltares, 2014). Therefore, only the formulae governing the bed load transport are presented in this section.

In Delft3D-FLOW, using Engelund-Hansen, the bed is updated by comparison of the bed/total transport gradients in the horizontal domain (Deltares, 2014). A morphological time scale factor

(MORFAC) may be used to speed up the morphological process and account for the different time-scales between hydrodynamic and morphological changes. The MORFAC simply scales up the speed of changes in morphology (Deltares, 2014).

$$\frac{\partial z_b}{\partial t} + f_{MORFAC}\left(\frac{\partial S_{b,x}}{\partial x} + \frac{\partial S_{b,y}}{\partial y}\right) = 0 \tag{15}$$

$S_{b,x/y}$ *Bed load transport in x/y-direction [kg/(ms)]*

z_b *Bed level [m]*

f_{MORFAC} *Morphological time scale factor [-]*

Bed Load Transport

Similar to the hydrodynamic parameters, the sediment transport parameters are determined at every grid cell during each time step. The sediment transport formulation of Engelund-Hansen initially derives the total sediment transport from the flow conditions according to Eq. 16 to 20. The outcomes of these formulae are corrected for the effects of bed level gradients in transverse and longitudinal directions based on the formulae presented in Van Rijn (1987).

$$S_b = \frac{0.05\alpha q^5}{\sqrt{g}C^3\Delta^2 D_{50}} \tag{16}$$

S_b *Bed/total load transport [kg/(ms)]*

α *Calibration coefficient [-]*

Δ *Relative density ($\rho_{sediment} - \rho_{water}$)/$\rho_{water}$ [-]*

q *Magnitude of flow velocity [m/s]*

D_{50} *Mean sediment diameter [m]*

The bed load transport in u/x- and v/y-direction can be found using Equation 17 to 20:

$$S_{b,x} = \frac{u_{b,x}}{|u_b|}|S_b| \tag{17}$$

$$S_{b,y} = \frac{u_{b,y}}{|u_b|}|S_b| \tag{18}$$

$$\overrightarrow{u_b} = \frac{\overrightarrow{u_*}}{\kappa}\ln\left(1 + \frac{\Delta z_b}{2z_0}\right) \tag{19}$$

$$u_* = \frac{\sqrt{g}}{C}\bar{u} \tag{20}$$

$S_{b,x/y}$ *Bed load transport in x/y-direction [kg/(ms)]*

$u_{b,x/y}$ *x- and y-components of velocity in bottom layer [m/s]*

u_* *Effective bed shear velocity [m/s]*

$\bar{u}$ *Depth-averaged velocity [m/s]*

κ *Von Kármán constant describing logarithmic velocity profile of boundary layer [-]*

Δz_b *Distance to grid point closest to bed [m]*

z_0 *Geometric roughness height [m]*

3. Methodology

With the background knowledge from chapter 2 at hand, a methodology can be derived to assess the hydrodynamic and morphological effects of the isle groyne. This chapter highlights the most important steps to be taken which should lead to the answers to the research questions.

As mentioned in chapter 1, a numerical study is performed with the use of Delft3D-FLOW. The description of the methodology can broadly be separated in two steps. The first concerns all activities related to the model set-up within Delft3D-FLOW, including a sensitivity analysis. The second includes all activities related to the analysis and validation of the results obtained from the numerical model.

Set-up of the model

To achieve the appropriate model set-up – presented in chapter 4 – several activities should be undertaken.

1. Schematization of the bathymetry and groynes: The effects of the isle groyne are assessed within a schematized representation of the river Waal. Based on average, representative values of the main channel of the Waal and its groyne fields, a straight river stretch – excluding floodplains – is constructed with the use of ArcGIS. Both the current and isle groyne are incorporated in the three-dimensional raster representation of the Waal. The dimensions of the isle groyne presented in Figure 3 are adjusted as such that the influences of the main characteristics of the isle groyne – the inlet and extended head – can be compared in isolated form to the current groynes in the river Waal.
2. Choice of the appropriate spatial and temporal steps: The flow and sediment transport should be calculated on a sufficiently small grid to model the large horizontal dynamic eddies with the Navier-Stokes equations (see § 2.4.2.1.). Refinement of the grid however leads to a significant increase of computational time. The proper spatial and temporal steps are chosen; refinement is applied whenever computational time and stability criteria allow.
3. Choice of the parameter settings: Flow and sediment transport parameter settings, including the initial and boundary conditions, as well as numerical parameter settings should be configured as such that the simulation best represents the desired conditions. These conditions correspond to the flow and sediment transport characteristics in the Waal during discharge conditions at which the water level (OLR + 1.0 meter) is just below the crest of the current, lowered groynes (i.e. OLR + 1.2 metres, see §2.1.2). This water level was adopted because measurements of Klop (2016) have shown that highest groyne flames occur after periods of relatively low discharges (§ 2.3). Furthermore, water levels below the groyne's crest prevent the possible influence of non-hydrostatic pressure gradients (not incorporated in the Delft3D-FLOW model) which would occur whenever groynes are overtopped.

   Most parameter settings can be adopted from previous research or measurements in the Waal, some require additional analyses:

a. Turbulence prevents the development of a stable equilibrium of the flow pattern. The induced bed shear stresses and consequential total transport might therefore differ every other time-step. The use of a MORFAC might in such cases have undesired side-effects. It may lead to the overestimation of bed level changes due to short, temporal flow patterns and negatively influence the flow and sediment transport in consecutive time-steps. The pattern of erosion and sedimentation is therefore compared using a MORFAC of 1, 10 and 100 to find out whether the MORFAC can be increased.
b. For many of the HLES-parameters, there is a range of plausible values. This bandwidth and resulting uncertainty gives rise to a short sensitivity analysis. For all HLES-parameters, the value of the average horizontal eddy viscosity has been determined within a domain downstream of the head of the current groyne. The results of the sensitivity analysis are used to get an idea of the potential impact of the present bandwidth on the uncertainty in the results.

Results

The results obtained from the numerical calculations in Delft3D-FLOW should be analysed and validated to derive answers to the research questions as presented in Chapter 1. This section is subdivided in a discussion on the methods to analyse (1) the differences in flow and velocity pattern, (2) the differences in turbulent motions, (3) the differences in groyne flames and (4) to validate the results.

1. The pattern of flow acceleration and deceleration is of high importance to the formation of groyne flames. The analysis of the flow and velocity pattern thus mainly focuses on this pattern and the factors influencing these velocity gradients.
   The flow and velocity pattern changes every other time step; dynamic eddies are shed from the groyne tip and interact with the primary eddy (§2.2.2.1.). The primary eddy on its turn influences the velocity in the main flow. The differences in the flow and velocity pattern between both groynes are therefore analysed by comparing (1) the vector representations of the flow field during several time-steps, by comparing (2) the mean and the range of the induced flow velocities and by comparing (3) the boxplots of the standard deviation of the velocities. The flow velocities are measured along two cross-sections (mean) – 21 m and 63 m downstream of the centreline of the groyne – and along a longitudinal profile 21 m away from the toe of the groynes (mean, 10^{th} and 90^{th} percentile). The boxplot presents the minima and maxima, the mean and the first and third quartile of the standard deviations of the velocities measured per time-step along the longitudinal profile 21 m away from the toe of the groynes.
   The comparison of the vector representations of the flow field (1) gives an idea of the strength and occurrence of the factors governing the changes in flow acceleration and deceleration. These factors include the prevention of flow deceleration due to the formation of a primary eddy, dynamic eddies which interact with the primary eddy and flow contraction near the

groyne tip. The comparison of the flow velocities along the longitudinal profile (2) as well as the boxplots (3) give an idea of the flow acceleration and deceleration induced by both types of groynes during the various flow conditions which appear in the dynamic equilibrium. The comparison of the flow velocities (mean) along the two cross-sections (2) gives an idea of the degree to which the flow acceleration near the groyne tip protrudes into the main channel.

2. The turbulence within the mixing zone and the horizontally rotating dynamic eddies play an important role in the formation of groyne flames. Both the strength of the turbulence and the degree to which the turbulence protrudes into the main channel are of importance.

   The turbulence is measured by means of the curl of the vector field of the velocity (the vorticity) in the bottom layer of the flow. As the horizontal motions are most interesting for this research (§2.3.1.), the z-component of the curl – i.e. the rotation on the horizontal plane – is determined following:

$$curl_z = \frac{\partial v}{\partial x} - \frac{\partial u}{\partial y} \tag{21}$$

   $curl_z$ z-component of the curl [s^{-1}]

   To determine differences in the intensity and orientation of the turbulence, the z-component of the curl ($curl_z$) is depicted in two ways. The first compares the magnitude of the $curl_z$ along several cross-sections around both types of groynes. This shows the intensity of the turbulence close to and further downstream of the groynes. The second – to determine the degree of protrusion of the turbulence into the main channel – compares the furthest 'in-channel' locations where the vorticity exceeds certain thresholds.

3. The effect of the groyne types on the groyne flames in the river Waal is evaluated by comparison of the impact of the groyne flames on the navigational quality of the river. This impact can be evaluated with further insight on the magnitude of the sedimentation – both the volume (1) and the height (2) – and the location of the sedimentation (3).

   The sedimentation induced by the isle groyne and current groyne is therefore first analysed by comparison of the maximum (time-averaged) sedimentation along the longitudinal profiles (row of cells) between two adjacent groynes (2). Furthermore, the furthest 'in-channel' location where the time-averaged sedimentation exceeds certain thresholds is compared (3). The effects of both groynes are also evaluated by comparison of the time-averaged sedimentation/erosion along four longitudinal profiles 3, 9, 15 and 21 metres away from the toe of the groynes (1 & 2).

4. The results obtained from the numerical calculations should be validated to interpret them in the broader context of the river Waal. Unfortunately, no measurements are available of the flow or the magnitude of groyne flames around the isle groynes. Also, the schematized representation of the Waal does not precisely meet the set-up of previous laboratory experiments measurements. This means that previous hydrodynamic and morphological measurements around the current groynes do not suffice for quantitative validation of e.g. flow acceleration and turbulence intensity. The validation of the results therefore reduces to the

following three activities. The results of these activities are presented throughout chapter 5 and 6. No specific section or chapter is assigned to the validation:

a. The qualitative comparison of the flow pattern around the current groynes. Comparison involves the analysis of the occurrence of dynamic eddies, the formation of the primary and secondary eddy and the flow contraction around the groyne tip.
b. The quantitative validation of the mean flow velocities within the centre of the main channel. The mean velocities in the centre of the main channel are compared with the mean velocities obtained from a WAQUA-model of the river Waal. WAQUA is the prescribed numerical model in the Netherlands for the evaluation of the impact of measures within the main channel and floodplains of the river Waal. This validation gives an idea of the representativeness of the flow conditions in the schematized river to the actual conditions present in the Waal during similar discharge conditions.
c. The semi-quantitative validation of the magnitude of the scour hole and the groyne flame. It is not possible to quantitatively compare the depth of the scour hole or the height of the groyne flame with field measurements; the constant flow conditions and idealized schematization would induce different quantitative morphological results. Semi-quantitative analysis of, respectively, the maximum depth and maximum height however gives an idea on whether the obtained values approximate the actual morphological features in the river Waal presented in Figure 5 and 6.

4. Model set-up

Chapter 3 presented the activities necessary to develop the applicable model set-up to reproduce the hydrodynamic and morphological features described in Chapter 2. The outcome of these activities – the model set-up – is presented in this chapter. This chapter elaborates on the exact geometric dimensions of the Waal schematization and the groynes (§4.1), will discuss the temporal and spatial steps applied (§4.2) and elaborates further on the physical and numerical parameters related to the transport of water and sediment (§4.3).

4.1. The bathymetries

The bathymetries considered consist of two 'building blocks'. The first building block is the base bathymetry, consisting of the flat, slightly sloping navigational channel and the adjacent groyne fields. The second building block consists of the groynes, which are superimposed on the base bathymetry. These groynes are part of the bathymetry since they can not be represented as hydraulic structures in Delft3D-FLOW, which are usually applied in large(r)-scale numerical calculations of the Waal. Hydraulic structures would not allow for friction along the structure. This would result in the absence of velocity gradients along groynes which are necessary for the induction of turbulence (§2.2.2.). The addition of non-erodible layers at the location of the groynes ensures that the groynes are not eroded over the course of the model run. The thickness of the erodible layer within the direct vicinity of the groyne is – for every cell – computed by subtracting the height of the groyne in case it were fully emerged (no sand) from the base bathymetry.

Idealized river: Base bathymetry

The base bathymetry within the straight idealized river stretch is based upon the typical characteristics of the main channel of the river Waal around Dodewaard as presented in section 2.1 (rkm 898 – 901). Floodplains have been excluded because they increase the computational time and since they lack importance for the purpose of this study. Furthermore, a flat bed – in transverse direction – was used in between two opposing groynes to more clearly visualize the effect of both groynes on the groyne flames. The slight inclination to the sides of the fairway has thus been excluded. At both sides of the main channel, groyne fields emerge.

Table 2: Measured average representative dimensions of the Waal near Dodewaard and used dimensions within the Waal-schematization in Delft3D-FLOW

	Measured	Used
Width in between two opposing groyne heads	220 m	221 m
Height of the bed	0 m +NAP	0 m +NAP
Slope of the bed	10^{-4}	10^{-4} [-]
Distance in between two adjacent groynes	200 m	200 m
Width of a groyne field	60 m	58 m
Length of Waal schematization	-	1602 m

The flat bed results in a rather steep slope at the toe of the groyne fields (1:4) to reproduce the groyne fields and their height to best extent. The length of this slope differs depending on the location within the groyne field. At the upstream end of the groyne field, the steep slope extends to 2.2 meters above the bed whereas the steep slope is only 1 meter high at the downstream end. This creates the pattern of asymmetric, bell-shaped groyne fields. Differing slopes within the groyne field cause both sides of the field to reach the same height as they reach the river's embankments (Figure 19). To overcome possible boundary effects, these embankments were implemented as steep slopes rather than vertical sidewalls

A total of seven groynes is constructed within the 1602 metres long schematization; each groyne is located 200 meters apart and a buffer of approximately 200 metres is maintained at both sides of the schematization. Zhang and Nakagawa (2008) concluded that hydraulic patterns from the 5th groyne onwards show similar effects. The construction of seven groynes should thus be enough to prevent the influence of initialization effects within the model results. To account for the slope in the river bed (10^{-4}) the groynes are designed with slightly different base heights.

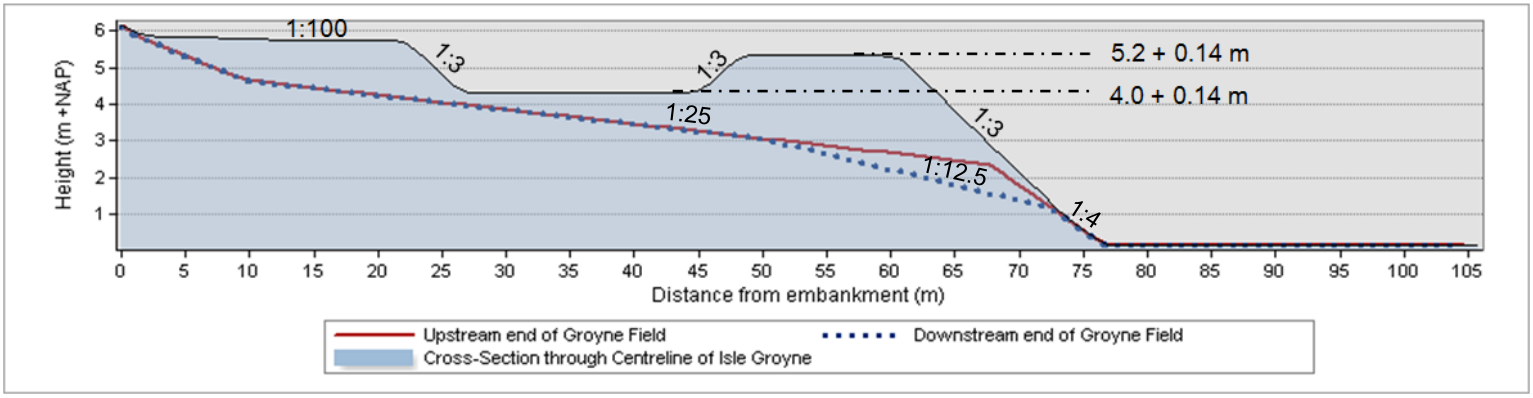

Figure 19: Cross-Sections of the Isle Groyne (adjusted to the crest level of the lowered groynes), of the upstream end of the groyne field (red line) and the downstream end of the groyne field (blue dotted line).

The main dimensions of the schematized Waal representation are presented in Table 2.

The groynes

The design of the current groyne is based on design drawings presented in chapter 2 and is adapted to the design limitations imposed by the river cross-section (width of the groyne fields). The groynes – measuring 60 meters in length – thus have a flat crest with a width of 12.5 meters and slopes with a gradient of 1:3. The crest level of the tip of the groyne is, in agreement with the height of the lowered groynes, 5.2 meters +NAP. In contrast to the groynes in the river Waal, the structures maintain this height along a distance of 6.25 meters towards the river embankment and then increase in height with a slope of 1:100.

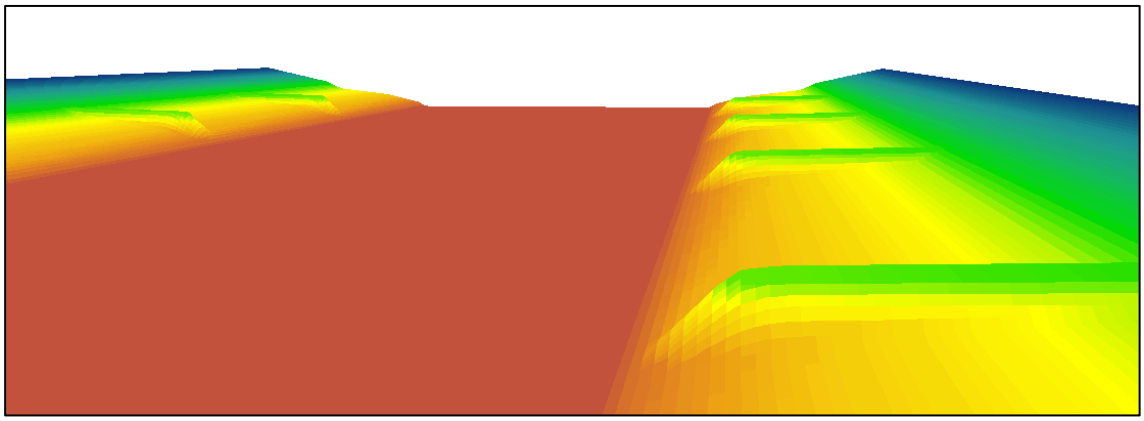

Figure 20: 3D-view of Waal schematization with current groynes. The downstream end of the groyne field shows a more gradual slope.

The isle groyne is constructed based on the design characteristics presented in section 2.1.3. However, as mentioned in the methodology, the design used in this analysis is adjusted to the lowered groyne level to assess the effect of its main characteristics – the elongated groyne head and the inlet – on the hydraulics and the morphology in the Waal in an isolated form.

The modifications made in comparison with the design presented in Figure 3 are visible in the isle groyne's cross-section presented in Figure 19. For further clarification, the changes are shortly enumerated in the list below.

- The crest level of the groyne head is reduced to a height of 5.2 meters + NAP. Similar to the current groyne, a wide crest of 12.5 meters is adopted.
- The slope of the groyne head/isle has, on each side, been changed to a gradient of 1:3.
- The isle groynes have a length of 60 meters from the tip of the isle to the root of the groyne. The part of the groyne which is attached to the river embankment has a transverse slope of 1:100 and – in line with the current lowered groyne – a flat buffer with a width of 6.25 meters has been used at the head of the landside part of the groyne.

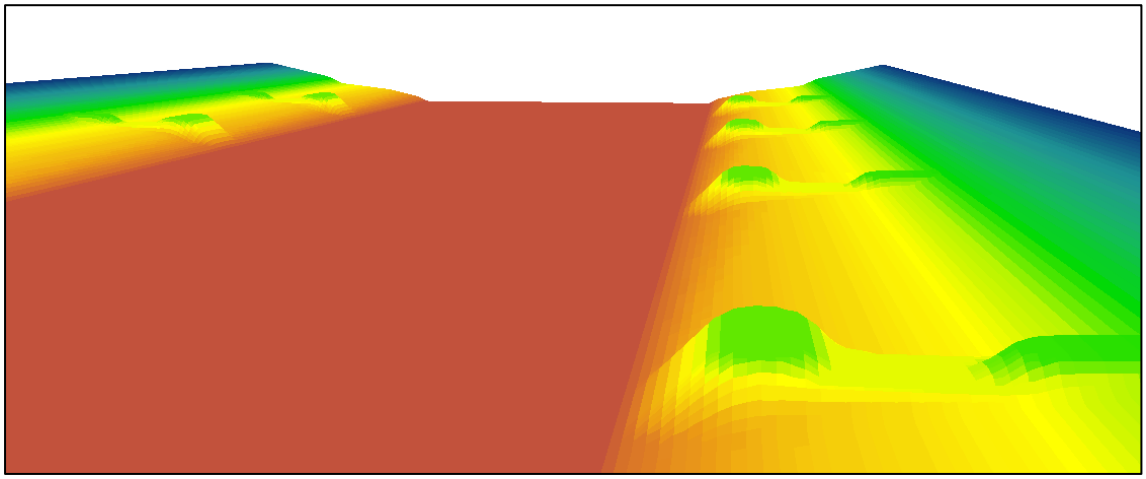

Figure 21: 3D-view of Waal schematization with isle groynes

4.2. The spatial and temporal steps

The hydrodynamics and morphological effects of both groynes are evaluated on a fine grid with corresponding small time-steps. The grids used for the numerical calculations differ based on the purpose of the run. For the simulations used to gain understanding about the turbulent motions around the groynes, domain decomposition has been applied in order to visualise the hydraulic patterns on a small scale (Figure 22). Grids of 9 by 9 metres, 3 by 3 metres and 1 by 1 metres are used, fulfilling the domain decomposition requirements of refining with a factor of (a multiple of) three. Not using domain decomposition and maintaining the smallest grid size of 1 by 1 metres would increase the computational time by, circa, a factor 30.

Domain decomposition poses challenges to the model configuration since, for example, the bed levels should be equal on the boundary of two adjacent domains. Since the small resulting bed level 'step' is amplified by the morphological processes – causing different flow and sediment transport patterns – a single mesh with grid cells of 3 by 3 meters was applied in the runs including sediment transport processes. A run with a single mesh with grid cells of 1 by 1 metres would take months. The larger minimum cell size of 3 by 3 metres had proven to be sufficiently small to model the turbulent patterns around a groyne. Analysis of the results of the hydraulic runs shows that – although the 1 by 1 meter grid cells provide a more precise image of all hydraulic patterns – the 3 by 3 meter grid cells were able to calculate the same major characteristics of the turbulence as the 1 by 1 meter cells. This included the migration of dynamic eddies in the vicinity of groyne heads. The results obtained with this medium-sized grid were also used for the analysis of the flow velocity patterns.

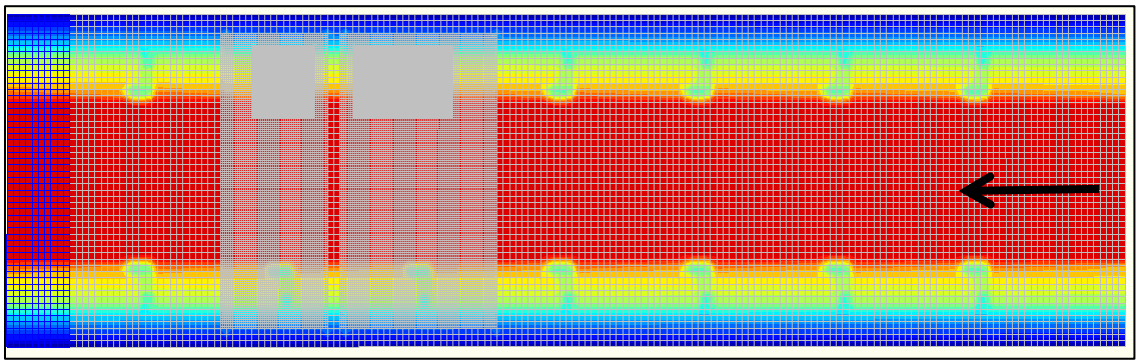

Figure 22: Topview of Waal schematization on the decomposed grid. The colours denote the bathymetry.

To fulfil the stability criteria of the model, temporal steps of 0.003 minutes (0.18 seconds) were used in the decomposed grid. The temporal step for the 3-by-3-meter grid was 0.1 minutes (6 seconds). Since domain decomposition requires the same temporal steps in all domains, the time step of 0.003 minutes has been applied to all domains in the hydraulic runs. The numerical calculations simulate respectively 2 hours (decomposed grid) and 6 days (3-by-3-meter grid).

4.3. Parameter Settings

This sub-chapter addresses the parameters which govern the flow and sediment transport. It subsequently addresses the initial and boundary conditions applied in the model runs, the physical flow parameters, including the turbulence parameters, and lastly the sediment transport parameters.

Initial and boundary conditions

The analysis of the effects of the isle groyne within the idealized Waal geometry focuses on discharge conditions corresponding to a water level just below the crest of the groyne, 5.0 metres +NAP. To reduce errors due to an initially propagating wave which causes momentary overtopping of groynes in case of an initial water level of 5.0 meters, an initial water level of 4.5 meters was applied over the entire domain.

Two open boundaries are defined, one on either side of the domain. At the downstream boundary, the initial water level of 4.5 meters is defined as a boundary condition during the first part of the simulation. After a period of 20 minutes and 24 seconds, the water level linearly increases to an eventual constant water level of 5 meters after 30 minutes. At the upstream boundary, a constant inflow of 1200 m^3/s is defined.

Physical flow parameters

For the Horizontal Large Eddy Simulation, several parameters must be specified. Since the turbulence plays an important role in this research, each of these will briefly be discussed. The results of the sensitivity analysis are presented in appendix V and may give an idea of the potential impact of the present bandwidth of plausible values on the uncertainty in the results.

- Slope in the log-log spectrum (α) = 5/3. As mentioned in section 2.4.2.1., this parameter represents the gradient in the graph of the energy density per wave number of the turbulence within the inertial subrange. Values of 5/3 and 3 are most applicable. In literature, the value of 5/3 is found to be used most often (Berselli, Illiescu, & Layton, 2006) and is most often stated as representative for the slope in the graph. Changing the value to 3 would result in higher values of the horizontal eddy viscosity.
- Dimensional number (n_D) = 2. Indicating the dimensionality of the turbulence, the value 2 is most appropriate for the simulation of the horizontally rotating eddies shedding from the groyne tip. A value of 3 would decrease the horizontal eddy viscosity downstream of the groyne tip.
- Prandtl-Schmidt number (σ_T) = 0.7. The turbulence Prandtl-Schmidt number represents the ratio between the Prandtl number – the ratio between momentum and heat diffusivity – and the Schmidt number – the ratio between the viscous and molecular diffusion rate. It was found that a value of 0.7 is appropriate for free turbulent flows and that the Prandtl-Schmidt number could not exceed a value of 1 (Winterwerp & Kesteren, 2004). Higher values of σ_T give higher values for the horizontal eddy viscosity.

- Spatial low-pass filter (f_{lp}) = 1/3. Higher values would result in lower values for the horizontal eddy viscosity. Lower values would result in significantly higher values of the horizontal eddy viscosity.
- Relaxation time (τ) = 8.658 minutes. The relaxation time is specified at a value twice the temporal scale of the largest horizontal eddies. It is used to make a distinction between the turbulent motions resolved by the Navier-Stokes equations and the motions that are modelled using the HLES SGS-model (Section 2.4.2.1.) (Deltares, 2014). A spectral analysis (Figure 23) of the velocities in u- (longitudinal) and y- (transverse) direction at a couple of locations directly downstream of the groyne head shows that the time scale of the large horizontal eddies is circa 4.33 minutes. In the calculation of the spectral density, only velocity values after the spin-up time (ca. one hour) are used. Since a temporal step of 0.003 seconds was used, a relaxation time of 8.658 minutes is applied. Higher values would lead to higher values of the horizontal eddy viscosity.

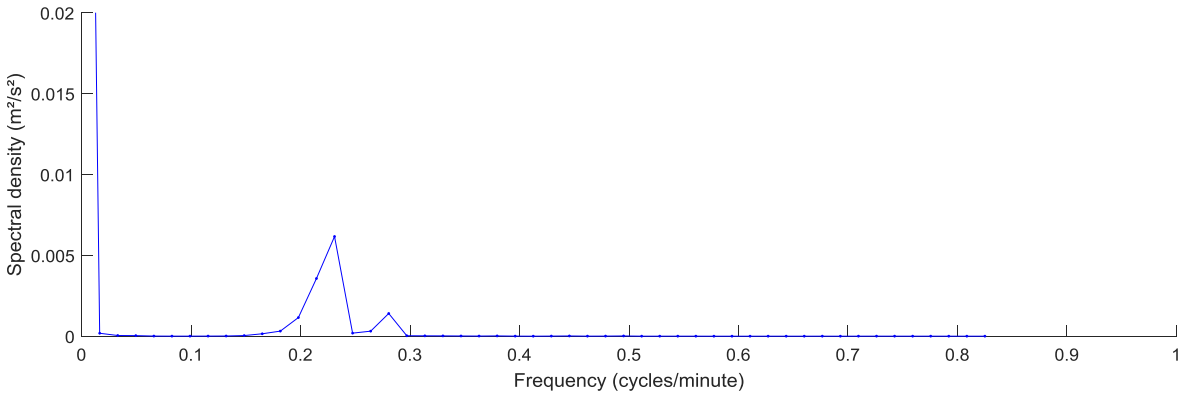

Figure 23: Periodogram of the velocity in transverse flow direction in the shear zone behind the current groyne

The values of the remaining physical flow parameters can be found in Table 3. The impact of changing the Chézy-coefficient on the horizontal eddy viscosity is also addressed in appendix V.

Table 3: Physical parameter values used within Delft3D-FLOW

Density of water	1000 kg/m³	α	5/3
Gravitational acceleration	9.81 m/s²	n_D	2
Chézy	50 $m^{1/2}/s$	σ_T	0.7
Slip condition	No-slip-condition	f_{lp}	1/3
Background horizontal & vertical eddy viscosity and diffusivity	0 m²/s	τ	8.658 minutes

Physical sediment parameters

To correctly model the morphological effects of the isle groyne, sediment values representative for the situation near Dodewaard are used. Several of these are highlighted in the text within this section, the additional parameters are found in Table 4.

Based on the D50-values in the main channel at Dodewaard used within the DVR-studies (Duurzame Vaardiepte Rijntakken) a median sediment diameter of 1450 micrometer is used. Furthermore, a sediment concentration of 0.04 kg/m³ is applied as initial condition everywhere in the domain and as a boundary condition both at the upstream and downstream side of the domain. This meets the average values of 37.7 mg/l (0.0377 kg/m³) – 39.9 mg/l (0.0399 kg/m³) that were measured in between 1980 and 1999 near Lobith (Brinke, Bolwidt, Snippen, & Hal, 2001).

A morphological factor of 100 is used to speed up the morphological processes within the model to account for the different time-scales of the hydrodynamic and morphological changes. Tests with morphological factors of 1 and 10 have shown that a value of 100 is still applicable to model the morphological development as they show qualitatively similar results (Appendix VI).

Table 4: Physical parameter values of sediment transport in Delft3D-FLOW

D50	1450 µm	*Morphological factor*	100
Sediment concentration	0.04 kg/m³	*Spin-up interval before morphological changes*	60 minutes
Specific density	2650 kg/m³	*Reference density for hindered settling*	1600 kg/m³
Dry bed density	1600 kg/m³		

5. Results: Hydrodynamics

The river, including both its bed and flowing water, is one coherent system which – under the assumption of stable boundary conditions – will reach a (dynamic) equilibrium. Morphological changes are governed by changes in the hydrodynamics in the river, and the other way around. To gain insight on the morphological evolution of the river due to the implementation of isle groynes and be able to understand the origin of the morphological changes, understanding the effect of the isle groynes on the hydrodynamics is thus of importance. This chapter highlights the results obtained on the flow and velocity pattern (§5.1) and the turbulence (§5.2) in the vicinity of both types of groynes. It presents the results by means of the methods described in chapter 3. Throughout section 5.1 a qualitative validation of the flow pattern and a quantitative validation of the mean flow velocities within the centre of the main channel are presented.

5.1. Velocity field

The flow field around both types of groynes is in a dynamic equilibrium due to the dynamic nature of the eddies which are shed from the groyne tip. This section first analyses the flow and velocity pattern around the current groyne. Emphasis is laid on the pattern's temporal variability and the influence of dynamic eddies. Secondly, a similar analysis is presented on the flow and velocity pattern around the isle groynes. The section then compares the flow and velocity pattern around the groynes with the use of boxplots and both the mean and range of the flow velocities along a longitudinal profile and two cross-sections around both types of groynes.

5.1.1. Current groynes

The flow pattern around the current groynes shows the characteristic convergence and divergence of the flow at all moments. The flow which penetrates the groyne field is forced to pass the groyne along its head creating a consecutive acceleration and deceleration of the flow in the main channel. The deflection of the flow – both in the direction of the channel's centreline and of the river's embankment – is mostly concentrated along a rather narrow part around the normal line between two adjacent groynes.

The magnitude of the velocity gradients in the main channel however differs every other time-step as the flow pattern within the groyne fields shows highly dynamic, unsteady behaviour. The main contributors to the temporal change of the flow pattern's planview are the dynamic eddies and the primary eddy. The primary eddy, rotating in clockwise direction on the right-hand side of the river, is omnipresent in the results of the Delft3D-FLOW model. The interference with the dynamic eddies however results in the primary eddy to take different forms and locations every other time-step; the 'breathing' of the primary gyre (section 2.2.2.1.). In the model results, these dynamic eddies are – as found in previous research – regularly shed from the groyne tip. They migrate in downstream direction along the mixing zone and eventually merge with the primary eddy.

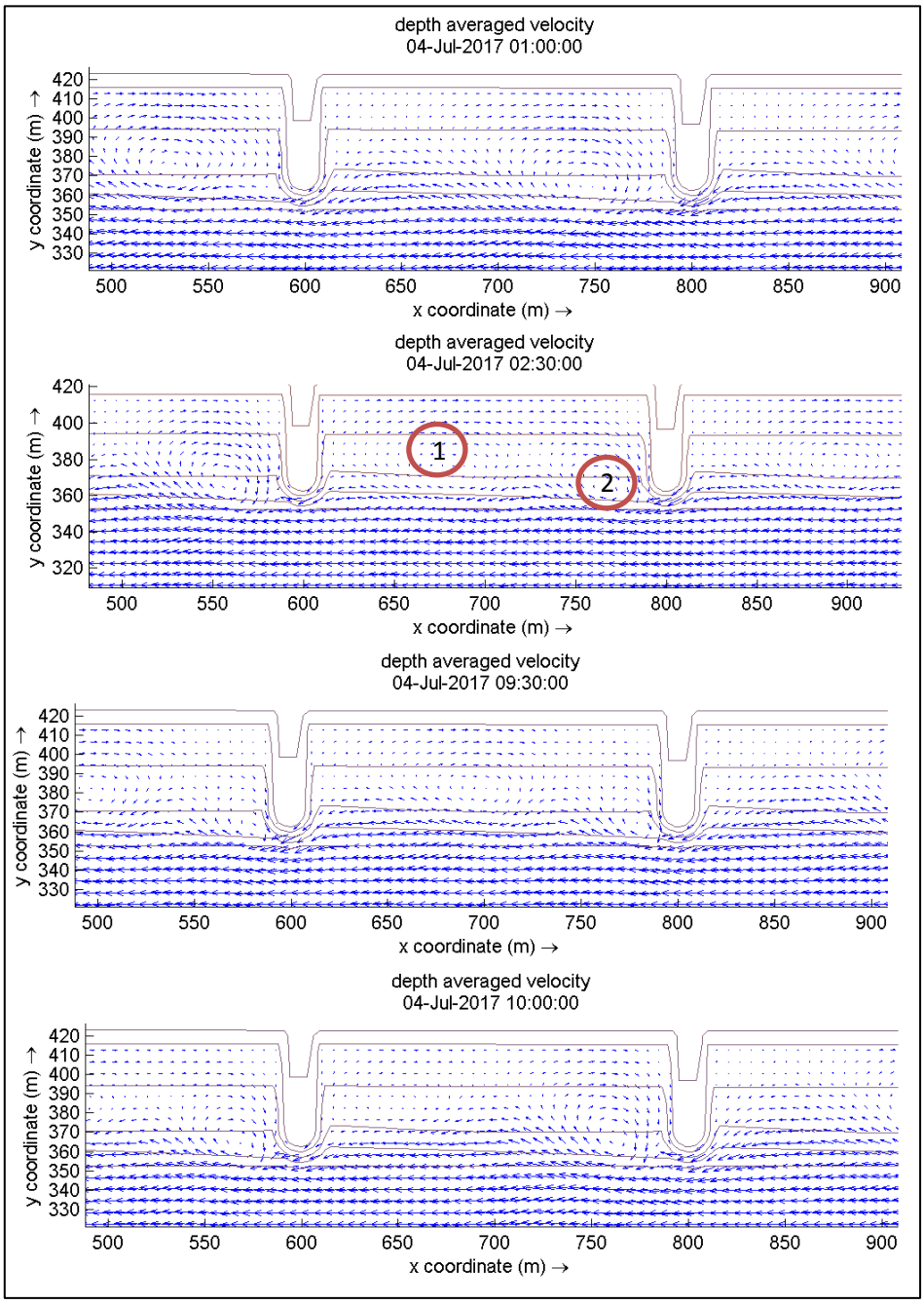

Figure 24: Instantaneous flow pattern at different moments in time. The flow pattern in the groyne field shows temporally varying behaviour. Point 1 represents the primary eddy which is formed in the downstream half of the groyne field after 2.5 hours. Point 2 indicates the presence of a dynamic eddy

The 'breathing' of the large primary eddy, partially preventing the divergence of the flow in the river Waal, causes the eddy to be alternately located in the upstream and downstream two-thirds of the groyne field. This consequentially results in a varying magnitude and location of the flow acceleration and deceleration. For example, after one hour, the primary eddy is located in the upstream two-thirds of the groyne field. The eddy has likely just merged with the dynamic eddy which is shed from the groyne tip. The location of the primary eddy induces additional flow contraction near the tip of the groyne as the return flow from the large stable eddy is 'launched' into the main channel. On the other hand, after two-and-a-half hours, the large primary eddy is located in the downstream two-thirds of the

groyne field (Point 1 in Figure 24). A dynamic eddy has just formed near the groyne tip (Point 2 in Figure 24). No additional convergence is induced near the groyne tip by the presence of the primary eddy and the divergence of the flow is prevented by the presence of the primary gyre in the downstream two-thirds.

The model results clearly show the presence of the primary eddy and the dynamic eddy. A second stable eddy, rotating in anti-clockwise direction at the upstream root of the groyne is only occasionally present in the results of the Delft3D-FLOW model with a 3-by-3-meter grid. During some moments in time this eddy emerges in the upstream corner of the groyne field. It should be mentioned that this eddy is more often present in results of the decomposed 1-by-1 meter grid (Point 1 in Figure 25).

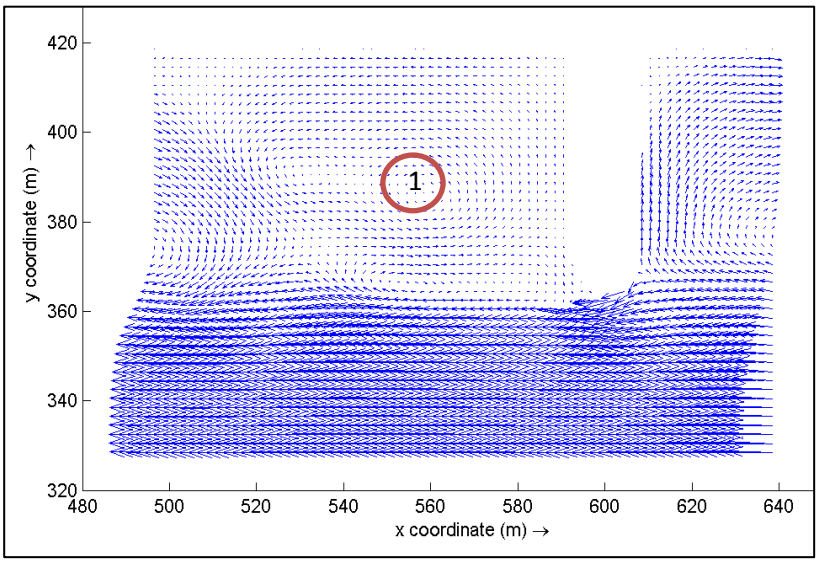

Figure 25: Instantaneous flow pattern (1-by-1 meter grid). The presence of the secondary eddy is denoted with point '1'

Despite the temporal variability in the magnitude of the velocity gradients, the divergence and convergence of the flow around groynes in general create slight acceleration in the vicinity of a groyne and deceleration further downstream (Figure 26). As the deflection of the flow is mainly concentrated at the sides of the fairway, acceleration is highest closer to the tip of the groyne and decreases as one moves in a direction normal to the main flow, away from the river's embankments. The average velocity along the centreline of the main channel is circa 1.05 m/s (Figure 26 and Figure 28). This shows good comparison with mean velocities obtained from a WAQUA-model, the prescribed numerical model in the Netherlands for evaluation of the impact of measures within the main channel and floodplains of the river Waal (appendix VII) (Kroekenstoel, 2017).

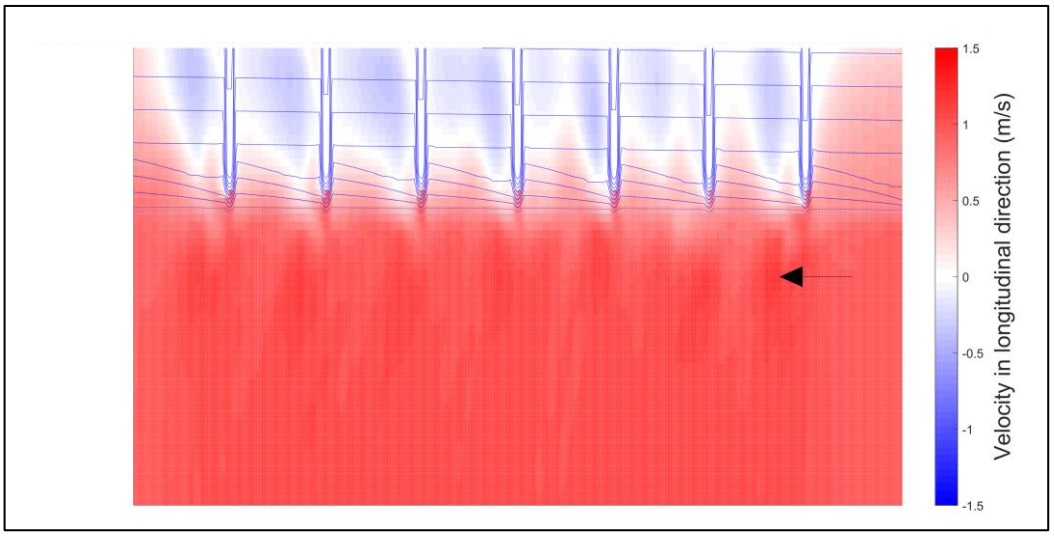

Figure 26: Flow velocity in the Waal representation after one hour. The flow accelerates around the groyne tips and decelerates adjacent to the groyne fields

The primary eddy induces average flow velocities of up to (-) 0.3 m/s in the groyne fields (Figure 30, cross-sections 63 m downstream of the groyne). This shows good comparison with literature. Yossef and Klaassen (2002) stated that the velocity within groyne fields reached around 30-40% of the velocity in the mean flow. The small difference could be the result of the temporal variability of the primary eddy; highest flow velocities are alternately present at different locations in the groyne field.

5.1.2. Isle Groyne

In contrast to the situation with the normal groyne, the isle groyne allows for the passage of flow through the isle groyne's inlet. In general, this is expected to reduce the average flow velocity in between two opposing groynes as the discharge through this narrow cross-section is reduced. Similar to the situation with the current groyne however, the flow pattern around the isle groyne shows some temporal variability, meaning that the situation does not allow for straightforward analysis of the acceleration around the groyne head and deceleration adjacent to the groyne fields. Depending on the

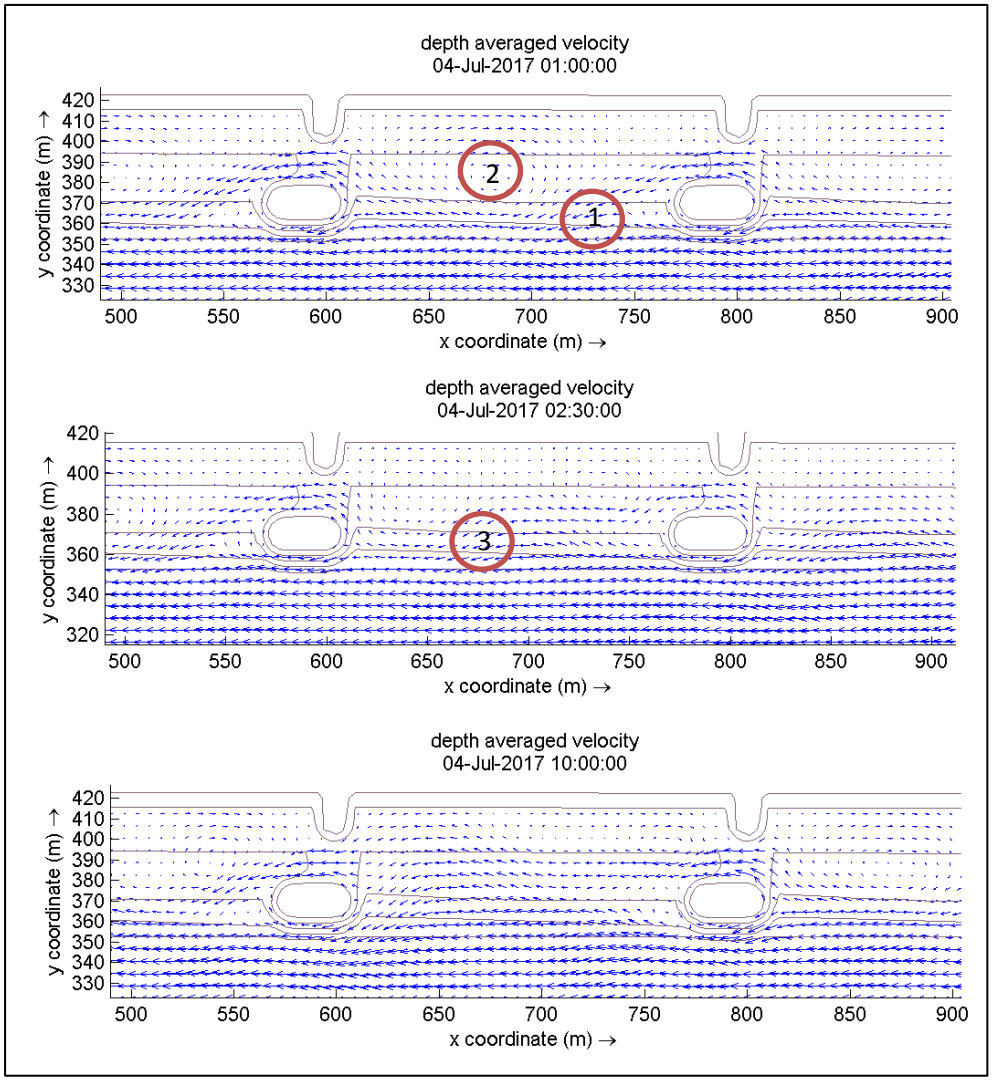

Figure 27: Instantaneous flow pattern at different moments in time. The flow pattern in the groyne field shows temporally varying behaviour. A parallel flow is formed during some moments in time (bottom figure). Point 1 and 3 denote the location where the bypassed flow is reattached tot he main flow. Point 2 indicates the presence of the primary eddy.

moment in time, the primary eddy may either be absent and disturbed by the discharge originating from the isle groyne's inlet or be present and dominating the flow pattern in the groyne field (Figure 27). In the latter case, the flow through the inlet does not penetrate into the primary eddy and is deflected in the direction of the main channel in the upstream half of the groyne field. This location, at which the inlet's discharge reattaches to the main flow, fluctuates over time due to the formation and migration of the dynamic eddy which is shed from the isle groyne's elongated head. Whenever this reattachment point is located relatively far downstream, a secondary eddy might be formed in the wake zone just downstream of the root of the isle groyne.

The temporal variability of the existence, location and magnitude of the primary eddy, causes the pattern of flow acceleration and deceleration to change over time as well. A closer look at the flow patterns at three time-steps indicates this variability (Figure 27).

- After one hour, the flow around the isle groyne forms a pattern of relatively strong convergence and divergence. The bypassed flow reattaches to the main flow in the upstream half of the groyne field (Point 1 in Figure 27). Downstream of this flow, a primary eddy (Point 2 in Figure 27) is present which prevents divergence in the middle of the groyne field. Close to the downstream end of the groyne field, the flow diverges along its course to the inlet. This pattern causes flow acceleration at the tip of the groyne and just downstream of the groyne. It causes flow deceleration along the groyne fields.
- After 2.5 hours, the amplitude of the velocity fluctuations has decreased. The reattachment point of the bypassed stream, being located further away from the upstream groyne (Point 3 in Figure 27), may contribute to this effect; it prevents the divergence of the flow along most of the groyne field.
- After 10 hours, the primary eddy has completely disappeared. This results in a relatively stable stream pattern in which the main flow and the bypassed flow propagate parallel to one another and little exchange of flow is present.

5.1.3. Comparison of the flow and velocity pattern around both groynes

Both the isle groyne and the current groyne create a temporally varying flow pattern, each resulting in a different succession of flow acceleration and deceleration. At each time-step, the comparison between the current groyne and the isle groyne would yield different results on the effects of the isle groyne on the flow acceleration and deceleration around groynes. Since it is not possible to evaluate all moments in time, the patterns are – as presented in the methodology – evaluated based on the mean and the range of the velocities.

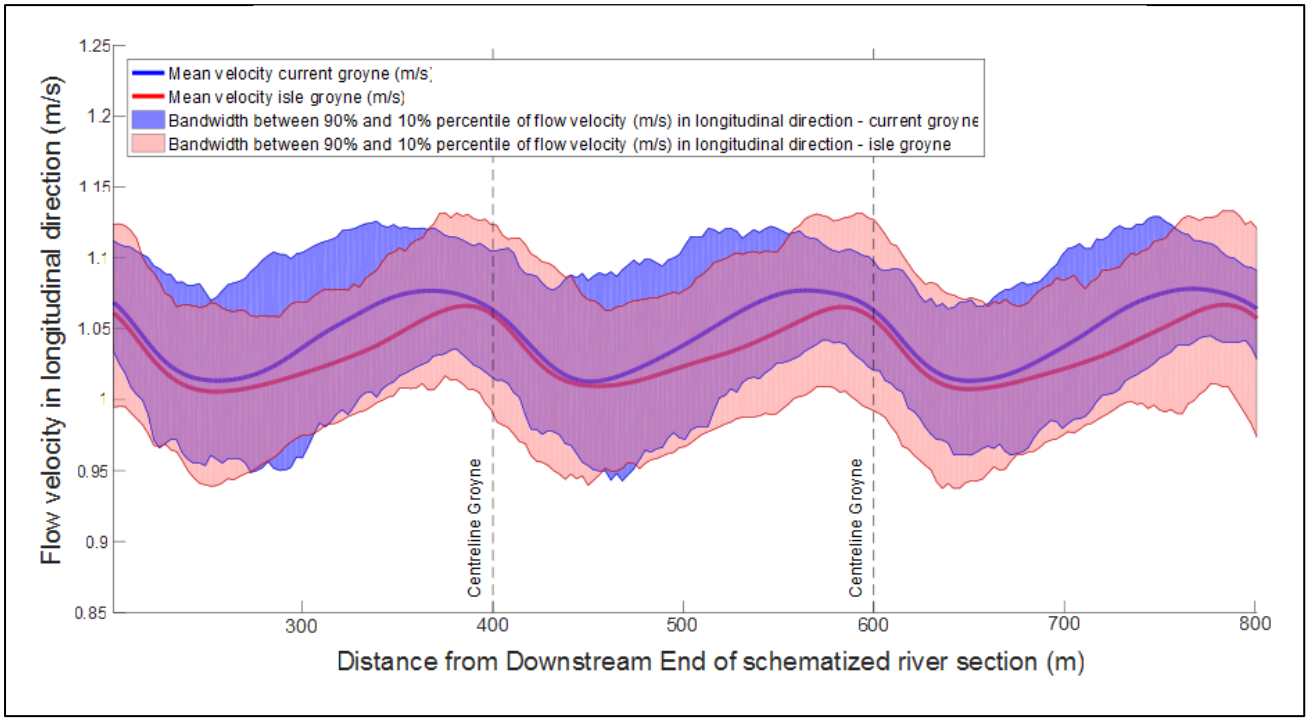

Figure 28: Mean, 10th percentile and 90th percentile of the flow velocity in longitudinal direction (m/s) around the current groyne and the isle groyne at a distance of 21 m away from the toe of the groynes

Comparison of the mean flow velocities and the 10th and 90th percentile of the flow velocities presented in Figure 28 gives some differences between both groyne types. On average, flow velocities are slightly lower in the schematized Waal with the implementation of isle groynes. The inlet increases the flow conveyance capacity of the river and decreases average velocities. The differences in mean flow velocities are highest along the upper half of the groyne field. This might result from the location where the bypassed flow reattaches to the main flow. The bypassed flow – reducing flow velocities in the main channel – is present in the upstream half of the groyne field during most time instances. It only proceeds into the downstream half whenever a continuous parallel flow is maintained (Figure 27). This occurs only occasionally. In the meantime, the main flow near the upstream region of the groyne field behind current groynes is characterized by additional flow contraction due to the primary eddy. The elongated groyne head and bypassed flow prevent the primary eddy to be formed in this upstream region behind isle groynes. Flow velocities thus decrease directly downstream of the isle groyne as a result of the bypassed flow and increase downstream of the current groyne because of the additional flow contraction, causing the relatively big velocity difference in this region.

Comparison of the 10th and 90th percentiles of the flow velocity shows a wider range of flow velocities in the direct vicinity of the isle groyne. This could result from the stronger temporal variability of the magnitude of the flow convergence around the isle groyne; little flow contraction occurs whenever a parallel flow is formed in the groyne field whereas the flow contraction is strong in other cases. The 90th percentile of the flow velocities even indicates stronger maximum flow acceleration around the isle groyne than around the current groyne. It is unknown what might cause this slightly higher peak. It

might be explained by the directions of the flow upstream of the groynes. Whereas the flow around normal groynes follows the expected wavy pattern of rather smooth but relatively strong convergence and divergence, the flow direction in the vicinity of the isle groyne is changed more abruptly. The flow which intrudes the groyne field follows a course in the direction of the isle groyne's inlet until the far downstream end of the groyne field (Figure 27). There, a part of the flow is deflected towards the main channel and another portion of the stream flows through the open notch. The more abrupt change of flow direction could cause stronger velocity gradients and a more in-channel location of the velocity peak near the groyne. This peak extends over a couple of tens of metres downstream because of the length of the head of the isle groyne.

Despite the above mentioned differences in mean and extreme flow velocities, the flow patterns around both types of groynes yield similar velocity gradients between the magnitude of the accelerated and decelerated flow. The boxplots in Figure 29 endorse this statement. These boxplots show – as presented in the methodology – the minima and maxima as well as the first, second and third quartile of the standard deviation of the flow velocity along the longitudinal profile 21 metres away from the toe of the groynes. The median standard deviations differ only 0.001 m/s and the minimum and maximum of the standard deviation also show close comparison to one another. The first quartile of the standard deviation shows the largest differences; the isle groyne's low values might be the result of the occasional occurrence of a parallel flow.

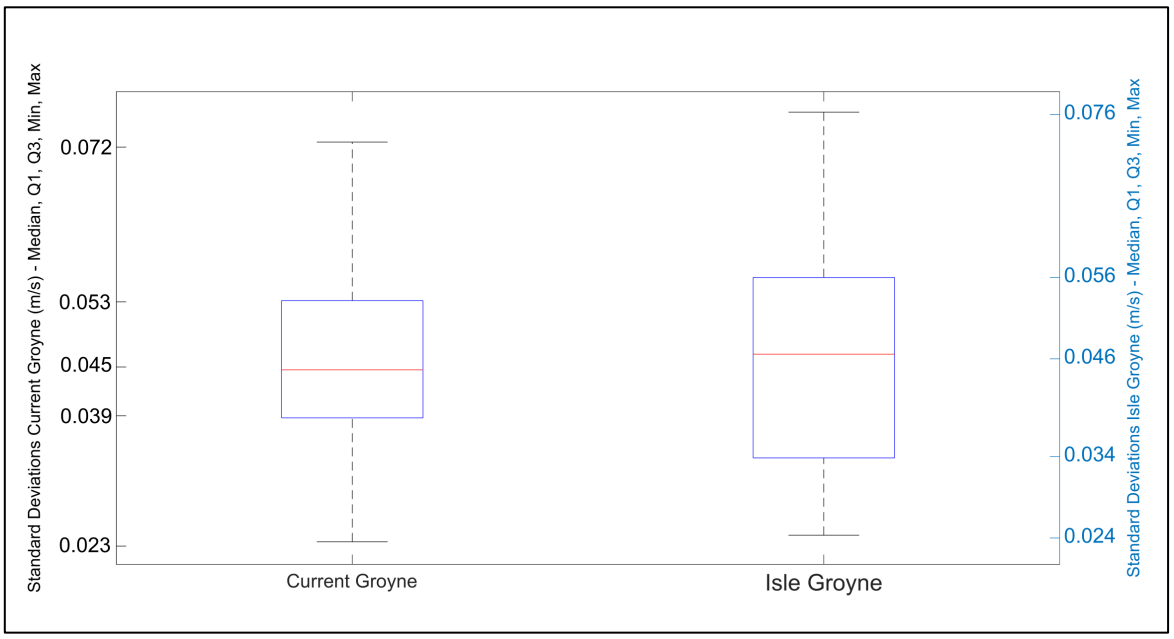

Figure 29: Boxplot of the standard deviations of the flow velocities per time-step. Used flow velocities: in longitudinal direction along a longitudinal profile 21 metres away from the toe of the groynes between the 4th and 7th groyne in downstream direction

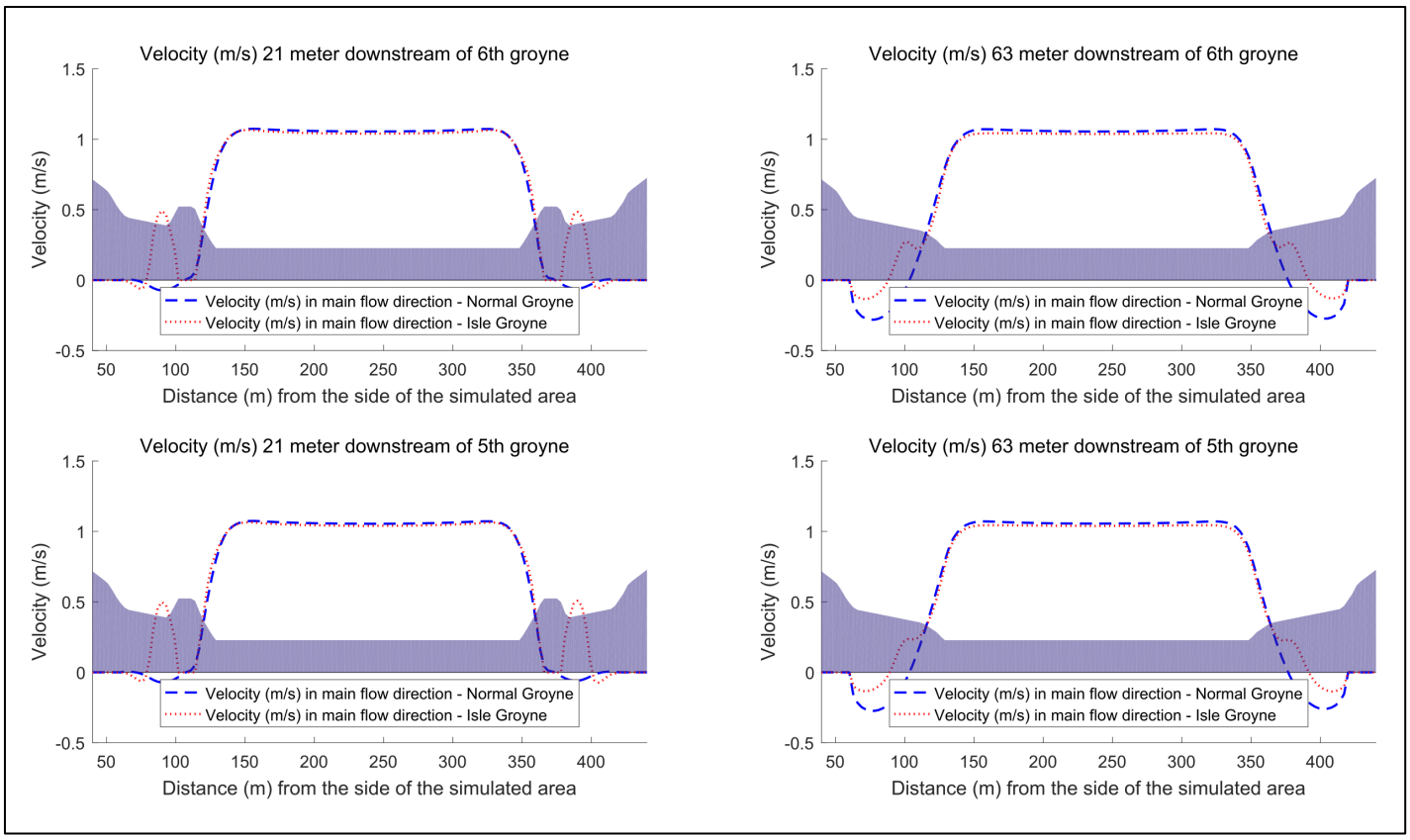

Figure 30: Average flow velocities along cross-sections 21 m and 63 m downstream of the 5th and 6th groyne (in downstream direction)

Comparison of the mean flow velocities along cross-sections 21 and 63 metres downstream of the groynes show only very small, insignificant differences for the flow velocities in the main channel. Flow velocities in the main channel are slightly lower around the isle groyne. Also, the flow acceleration shows a minor decrease around the isle groyne, especially further downstream (i.e. 63 metres downstream). The velocities within the groyne field show significantly different values. The bypassed flow and accompanying positive flow velocities compensate and replace the negative flow velocities from the primary eddy.

Summary of the observed effects of the isle groyne on the flow and velocity pattern: The isle groyne induces a different flow pattern in the groyne fields compared to the current groynes. The bypassed flow penetrates and disturbs the primary eddy in the groyne field during several moments in time. The flow field is however variable in time and periods with persistent flow parallel to the main channel change on regular basis with the appearance of primary eddies within the groyne field. This alternating flow pattern creates similar temporal variability in the observed acceleration and deceleration in the main channel.

On average, flow velocities are slightly lower around the isle groyne than around the current groyne. This is particularly the case in the part of the main channel next to the upstream half of the groyne fields. The isle groyne further shows large(r) temporal variability of the flow acceleration around the groyne head. These changes do however not result in significant alterations to the velocity difference between the accelerated and decelerated flow; standard deviations of the flow velocity along a

longitudinal profile close to the groynes per time-step show similar results for the isle and current groyne.

5.2. Turbulent motions

As presented in section 2.2.2, turbulence plays an important role in the formation of groyne flames. This section elaborates on the differences between the turbulence induced by the current groyne and the isle groyne by presenting the vorticity near the groynes. Using the z-component of the curl of the velocity field – further explanation is given in Chapter 3 - allows for analysis of the horizontal turbulent motions around groynes. The analysis thus focuses on the vorticity in the horizontal plane. In this way, the vorticity originating from the quasi-2D dynamic eddies and the turbulence in the mixing zone are analysed.

Horizontally rotating turbulent structures, including the horseshoe vortex, are not simulated correctly in Delft3D-FLOW due to the use of Horizontal Large Eddy Simulation rather than 3D-Large Eddy Simulation. The latter is not available within Delft3D-FLOW. It is thus of nu use to simulate the vorticity along the horizontal axis.

This section first elaborates on the occurrence of dynamic eddies in the model results and then continues with a comparison of the turbulence around the isle groyne and current groyne.

The velocities (in each of the three directions) from the 1-by-1-meter grids are used.

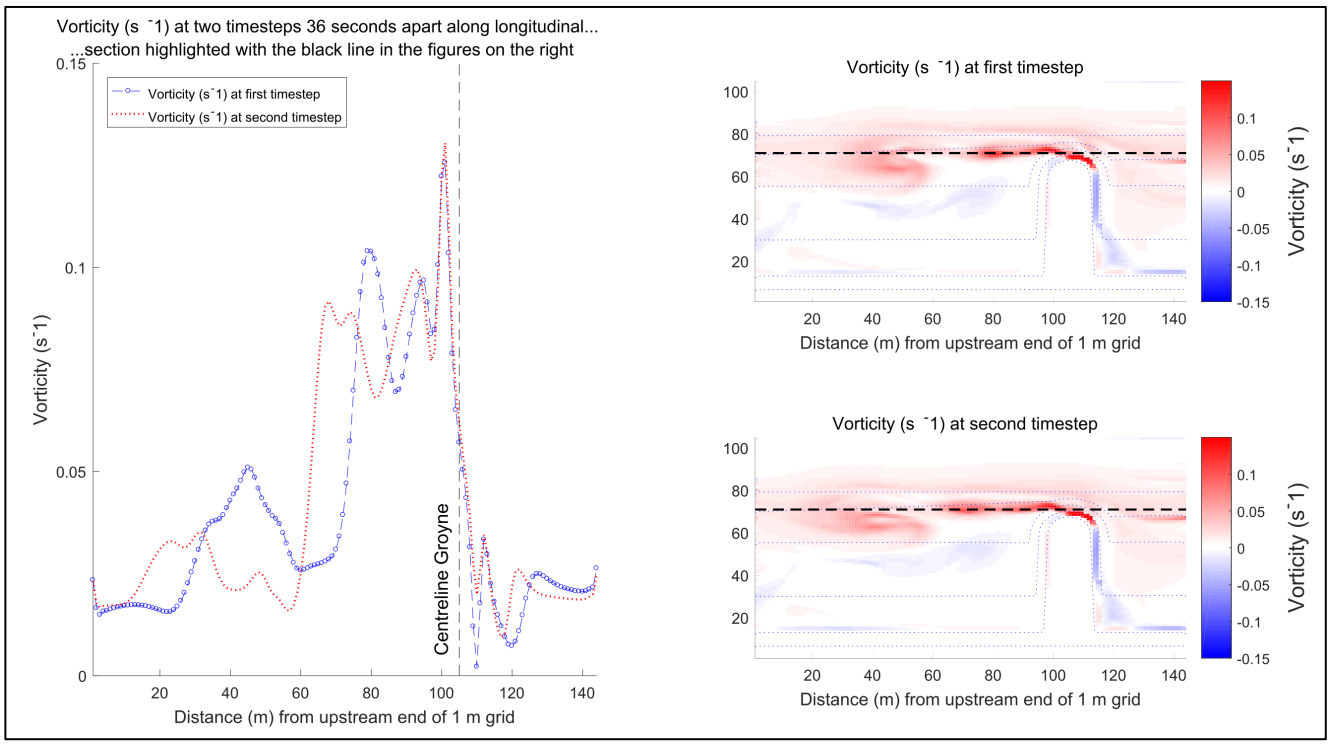

Figure 31: The migration of the dynamic eddies. The eddies which are shed from the tip of the current groyne move in downstream direction, causing a downstream shift of the patches of high vorticity (s^{-1}) on the horizontal plane (in the bottom layer) at two consecutive time-steps.

5.2.1. Dynamic eddies in detached shear layer

The flow around groynes is characterized by dynamic eddies which are shed from the tip of the groyne and migrate downstream (§2.2.2.1.). The model results confirms the formation of these eddies and their downstream migration. A street of high vorticity is formed from the tip of the groyne onwards (Figure 31), likely induced by flow separation around the tip of the groyne and intense mixing in the shear zone downstream of the head of the groyne. At both of these locations, high velocity gradients are present. Within this street of high vorticity, regularly shed dynamic eddies are migrated in downstream direction. Analysis of the calculated vorticity shows that Delft3D-FLOW is also able to reproduce the temporal behaviour of these dynamic eddies (Figure 31). As time proceeds, eddies, formed near the tip of the groyne, are migrated in downstream direction; the peak of the vorticity is moved to the left (Figure 31). After a certain distance, the eddy loses its coherence and strength and the vorticity decreases.

5.2.2. Comparison between the isle groyne and current groyne

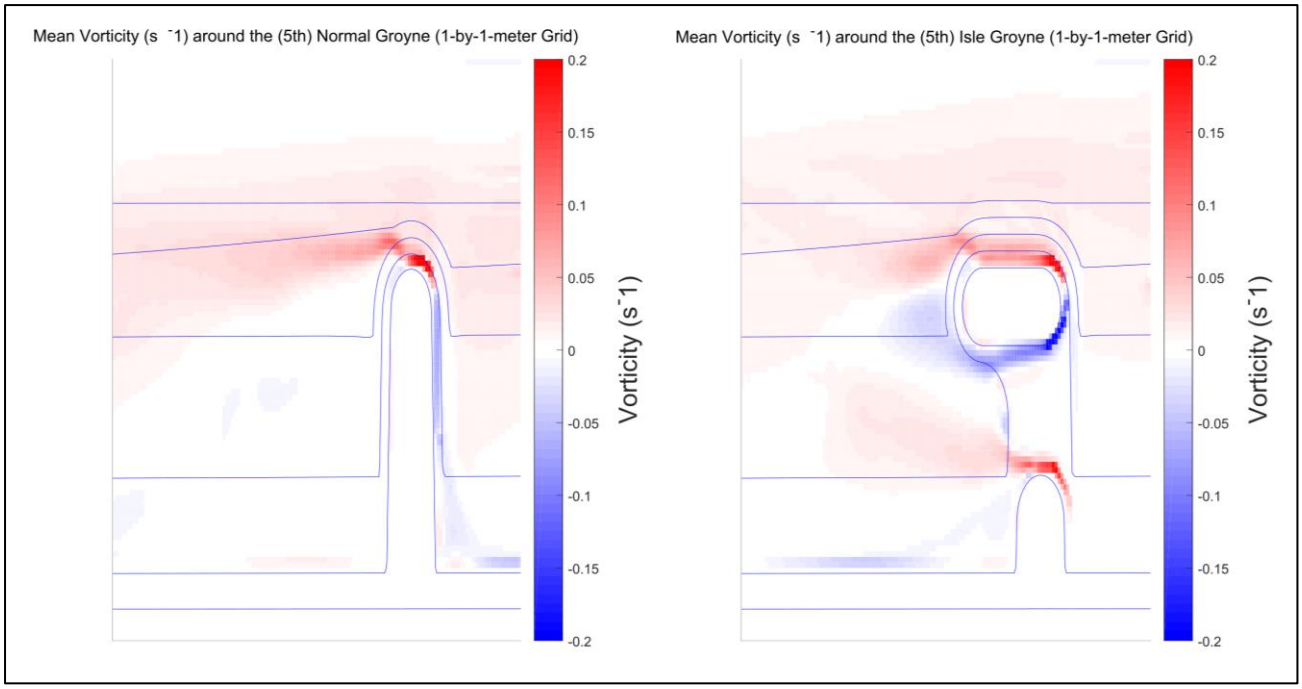

Figure 32: The average vorticity (s^{-1}) - rotation in the horizontal plane (bottom layer of the flow) - around the isle groyne (right) and the current groyne (left)

The altered design of the isle groyne is expected to change the turbulence characteristics and the contribution of the eddies within the detached shear layer to the magnitude and orientation of groyne flames. To get a proper insight in this contribution, both the intensity of the turbulence and the furthest in-channel location are of importance. Results on these are given in the upcoming paragraphs. For further analysis of the turbulence in the vicinity of both types of groynes, the vorticity is averaged over time over a period of one hour after the flow has reached its dynamic equilibrium; the temporally varying dynamic eddies can not be compared adequately using instantaneous flow and velocity patterns.

Two main qualitative differences are present between the vorticity near the isle groyne and the vorticity near the current groyne. The first being the turbulence induced at both sides of the isle groyne's inlet and the accompanying shear zones downstream. This turbulence is the result of high velocity gradients present between the fluid which is transferred through the inlet and the rather stationary flow near the downstream root of the isle groyne on the one side and the wake of the head of the isle groyne on the other side. The induced turbulence near the embankment's side of the inlet is of significantly smaller magnitude than the turbulence at the channel-side of the inlet (higher absolute values); the depth of the approaching flow is bigger as a result of the sloping groyne field, likely resulting in this higher value of the vorticity. The second qualitative difference is the enlarged patch of turbulence along the groyne head as a result of the elongated area of high velocity gradients between the main flow and the stationary flow along the groyne head (Figure 32).

Although additional areas with high values for the two-dimensional turbulence are formed within the groyne field, changes which could favour the reduction of the height of the groyne flames occur in the main channel. A significant reduction of the turbulence is present alongside the elongated groyne head of the isle groyne (Point 1 and 2 in Figure 33). Several factors could be the driver of this effect, including the reduction of the strength of the vortices due to friction with the elongated groyne head and lower velocity gradients due to decreased flow velocities in the main channel.

Further downstream, the vorticity induced by the isle groyne shows higher values (Point 3 in Figure 33). This could however simply be the result of the downstream shift of the wake zone behind a groyne's head due to the elongated form of the isle. The wake zone behind a groyne gives rise to high velocity gradients and consequential stronger turbulence.

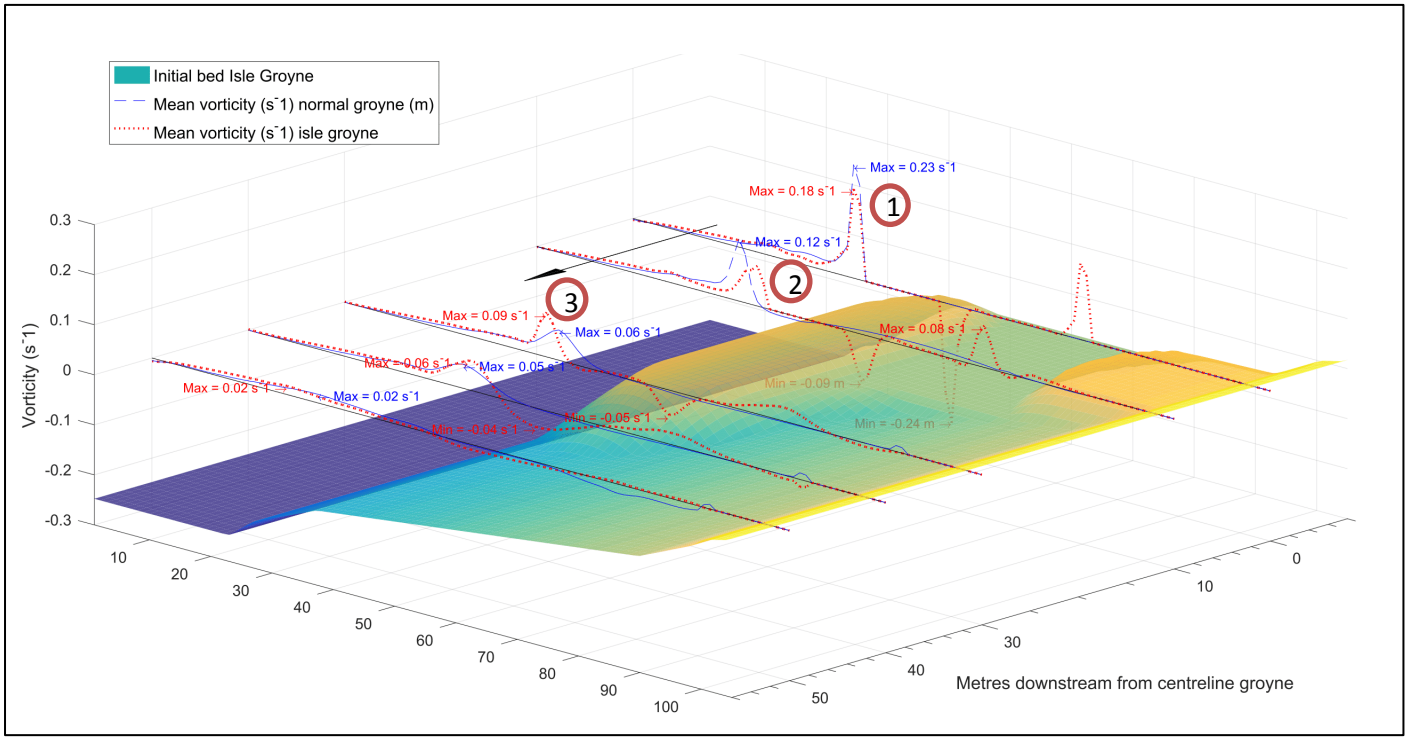

Figure 33: Average vorticity (s^{-1}) ($curl_z$) in the bottom layer of the flow around the current groyne and isle groyne along several cross-sections. The isle groyne induces a reduction of the vorticity alongside the isle groyne's head (point 1 and 2). Vorticity is increased at point 3.

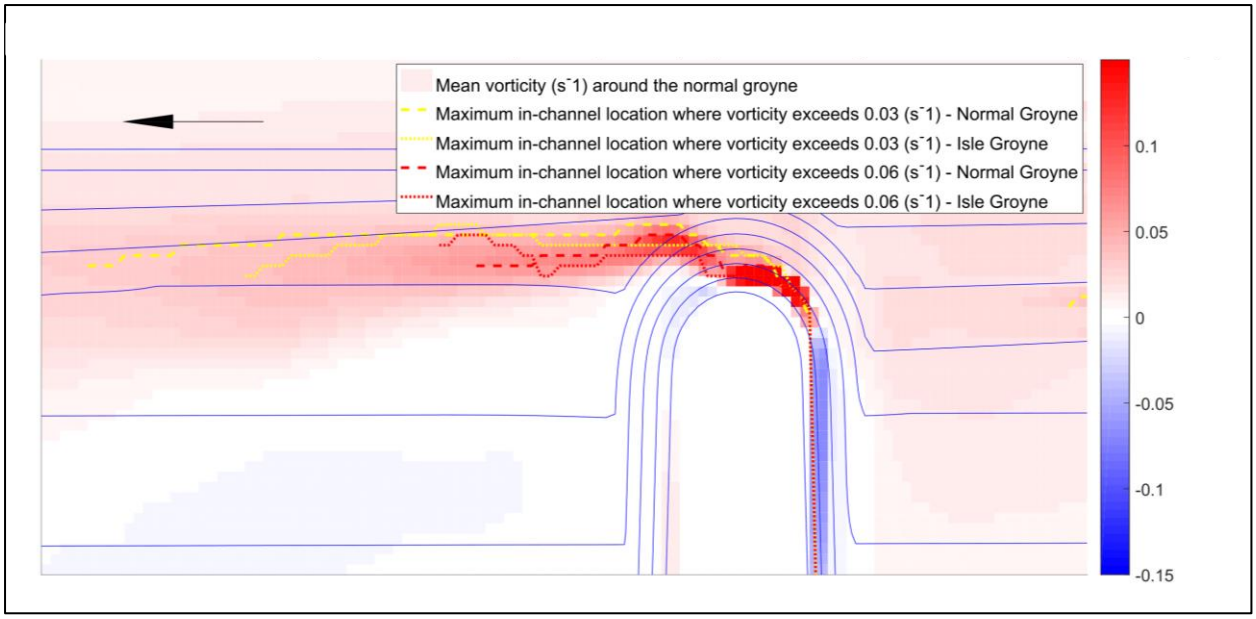

Figure 34: Furthest "in-channel" location where the average vorticity (s^{-1}) exceeds either 0.06 s^{-1} or 0.03 s^{-1} for the isle groyne and the current groyne (5th groyne). The presented vorticity (in the bottom layer of the flow) is the z-component of the vorticity

This effect of increased turbulence downstream of the isle groyne is not visible over the entire domain downstream of the groyne. Analysis of the spots located furthest into the navigational channel and increasing a threshold of low (0.03 s^{-1}) and medium (0.06 s^{-1}) vorticity shows that the (weak) turbulence in the wake of the current groynes expands further downstream than the turbulence around the isle groyne (Figure 34). It is furthermore shown that the turbulence induced by the current groynes intrudes slightly further into the main channel alongside the isle groyne's head (Figure 34). The peak of vorticity is at this location (point 2 in Figure 33) also located closer to the groyne. The exception is – in accordance with the results on the magnitude of the mean vorticity – the location at the far downstream end of the isle where isle-groyne-induced turbulence is deflected further away from the groyne field.

Summary of the observed effects of the isle groyne on the vorticity: The isle groyne induces increased turbulence within the groyne field as a result of the velocity gradients between the flow which is transported through the inlet on the one hand and the adjacent groyne slopes and zones of stationary flow on the other hand. The strong vorticity alongside the upstream part of the groyne head is significantly decreased. Contrarily, the turbulence increases in the vicinity of the downstream end of the isle. The rather weak turbulence far downstream of the groyne head is further reduced in comparison to the situation with the current groynes. This last change is however relatively small. The vorticity is in general also located closer to the groyne field. This difference, albeit small, could favour the navigational quality of the Waal. At one location, near the downstream end of the isle groyne's head, the turbulence is located further into the main channel.

6. Results: Morphology

The altered hydrodynamics cause – in accordance with the morphological loop presented in Figure 18 – bed level changes. The differences in flow patterns and turbulence between both groyne types, presented in section 2.2., induce a different sedimentation and erosion pattern. This section focuses on the differences in magnitude of the groyne flame and its orientation towards the main channel. However, first the general (temporal) development of the bed is discussed to obtain a first insight in the morphodynamics caused by the flow obstructive nature of the groynes and on whether the (dynamic) equilibrium has been reached within the modelled time domain.

6.1. General (temporal) development of the bed

Over the course of the 600 simulated days (six days times a MorFac of 100), the bed changes significantly. General degradation of the bed causes the decrease of bed levels – on average – over the entire domain. Groyne fields are eroded in a way which further amplifies the asymmetric plan view of the groyne fields; the main channel is wider at the downstream end of the groyne field. Furthermore, as time proceeds, a pattern of dunes with amplitudes of circa 0.5 – 1 meters is formed which propagate within a dynamic equilibrium through the system (Figure 35). The model not only requires a temporal spin-up, but also a spatial spin-up of circa three groyne fields to generate these characteristic bars.

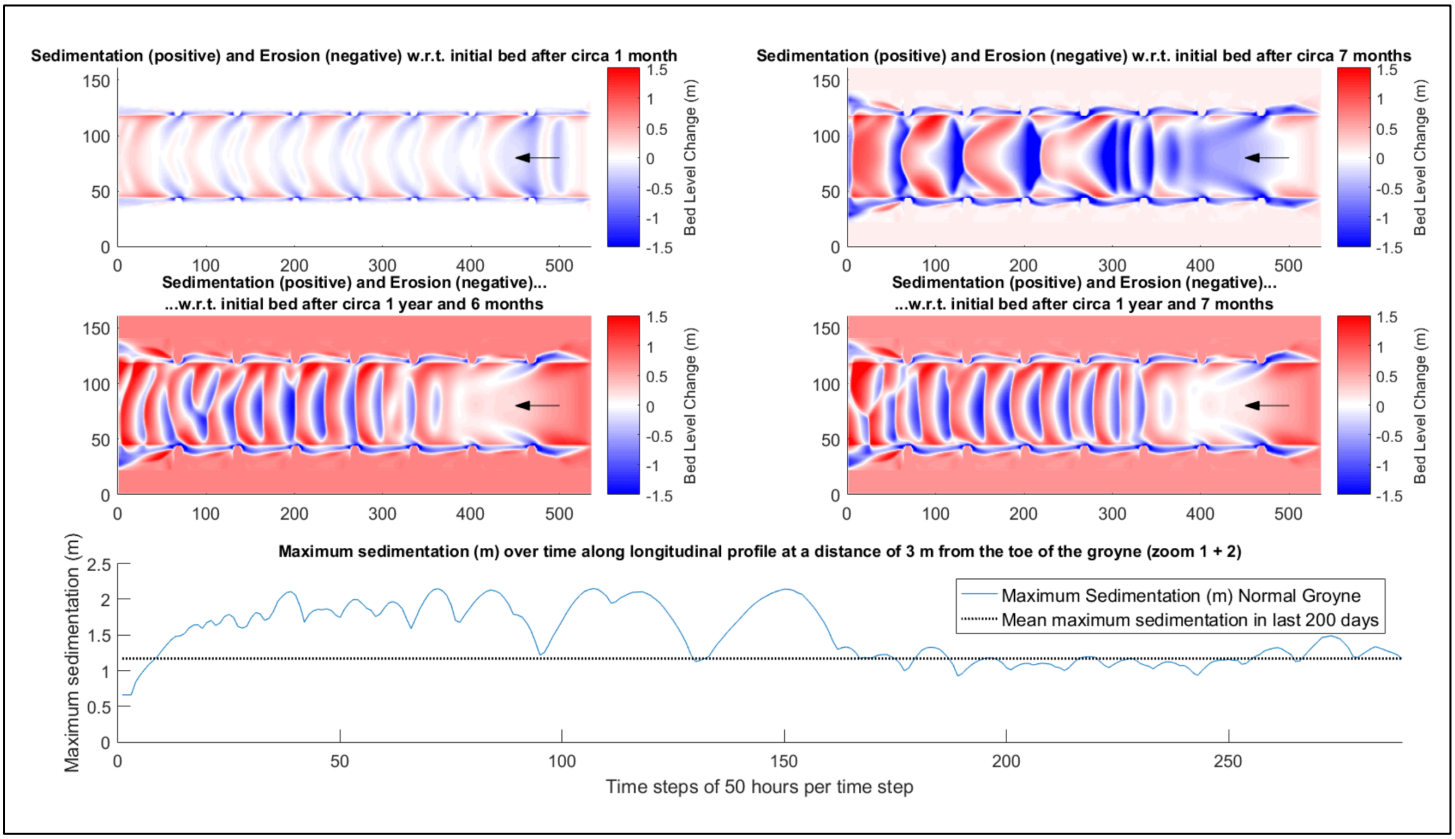

Figure 35: Temporal development of the cumulative sedimentation and erosion in the Waal - current groyne. The cumulative sedimentation and erosion in the top four figures is corrected for the average degradation of the bed observed at that moment in time. After more than a year, a dynamic equilibrium is reached.

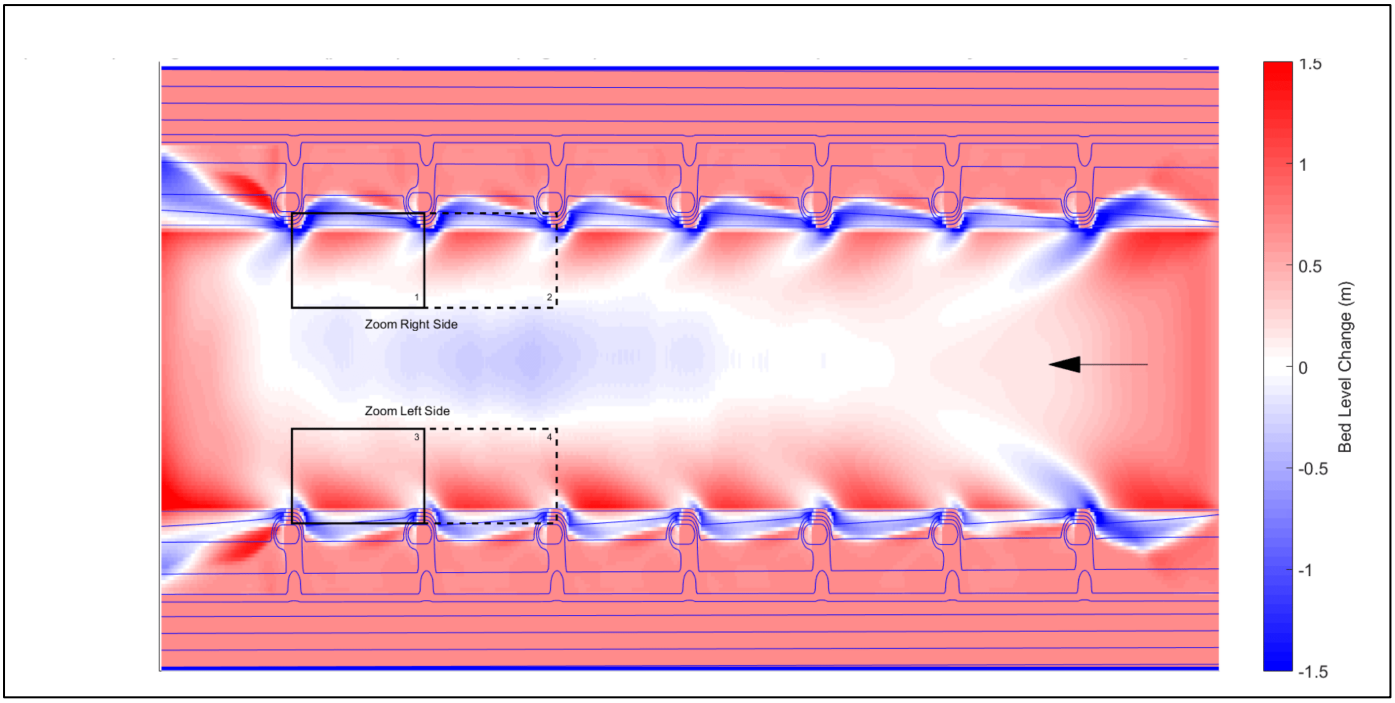

Figure 36: Mean cumulative sedimentation and erosion – after the dynamic equilibrium is reached – induced by the presence of the current groyne. Scour holes and groyne flames are formed. The cumulative sedimentation and erosion is compensated for the average degradation of the river bed.

The latter effect – the formation of bars – blurs the view of the scour holes and groyne flames which are formed in the vicinity of groynes. The bars interfere with this morphological evolution in a way which varies over time (Figure 35); as a bar passes a scour hole, the high bed level compensates for the scour which occurs at the groyne head whereas the scour hole extends over a large part of the channel whenever a trough passes the groynes. Adjacent to the groyne fields, groyne flames reach out to the bars, altering the orientation of groyne flames over time depending on the location of the closest migrating bar.

Further analysis on the magnitude of groyne flames and the differences as a result of the implementation of the isle groyne is only possible when the cumulative values of erosion and sedimentation are averaged over time in such a way that the bars are evened out. The averaging has taken place over the last 167 days of the model run during which the dynamic equilibrium of propagating bars with stable magnitudes was formed (Figure 35). The acquired pattern is further adjusted for the overall degradation occurring over the entire domain by increasing the bed levels with the average degradation within the centre three-quarters of the main channel (Figure 36).

On average, the characteristic pattern of scour holes and groyne flames is clearly visible. Scour holes extend to depths of over 1.5 meters and groyne flames reach up to circa 1 meter – both in the same order of magnitude as the observed values in the Waal (Figure 5 and Figure 6). The deepest points of the scour holes are formed directly around the entire head of the groyne. The patch of erosion extends downstream at an angle directed downstream and towards the centre of the main channel. The groyne flame – highest near the groyne field, lower near the main channel – is formed downstream of the scour hole (Figure 36).

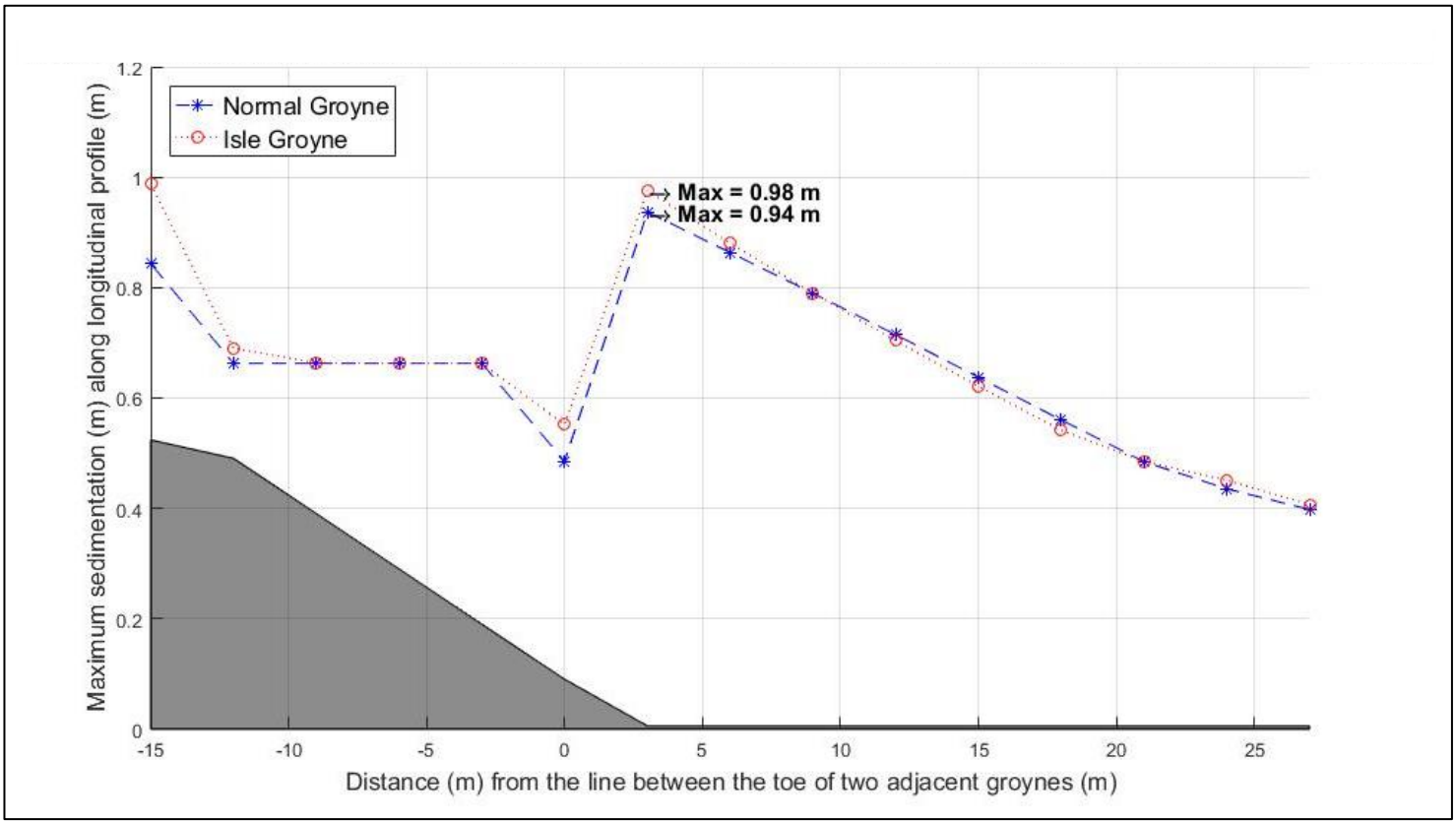

Figure 37: Maximum mean sedimentation along longitudinal profiles between two adjacent isle groynes and current groynes within zoom 1+2

6.2. Comparison current groyne and isle groyne

A similar qualitative pattern of sedimentation and erosion is formed around the isle groyne. Groyne flames around the isle groyne – focus on zoom 1 and 2 in Figure 36 - do not show significant differences compared to the groyne flames around the current groynes. On average, the former only slightly differ from the groyne flames induced by the flow structure around the current groyne. The difference is negligible.

The maximum average sedimentation along each of the longitudinal profiles between two groynes (Figure 37) is only barely lower further away from the normal line. Closer to the normal line, the values for the isle groyne are even slightly higher, possibly indicating a shift of the groyne flame to a position more parallel to the groyne field.

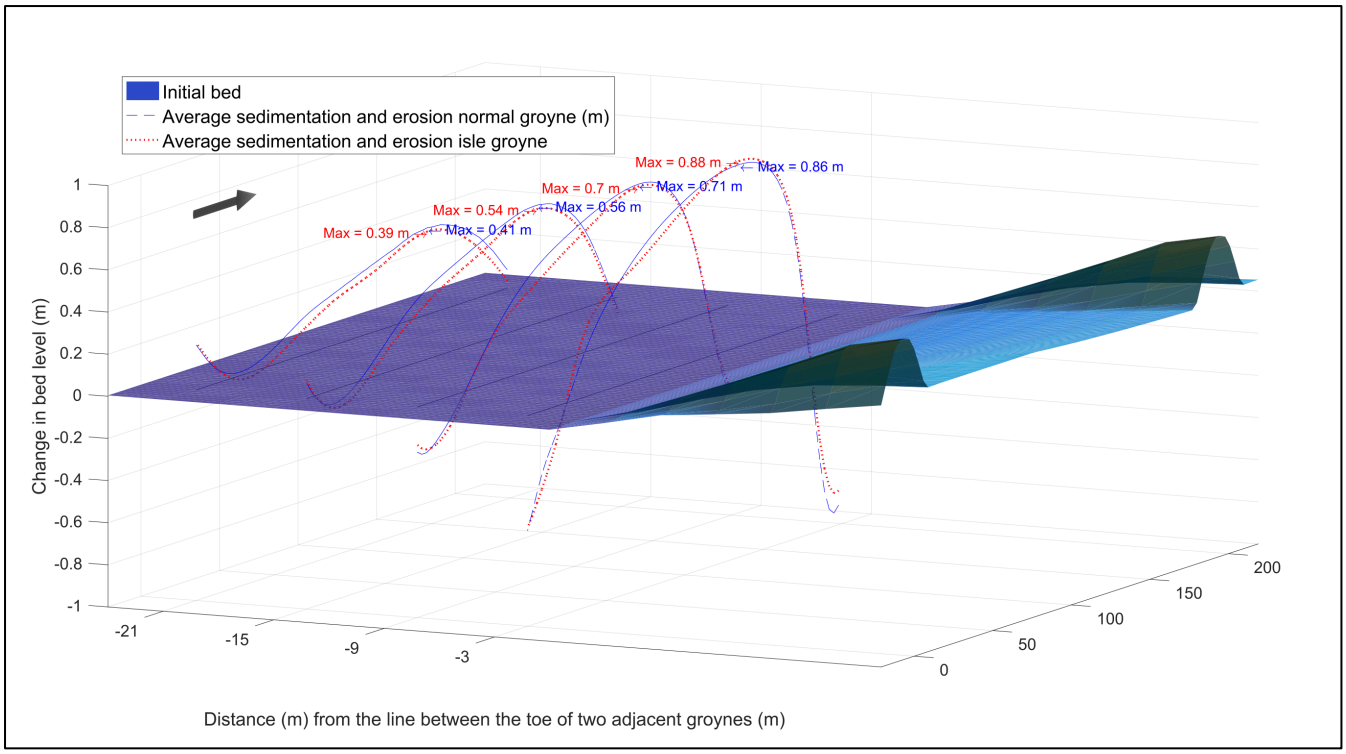

Figure 38: Average sedimentation and erosion (m) with respect to the initial situation along several longitudinal profiles parallel to the normal line between the isle groyne and current groyne (zoom 1)

Although the isle groyne does thus not decrease the maximum values for the average sedimentation, the isle groyne has a minor positive effect (decrease) on the total volume of the groyne flame (Figure 38). The groyne flames are slightly lower – a couple of centimetres – along the majority of each longitudinal profile, possibly reducing the stress imposed by the groyne flames on the dredging activities.

Furthermore, the model results do not show much difference in the intrusion of both groyne flames into the main channel (Figure 40). The differences which exist between the groyne flames near two adjacent groyne fields are big enough to compensate for possible differences between the two type of groynes; the isle groyne creates the groyne flame which intrudes the main channel furthest in ‘zoom 2’ whereas the effect is opposite in ‘zoom 1’.

It should further be highlighted that the differences described above are those found in the groyne flames generated on the northern side (right side in flow direction) of the river. The qualitative pattern of the difference between the two groynes is similar on the left side (Appendix IIX). However, the groyne flames along this side of the river are in general slightly higher.

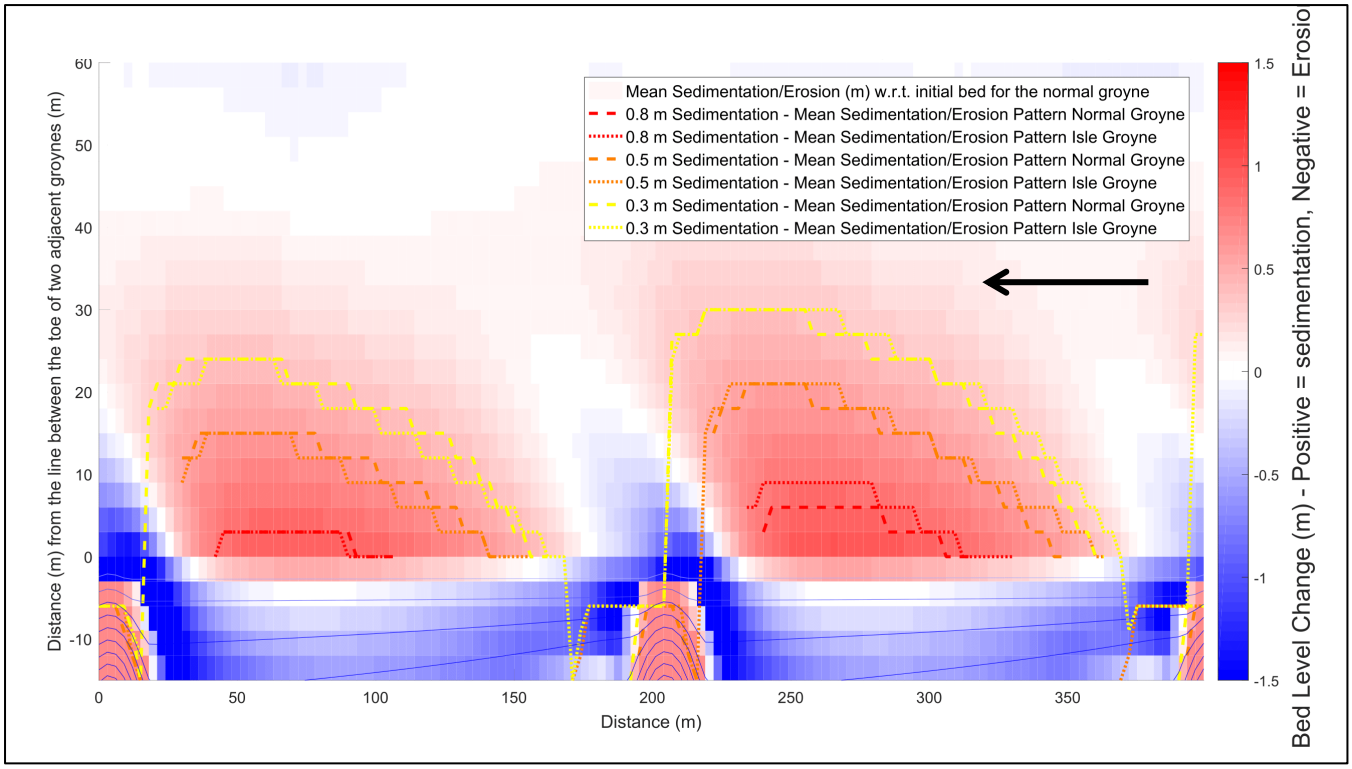

Figure 40: Furthest "in-channel" location where sedimentation exceeds 0.3, 0.6 or 0.9 m for the current and isle groyne

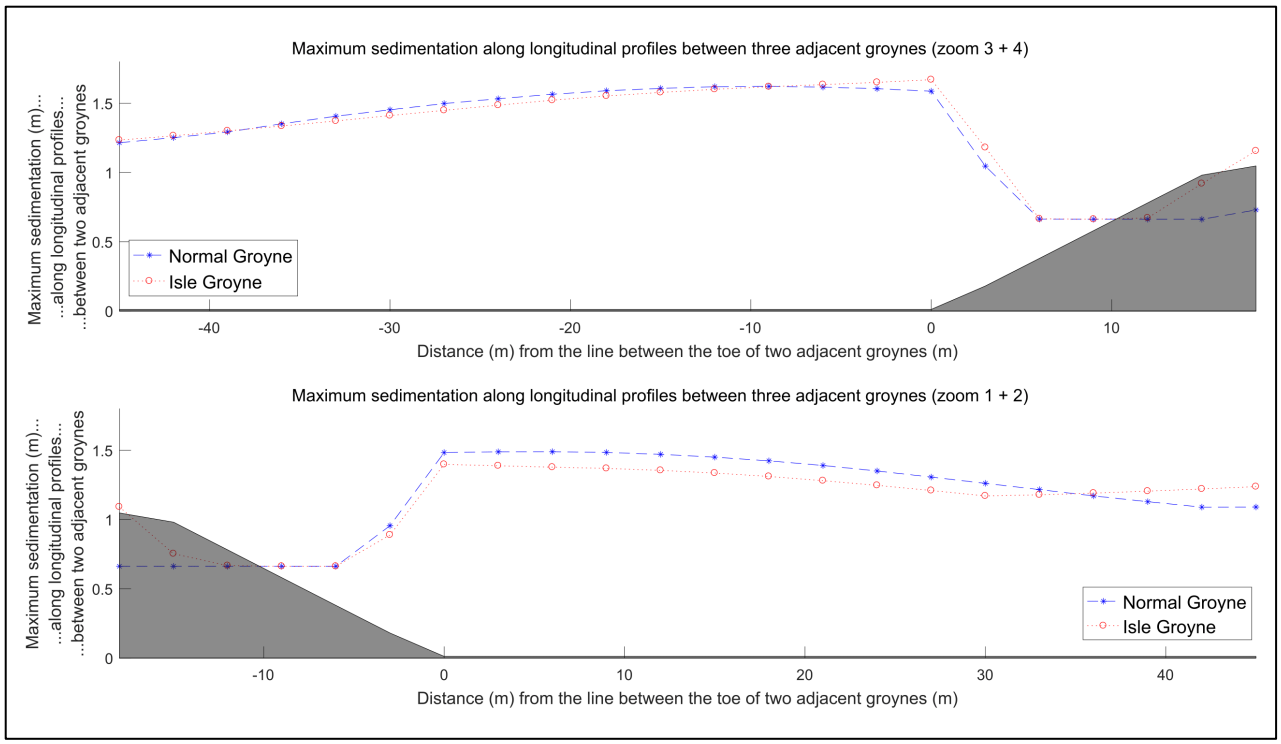

Figure 39: Maximum sedimentation observed along the longitudinal profiles between two adjacent isle groynes and current groynes within zoom 1+2. The figures depict a cross-section of a part of the main channel.

Analysis of the maximum sedimentation (no averaging) shows slightly more promising results for the isle groyne. The maximum sedimentation (Figure 39) along each of the longitudinal profiles between two groynes is up to 10 centimetres lower around the isle groyne on the sides of the main channel (zoom 1 + 2). However, the maximum sedimentation within the groyne flames on the left side of the river (zoom 3 + 4) shows results alike the maximum average sedimentation; the isle groyne induces more sedimentation close to the groyne field and smaller sedimentation closer to the centreline of the navigational channel.

Summary of the observed effects of the isle groyne on the groyne flames: The expected reduction of the impact of groyne flames on the navigational quality of the river Waal is not supported by the model results. Only small changes are present in the magnitude of the groyne flame. The groyne flames induced by the isle groyne have a slightly smaller volume, but higher maximum heights. These changes are however insignificantly small. Furthermore, no significant change is visible in the total intrusion of the groyne flame into the main channel.

7. Discussion

The results have shown that the isle groyne induces some differences in the hydrodynamics in Delft3D-FLOW compared to the current groyne. These differences do however not cause significant changes in the morphological pattern calculated modelled in Delft3D-FLOW. This discussion elaborates on the representativeness of the results for the river Waal. The chapter first discusses whether shortcomings in the Delft3D-model influence the hydrodynamics and morphological features in the adopted Waal schematization. It subsequently discusses the possible implications for the actual flow and velocity pattern, the turbulent motions and the groyne flames. Secondly, the chapter discusses the implications of the applied schematized Waal representation and discharge conditions on the obtained results.

Recommendations on river training measures and future research are presented in chapter 9.

7.1. Implications of model shortcomings on the results

Unfortunately, measurements of flow and sediment transport in the vicinity of isle groynes are not available. Quantitative validation of the model results on the hydrodynamic and morphological effects of the isle groyne in comparison with the current groyne is thus not possible. It is however expected that several shortcomings of Delft3D-FLOW influence the obtained results. The expected implications of the most important shortcomings on the flow and velocity pattern, the turbulent motions and the groyne flames are addressed.

Flow and velocity pattern

Model results on the flow and velocity pattern show temporally varying behaviour around the current groyne and the isle groyne. Around the current groyne, a primary eddy is formed which interacts with the frequently shed dynamic eddy. A secondary, anti-clockwise rotating eddy is however not always present in the model results presented in section 5.1. In line with previous research by e.g. Uijttewaal et al. (2001), the decomposed 1-by1-meter grid which is used for the analysis of the turbulent motions shows a more profound formation of the secondary eddy (Figure 25). The presence of the secondary eddy would partly prevent the primary eddy from intruding into the far upstream end of the groyne field. This intrusion occasionally occurs in the results of the model runs which utilised the 3-by-3 meter grid. Under the assumption that the 1-by-1-meter grid gives better results, this would mean that the use of a 3-by-3-meter grid has resulted in slight upstream shift of the average location of the ‘launch’ of the flow of the primary eddy into the main channel. This could potentially have resulted in increased flow acceleration near the tip of the current groyne in the model results because of the local increase of flow contraction. Although this effect is not expected to be significant because of the infrequency of the event, this could imply that the isle groyne has even fewer beneficial effects on the pattern of flow convergence and divergence than described in section 5.1.

It could furthermore be questioned whether the ‘no slip’-condition in Delft3D-FLOW – which reduces the flow velocities along the river’s embankments to zero – could hamper the formation of an anti-

clockwise rotating secondary eddy. The results of a run with partial slip (roughness length 0.3 m) however show similar flow patterns in the groyne fields.

Another shortcoming of the adopted model which could influence the flow pattern in the groyne field is the lack of incorporating non-hydrostatic pressure gradients. The presence of non-hydrostatic pressure gradients could slightly alter the velocity field in the vicinity of the inlet. At this location, the sudden change in bed geometry could result in changes of the non-hydrostatic pressure and thus of the stream velocity. It is not expected that this will significantly alter the flow pattern in the groyne field since the flow through the inlet is relatively small.

Turbulent motions

The more frequent presence of a secondary eddy, as described in the previous paragraphs, could intensify the formation of dynamic eddies around the current groyne. The increased velocity gradients gives rise to stronger dynamic eddies. Around the isle groyne, the flow through the inlet prevents the secondary eddy from being located next to the main flow. This implies that this shortcoming of the applied Delft3D-model (3-by-3-meter grid) reduces the beneficial effects of the isle groyne on the mitigation of the formation of dynamic eddies compared to the current groyne in the model results.

This effect is amplified due to the use of rectangular grid cells. This grid results in a 'staircase'-effect in the representation of groynes. Independent of the approaching flow or of the slope of the structure, this 'staircase'-effect induces flow separation. The 'artificial' flow separation – causing high velocity gradients on the boundary between the main and stationary flow – could induce additional turbulence which would in reality not be present. As the isle groyne is thought to generate less flow separation along the channel-side of the groyne head, this shortcoming could have resulted in an artificial increase of the turbulence in the upstream part of the mixing zone along the isle groyne. The model could thus have decreased the potential beneficial effects of the isle groyne on the turbulent motions around groynes further.

Additionally, a certain range of plausible values is present for several of the SGS-model parameters of the Horizontal Large Eddy Simulation. A sensitivity analysis (Appendix V) has shown the effect of changes within these parameters. It is however not known whether the adopted parameters or slightly higher or lower values are most applicable for the simulations. Changing these parameters could affect the turbulence around both types of groynes but is not expected to affect the difference between the effects of both types of groynes.

Lastly, Delft3D-FLOW is not capable of capturing the vertically rotating horseshoe vortex. The HLES is capable of simulating the dynamic eddies, rotating along a vertical axis, to good extent. 3D-LES is however necessary to capture the horseshoe vortex, a feature which is not supported by Delft3D-FLOW. As presented in section 2.2.2.2., it is questioned to which extent this vortex is formed around the groynes in the Waal. It is however expected that the horseshoe vortex would be (even) weaker in

the vicinity of isle groynes (Heereveld, 2006); the inlet reduces the adverse pressure gradient and thus the strength of the horseshoe vortex.

Groyne flame

The effect of the limitations of Delft3D-FLOW on the differences in hydrodynamics induced by the isle groyne and the current groyne also affects the morphology. The two hydrodynamic implications of the limitations which are thought to have the most profound impact on the morphology are those concerning the effects of the 3-by-3-meter, rectangular grid. The likely artificial reduction of the formation of dynamic eddies around the current groyne and the artificial increase of flow separation around the isle groyne lead to a probable underestimation of the beneficial effects of the isle groyne on the magnitude of the groyne flames within the present Waal schematization.

The inability of the model to simulate the horseshoe vortex likely leads to a further underestimation of the benefits of the isle groyne. This effect is however thought to be small as the horseshoe vortex only indirectly influences the magnitude of groyne flames. Contrarily, the slight reduction of the flow contraction around the current groyne due to the presence of a secondary eddy could have had a small negative impact on the relative morphological effects of the isle groyne.

A shortcoming of the morphological modelling in Delft3D-FLOW originates from the way the sediment transport is modelled. Since the modelling of suspended sediment transport has several drawbacks, the total transport formula of Engelund-Hansen was used to evaluate on the morphological development of the river bed. Arailopoulos (2014) for example found 'strange' behaviour in the erosion and sedimentation patterns in river bends with the use of transport formulae that included suspended sediment transport. Within the present research it was also found that the morphological development showed aberrant characteristics; the inlet of the isle groyne soon silted up (Appendix IX) and several locations were identified with sedimentation values far exceeding the realistic limits. Since a total transport formula like Engelund-Hansen models both the bed and suspended load as bed load, this might lead to some mistakes in the simulation of the bed level change. It is however not expected that this will affect the difference in the morphological effects of the isle groyne and the current groyne. It is furthermore found that the transport formulae of Meyer-Peter-Muller yield similar qualitative results (Appendix IX).

Additional shortcomings in the sediment transport are related to the turbulence. Turbulence affects the morphological processes in Delft3D-FLOW by influencing the local flow velocities. However, since the sediment transport formulae are not specifically designed for the purpose of simulating the effect of turbulence on the morphology, some mistakes might be present. As for the implications of the use of the formulae of Engelund-Hansen, it is not expected that this will influence the relative impact of the isle groyne.

All in all, the limitations of Delft3D-FLOW likely result in the underestimation of the beneficial effects of the isle groyne on the magnitude and orientation of the groyne flame. However, it is not thought that

these will affect the overall conclusion on the effect of the isle groyne on groyne flames. This effect is still thought to be minimal for the present Waal schematization under constant discharge conditions.

7.2. Implications of the Waal schematization and discharge conditions

To derive any conclusions on the effects of the isle groyne in the actual Waal in comparison with the current groynes, it is also important to discuss the implications of the constant discharge condition and the schematized representation of the Waal.

The model has only been run for a discharge corresponding to a water level just underneath the crest of the groyne. It is thought that realistic variable discharge conditions will decrease the beneficial impact of the isle groyne on the groyne flames since differences in hydrodynamics will likely decrease. The constant discharge adopted in the present research is lower than the average discharge in the river Waal. As both groynes allow for overflow with higher discharges, the hydrodynamic effects of the isle groyne's inlet are minimized. The expected positive effects of decreased convergence and divergence due to the elongated groyne head are reduced; the overtopping of the current groyne allows the flow to maintain its straight flow pattern. Furthermore, the benefits of the induced reduction of the formation of dynamic eddies around isle groynes are also minimized. The higher discharge leads to a decrease of velocity gradients along the mixing zone and decreased flow separation at the head of both types of groynes. Consequentially, the turbulence in the mixing layer and the strength of the dynamic eddies are reduced around both the current groyne and isle groyne and differences in turbulent motions between the isle groyne and the current groyne decrease.

The schematized representation of the Waal also influences the effects of the groyne types on the groyne flames. The Waal and its groyne fields are not uniform over the river's entire length. Different aspect ratios of groyne fields, another orientation of groynes, the position of groyne fields in river bends and spatially varying bed levels could all locally influence the magnitude and orientation of groyne flames and the differences between the isle groyne and current groyne.

Another implication of the schematized representation of the Waal might originate from the relatively steep bed level gradient (1:4) at the toe of the groyne field (Figure 19). This steep gradient was, as explained in section 4.1., designed to compensate for the flat bed in the main channel. It could however be that this rapid bed level increase affects the flow by partially preventing it from intruding into the groyne field. This would mean that the model underestimates the flow divergence and possibly the size of the groyne flames around the current groyne, leaving little room for improvement for the isle groyne.

Altogether, it can be expected that the differences in the hydrodynamic and morphological results between both types of groynes are likely mitigated whenever the Waal was simulated with a realistic bathymetry and under realistic variable discharge conditions. Locally, bathymetric characteristics can either result in stronger, respectively weaker, benefits of the isle groyne on the magnitude and orientation of groyne flames.

8. Conclusion

This research has offered insights in the effects of the isle groyne on the hydrodynamics and morphology in the river Waal. Conclusions were derived with the use of a numerical calculation of the flow and sediment transport within a schematized Waal representation under constant discharge conditions. Based on the analysis of the Delft3D-FLOW model results and the consecutive discussion, the following conclusions can be derived:

1.a. What are the effects of the isle groyne on the flow and velocity pattern in the river Waal in comparison with the current groynes?

Under the assumption of low discharge in the Waal, the isle groyne changes the temporally varying flow and velocity pattern around groynes. The flow through the inlet of the isle groyne causes a different – albeit time-varying – flow pattern in the groyne field. At some time instances, the bypassed stream is strong enough to penetrate into the primary gyre, disturbing its nature and creating a pattern of continuous flow parallel to the main flow from the one inlet to the other. At other time instances, the flow through the inlet soon deflects in the direction of the main channel and reattaches to the main flow upstream of the primary eddy.
The model results show an average decrease of the flow velocity in the main channel of the river Waal. This decrease is most profound along the upstream half of a groyne field. Here, the bypassed flow is still unattached to the main flow during most moments in time. The isle groyne further induces a slightly larger temporal variability of the magnitude of the flow acceleration around the groyne's head due to the irregular appearance of the primary eddy and the parallel flow. These differences do however not induce a significant change in the observed difference between the magnitude of the accelerated and decelerated flow velocities.

It is expected that these model results are representative for the actual Waal under constant (low) discharge conditions. Only a minor reduction of the flow acceleration around the tip of the current groyne is expected due to the likely incorrect infrequency of the occurrence of a secondary eddy downstream of the current groynes in the model results.
Under higher discharge conditions, differences between the isle groyne and the current groyne are thought to be mitigated. These discharges allow for flow over the current groynes and lead to the consequential reduction of the formation of eddies and the pattern of convergence and divergence around both groynes. The flow patterns around both types of groynes become more alike.

It can thus be concluded that the isle groyne causes changes in the temporally varying flow pattern in the Waal under low discharge conditions. Flow through the inlet disturbs the characteristic flow pattern in the groyne field and occasionally creates a persistent parallel flow. Under these conditions, the isle groyne does not cause significant differences in the

magnitude of the difference between the velocities of the accelerated and decelerated flow. Under variable discharge conditions, differences between the isle groyne and current groyne are in general thought to be small.

1.b. *What are the effects of the isle groyne on turbulent motions in the river Waal in comparison with the current groynes?*

The isle groyne influences the turbulence pattern in the vicinity of groynes. Within the schematized representation of the Waal in Delft3D-FLOW, the isle groynes reduce the weak vorticity relatively far downstream of the groynes during discharges slightly below the groyne's crest. The turbulence at the upstream end of the groyne's head at the side of the main channel is also decreased. Stronger turbulence is present around the isle groyne's inlet and at the downstream end of the isle along the boundary of the main flow and the wake zone behind the groyne's head. These effects of respectively reduced (upstream) and stronger (downstream) turbulence along the isle groyne's head are accompanied by corresponding fewer and further intrusion of relatively strong turbulence into the main channel.

It is expected that the isle groynes will – in reality – further reduce the turbulence in the mixing zone since the model likely underestimates the formation of dynamic eddies behind the current groyne. The turbulence directly around the isle groyne's head is also expected to be decreased further as the use of a rectangular grid has possibly led to an overestimation of the flow separation around the (isle) groynes.
During higher discharge conditions – when groynes are overtopped – differences in turbulent motions between the two groyne types in the river Waal are reduced as the flow patterns become more alike.

It can be concluded that the isle groyne is able to decrease the strength of the turbulent motions along the groyne's head and the mixing zone in the river Waal under low discharge conditions. The isle groyne increases turbulence within the groyne field. Under higher discharge conditions, effects are thought to be minimal. Furthermore, no conclusion can be derived on the effect of the isle groyne on the horseshoe vortex.

2. *What are the effects of the isle groyne on groyne flames in the river Waal in comparison with the current groynes?*

The differences in the velocity and vorticity patterns do not result in significant changes in the magnitude and orientation of groyne flames. Only minor differences are present in the model results for the volume (reduced) and maximum time-averaged heights (increased close to the groyne field, decreased further away from the groyne field) of the groyne flames. Also, no significant changes are present in the extent of intrusion of the groyne flame into the main

channel. Slightly more promising effects are visible for the maximum non-averaged heights of the groyne flames.

It is expected that these results are representative for the river Waal. The model shortcomings – especially the expected slight underestimation of the turbulence reduction around isle groynes – might have led to reduced benefits of the isle groyne in the model results. It is however not expected that a better representation of the turbulent motions would cause significantly different morphological effects of the isle groyne.
Variable discharges would further decrease the potential benefits of the isle groyne on the magnitude of the groyne flame as hydrodynamic characteristics become more alike during high discharge conditions.

It can thus be concluded that the effects are too minimal to conclude on positive effects of the isle groyne on the magnitude and orientation of the groyne flame compared to the current groyne in the river Waal.

9. Recommendations

Based on the discussion and conclusion, several recommendations can be made. These are divided in recommendations on future research on the one hand and a recommendation to river managers in the Netherlands on the other hand.

9.1. Recommendations for future research

This section includes advice on the extension or improvement of the hydrodynamic and morphological simulation within the present research given the current Waal and groyne schematization. It further includes possible alterations in this model set-up to acquire additional, possibly confirmative insight on the effects of the isle groyne on groyne flames.

To improve the representation of the hydrodynamics and morphology in the vicinity of groynes, it is advised to use curvilinear grids to overcome potential problems regarding the 'stair-case'-representation of the groynes. It would be interesting to see how this will affect the turbulence along the groynes and the morphology. Also, a more in-depth analysis of the turbulence around the groynes – including three-dimensional turbulence – could be interesting for further insight on the effects of the isle groyne and other groynes alike. It would as well excite one's curiosity to see what the effect would be of applying 1-by-1 meter grid cells. Although computationally challenging, the more profound formation of the secondary eddy and dynamic eddies could possibly influence the evolution of the bed.

Extended research could furthermore focus on an alteration of the model set-up. Research could range from the comparative analysis of higher normal groynes and corresponding higher isle groynes (alike the initial design) to the analysis of the effects during higher discharges and to the analysis of the effects of the proposed optimizations of the isle groyne design (§9.2). Furthermore, it could be of interest to prevent the potential influence of the rather steep transverse slope at the boundary between the groyne field and the main channel. It would be interesting to see whether the average bed levels of the Waal – without already existing groyne flames and time-varying bed patterns like bars and ripples – could be applied and whether these would induce different results on the hydrodynamic and morphological pattern around both types of groynes.

Additionally, flume experiments to validate the results from the numerical researches could provide interesting insights on the topic of groyne flames in the vicinity of (isle) groynes.

9.2. Recommendations to river managers

Based on the present research, it can be concluded that the construction of the isle groyne would not result in a significant reduction of the impact of groyne flames on the navigational quality of the river Waal. Although additional research is recommended to endorse this statement, it is not likely that these will qualitatively alter the results of this research. Whereas several model improvements would probably positively affect the impact of the isle groyne (e.g. finer grid), others would probably decrease the isle groyne's beneficial effects (e.g. variable discharge). It is therefore not advised to construct the

isle groyne, with its present design, on a large scale in the Waal as an alternative to the present, lowered groynes as a mean to reduce the navigational impact of the groyne flame.

This does however not mean that the isle groyne has no future. Local conditions, improvements in the design of the isle groyne and side-effects of the hydrodynamics around the isle groyne, could benefit the future prospects of the groyne.

- The present research focuses on the comparison of the isle groyne with the current, lowered groynes in the Waal. The lowering of groynes has likely mitigated turbulence and the pattern of flow acceleration and deceleration around groynes. The reference situation in this research therefore represents relatively optimal flow conditions. The isle groyne could have more beneficial effects if constructed as an alternative to higher groynes. The increased size of the inlet would then lead to a larger reduction of turbulent energy. It is questioned whether the velocity gradients would decrease as well. The increased discharge through the groyne's inlet could lead to a more frequent disturbance of the primary eddy and the consequential parallel flow in the groyne field. However, the increased water depth also leads to a stronger development of the primary eddy.
- The beneficial effect of the isle groyne on the magnitude groyne flames can possibly be improved by optimization of its design. Further elongation of the groyne's head is likely the most promising. This design alteration could further decrease the intrusion of the main flow into the groyne field and, most importantly, facilitate a more frequent parallel flow through the groyne fields. In the present design, the discharge through the isle groyne's inlet alternately deflects into the main channel or continues its course parallel to the main flow.

  Talstra (2011) – investigating the effect of the construction of a pile sheet in front of the groyne head – concluded that the pile sheet was located optimal for the reduction of the groyne flame if constructed downstream of and perpendicular to the groyne. Based on these findings, it is thought that a more upstream placement or the inclination of the isle groyne's head would not result in more favourable results on the reduction of the magnitude of groyne flames.

  Design improvements could also focus on the reduction of the isle groyne's costs. The extension of the groyne head is likely rather costly. It is advised to investigate whether the downstream part of the isle groyne's head may be replaced by a pile sheet. This might result in a decrease of the smoothness of the stream guidance but could reduce the isle groyne's costs.
- Benefits of the isle groyne could also originate from reasons other than the reduction of the magnitude of the groyne flame. This research has shown that construction of the isle groyne creates a parallel flow within the groyne field during a portion of the time. This flow would facilitate a calmer flow pattern, especially during the passage of large vessels.

  Large vessels currently alter the flow pattern in groyne fields and generate a strong return flow from the groyne fields into the main channel. This flow reaches high velocities, leads to a significant drawdown of the water level in groyne fields and entrains sediment (Yossef, 2002).

During low discharges, this results in significant erosion of the groyne fields and thus in additional sediment supply to the main channel. Furthermore, the highly dynamic flow induced by the passage of ships does not favour the ecological potential of the groyne fields. The parallel flow might reduce the drawdown of the water level and, most importantly, protect the groyne field on the embankment's side of the parallel flow from the strong return flow. Additionally, the elongated groyne head also protects the groyne field from the effects of passing vessels. The protection of (a part of) the groyne field from highly dynamic flow increases the ecological potential and reduces the sediment supply to the main channel which had increased as a result of the groyne lowering (Dongen, 2016). Additional elongation of the groyne head could increase the potential of these benefits as it may favour the parallel flow and further protect the groyne field from the dynamic flow conditions.

Nature could further benefit from the isle groyne as the inlet allows fish to migrate from one groyne field to another in relatively calm flow conditions. Also, better visibility is achieved by the elongation of the groyne head. This reduces the chance of collision of ships.

10. Bibliography

Anderson, J. (2011). *Fundamentals of Aerodynamics.* McGraw Hill Education - Europe.

Arailopoulos, I. (2014). *Morphodynamic modelling with suspended sediment transport in river bends.* Delft: TU Delft.

Berselli, L., Illiescu, T., & Layton, W. (2006). *Mathematics of Large Eddy Simulation of Turbulent Flows.* Springer.

Brinke, W. t., Bolwidt, L., Snippen, E., & Hal, L. v. (2001). *Sedimentbalans Rijntakken 2000.* Arnhem: Directoraat-Generaal Rijkswaterstaat.

Busnelli, M., Schuurman, F., Sieben, A., Wal, M. V., & Hector, H. (2011). Morphodynamic responds of groyne fields to the lowering of crest level of the groynes in the Waal River, The Netherlands. *River, Coastal and Estuarine Morphodynamics*.

Consortium Kribben. (2006). *Louvrekrib: Hoofdrapport en achtergronddocument.*

Deltares. (2014). *User Manual Delft3D-FLOW: Hydro-morphodynamics.* Delft: Deltares.

Dongen, B. v. (2016). *Morfologische Ontwikkeling Oevers na Kribverlaging op basis van Laseraltimetrie Gegevens 2010 t/m 2015.* Amersfoort: Arcadis.

Havinga, H., Taal, M., Smedes, R., Klaassen, G., Douben, N., & Sloff, C. (2006). Recent training of the lower Rhine River to increase Inland Water Transport potentials: A mix of permanent and recurrent measures. *International conference on fluvial hydraulics* (pp. 31 - 50). Lisbon: River Flow.

Heereveld, M. v. (2006). *Kribben van de toekomst: Eilandkrib.* Nijmegen: Haskoning Nederland.

Henning, M., & Hentschel, B. (2013). Sedimentation and flow patterns induced by regular and modified groynes on the River Elbe, Germany. *Ecohydrology, 6*, 598-610.

Hinterberger, C., Fröhlich, J., & Rodi, W. (2007). Three-dimensional and depth-averaged large-eddy simulations of some shallow water flows. *Journal of Hydraulic Engineering, 133*(8), 857-872.

Kang, J., Yeo, H., Kim, S., & Ji, U. (2011). Experimental Investigation on the local scour characteristics around groynes using a hydraulic model. *Water and Environment Journal, 25*, 181-191.

Karami, H., Basser, H., Ardeshir, A., & Hosseini, S. (2014). Verification of numerical study of scour around spur dikes using experimental data. *Water and Environment Journal, 28*, 124-134.

Kisoensingh, J. (2015). *Impact of recent changes in river management on maintenance dredging in the Waal river.* MSc Thesis, Delft.

Klaassen, G., & Sloff, C. (2000). *Voorspelling bodemligging en herstelrelaties t.b.v. baggeren op de Waal: Eenvoudig relaties en benodigd onderzoek.* WL|Delft Hydraulics.

Klingeman, P., Kehe, S., & Owusu, Y. (1984). *Streambank Erosion Protection and Channel Scour Manipulation Using Rockfill Dikes and Gabions.* Corvallis: Oregon State University.

Klop, E. (2016). *Morfologische ontwikkeling hoofd- en vaargeul na kribverlaging op basis van multibeamgegevens in periode 2009-2015.* Amersfoort: Arcadis.

Koken, M., & Constantinescu, G. (2008). An investigation of the flow and scour mechanisms around isolated spur dikes in a shallow open channel: 1. Conditions corresponding to the initiation of the erosion and deposition process. *Water Resources Research, 44*, 19.

Kroekenstoel, D. (2017). *Rivierkundig Beoordelingskader voor ingrepen in de Grote Rivieren.* Rijkswaterstaat Water, Verkeer en Leefomgeving.

Li, G., Lang, L., & Ning, J. (2013). 3D Numerical Simulation of Flow and Local Scour around a Spur Dike. *2013 IAHR World Congress.* Chengdu.

Liek, G. (2000). *Horizontal Large Eddy Simulation using Delft2D-MOR.* Delft University of Technology, Faculty of Civil Engineering and Geosciences. Delft: TU Delft.

McCoy, A., Constantinescu, G., & Weber, L. (2008). Numerical Investigation of Flow Hydrodynamics in a Channel with a Series of Groynes. *Journal of Hydraulic Engineering, 134*(2), 157-172.

Nieuwstadt, F., Boersma, B., & Westerweel, J. (2016). *Turbulence: Introduction to Theory and Applications of Turbulent Flows.* Springer International Publishing.

Ouillon, S., & Dartus, D. (1997). Three-dimensional computation of flow around groyne. *Journal of Hydraulic Engineering, 123*(11), 962-970.

Rijn, L. V. (1993). *Principles of Sediment Transport in Rivers, Estuaries and Coastal Seas.* Amsterdam: Aqua Publications.

Robert, A. (2003). *River Processes: An Introduction to Fluvial Dynamics.* London: Hodder Education.

Rupprecht, R. (2004). *Modelling of the Morphological Interaction between a River and its Groyne Fields.* Delft: TU Delft.

Saberi, O., & Galoie, M. (2017). Numerical Modeling of Flow Around Groynes with Different Shapes Using TELEMAC-3D Software. *American Journal of Water Science and Engineering, 2*(6), 43-52.

Saeedipour, M., Schneiderbauer, S., Pirker, S., & Bozorgi, S. (2014). Numerical simulation of turbulent liquid jet breakup using a sub-grid criterion with industrial application. *28th Annual Conference on Liquid Atomization and Spray Systems.* Bremen: ILASS.

Safarzadeh, A., Neyshabouri, S., & Zarrati, A. (2016). Experimental Investigation on 3D Turbulent Flow around Straight and T-shaped Groynes in a Flat Bed Channel. *Journal of Hydraulic Engineering, 142*(8), 15.

Schuurman, M., Nagtegaal, L., & Karelse, M. (2010). *Ruimtelijke Kwaliteit Waalkribben: Ambitiedocument.* DHV.

Sodja, J., & Podgornik, R. (2007). *Turbulence models in CFD.* Ljubljana.

Talstra, H. (2011). *Large-scale turbulence structures in shallow separating flows.* PhD Thesis, Delft.

Uijttewaal, W., Lehmann, D., & Mazijk, A. v. (2001). Exchange processes between a river and its groyne fields: model experiments. *Journal of Hydraulic Engineering, 127*(11), 928-936.

Verheij, H. (1997). *Effectiviteit van kribben.* Waterloopkundig laboratorium.

Winterwerp, J., & Kesteren, W. v. (2004). *Introduction to the physics of cohesive sediment in the marine environment.* Delft: Elsevier.

Yazdi, J., Sarkardeh, H., Azamathulla, H., & Ghani, A. (2010). 3D Simulation of flow around a single spur dike with free-surface flow. *International Journal of River Basin Management, 8*(1), 55-62.

Yossef, M. (2002). *The Effect of Groynes on Rivers.* Literature Review PhD Study, Delft University.

Yossef, M. (2005). *Morphodynamics of rivers with groynes.* PhD Thesis, Delft.

Yossef, M., & Klaassen, G. (2002, January). Reproduction of groynes-induced river bed morphology using LES in a 2-D morphological model. *International Conference on Fluvial Hydraulics.* Louvain-la-Neuve.

Yossef, M., & Vriend, H. d. (2011, May). Flow Details near River Groynes: Experimental Investigation. *Journal of Hydraulic Engineering, 137*(5), 504-516.

Yossef, M., Jagers, H., Mosselman, E., & Sieben, A. (2007). Shear stress enhancement to account for increased turbulence in mixing layers along river groynes. *5th IAHR Symposium on River Coastal and Estuarine Morphodynamics*, (p. 28). Enschede.

Zhang, H., & Nakagawa, H. (2008). Scour around Spur Dyke: Recent Advances and Future Researches. *Annuals of Disas. Prev. Res. Inst., 51 B*, 20.

Appendix I: History of groynes in the river Waal

Over the past centuries, the river Waal has changed from a freely meandering river through the lowlands of the Netherlands to a heavily regulated river, kept in place by the presence of groynes and levees. The need to regulate the river and restrict its impact on the surrounding land increased with increasing amounts of activities in the vicinity of the river. Embankments both protected the hinterland for inundation during high waters and prevented the river from migrating through its delta whereas the first groynes preserved the surrounding land by preventing erosion of the river banks (Yossef, 2002). These groynes were however constructed by individuals and the irregularity of the presence of groynes caused impedance of flow by sand bars and – during winter time – of ice dams which increased the risk of flooding. A consequential ban on the construction of groynes had little effect which led to a second round of groyne construction around 1820 which aimed on the prevention of flood events. Despite the increasing importance of the waterway as a mean of transport, it took until the late 19th century until one decided on the structured constriction of the river to improve navigation over the Waal (Yossef, 2002). Regulation did however not stop. Recently, the Room for the River program – adopting the idea of lowering water levels rather than heightening levees to protect the land from flooding – caused other major changes. Measures included widening of the floodplains, the formation of bypasses but also the lowering of groynes, all to increase the flood conveyance capacity (Havinga, Taal, Smedes, Klaassen, Douben, & Sloff, 2006). The latter measure was possible without hampering the functioning of the groynes as autonomous subsidence of the river bed had caused the groynes to be relatively higher than initially intended and necessary (Schuurman, Nagtegaal, & Karelse, 2010).

The combination of the measures described above have given the Dutch riverine landscape their characteristic, regulated features as present nowadays.

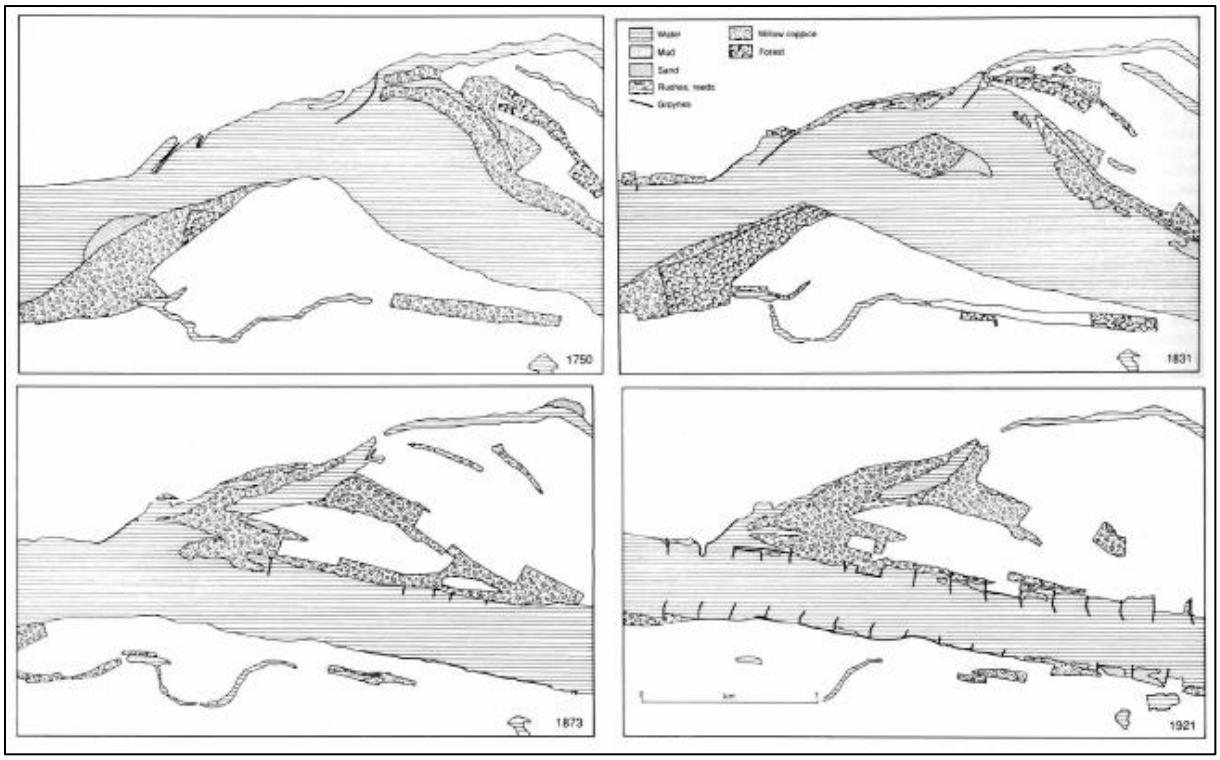

Figure 41: Evolution of the river Waal near Dodewaard as a result of river regulations over circa 200 years (Yossef, 2005)

Appendix II: Different Scales of Turbulent Structures and the Energy Cascade

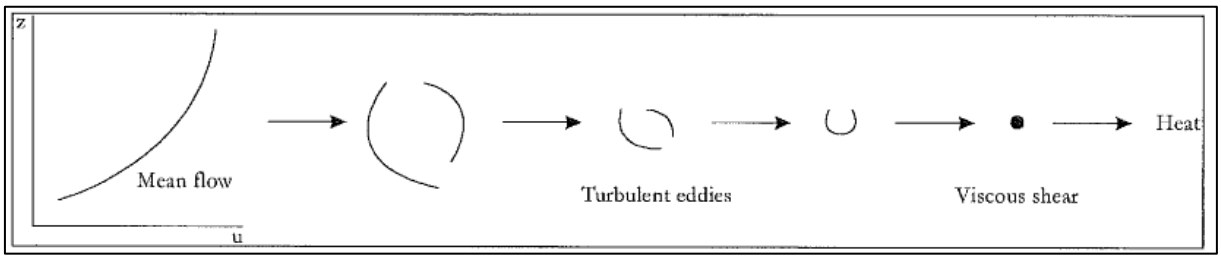

Figure 42: The energy cascade, energy is transferred from larger to smaller eddies in which viscosity transfers kinetic energy to heat (Liek, 2000)

Turbulence can occur at many different scales and turbulent flow can be considered to consist of eddies of multiple sizes, each coherent within the region of its length scale. In general, regions with large eddies also contain smaller eddies with smaller length scales. These length scales can be classified within three length scale ranges, being the 'energy containing range', the 'inertial subrange' and the 'dissipation range' (Figure 43) (Saeedipour, Schneiderbauer, Pirker, & Bozorgi, 2014). Each of these ranges is discussed separately in this appendix. First, the energy containing range is discussed. Then, the smallest structures present within the dissipation range are presented. The inertial subrange is discussed last.

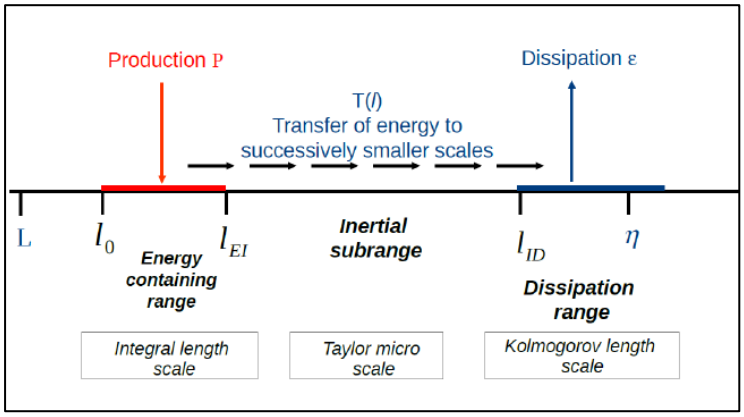

Figure 43: The different ranges of turbulence (Saeedipour, Schneiderbauer, Pirker, & Bozorgi, 2014)

The largest dimensions – within the *energy containing range* – are referred to as the macrostructure. This scale is directly influenced by the geometric characteristics of the flow; its vortex structures are directly produced by the mean flow and the eddies within this so-called 'integral scale' receive their kinetic energy through instability processes within the mean flow (Nieuwstadt, Boersma, & Westerweel, 2016). The bulk of the energy of turbulent motion is contained within these larger structures. The structures maintain this energy over a characteristic length scale L – the distance (mixing length) a particle travels until it loses its original characteristics (Robert, 2003) – during a time scale determined by the velocity and length scales of the turbulent motions (Nieuwstadt, Boersma, & Westerweel, 2016).

The energy is eventually dissipated into heat. However, this transformation can only take place through viscous effects which barely play a role at the large turbulent scales (Nieuwstadt, Boersma, & Westerweel, 2016). The energy dissipation can thus only occur in the smaller turbulent scales where velocity gradients can become large enough for viscous effects to be significant and for kinetic energy to be transformed into heat (Nieuwstadt, Boersma, & Westerweel, 2016). These smaller turbulent

structures are formed through a process in which larger turbulent structures become unstable and are broken down into smaller structures. This process continues until the microstructure is obtained at the smallest turbulent scale called the Kolmogorov scale within the *dissipation range*. It is within this range that the velocity gradients are large enough for the dissipation of turbulent kinetic energy to heat to occur (Nieuwstadt, Boersma, & Westerweel, 2016). The transfer of energy to heat thus takes place at the end of a sequence of break-down processes, making the rate of dissipation of kinetic energy into heat related to the length and velocity scales of the macrostructure as these govern the rate at which the dissipated energy is transferred to the microstructure. This dependency (Nieuwstadt, Boersma, & Westerweel, 2016) between the largest and smallest structures is referred to in the formulation of turbulence within so-called closure models within numerical models like Delft3D-FLOW (Section 2.4.2.). The process from kinetic energy towards its dissipation into heat is referred to as the *energy cascade.*

Kolmogorov's first similarity hypothesis states that the turbulent motions have, at this very small scale, a universal form which is determined by the dissipation of the energy (ε) and the kinematic viscosity (ν) (Nieuwstadt, Boersma, & Westerweel, 2016). He thus argued that the geometric information of the larger eddies – formed by the mean flow – are lost in the process of the energy cascade. The universal form of turbulence at the smallest scale eases the numerical modelling of turbulent structures (Section 2.4.2.1.)

The third subrange that can be identified is referred to as the *inertial subrange*, in which the turbulent motions do also exhibit a universal form. This universal form is uniquely determined by the energy dissipation (ε). The size of the eddies within this range are in the order of magnitude of at least six times smaller than the eddies within the energy containing range but significantly bigger than the eddies within the dissipation range.

Appendix III: The Closure Problem

In case of a well-posed problem – like laminar flow – a system of Navier-Stokes equations, in addition with realistic boundary and initial conditions with sufficient accuracy, leads to a unique and stable solution. These linear problems are thought to be predictable.

However, the procedure of Reynolds-Averaging introduces a new nonlinear advection term in the set of momentum equations. This term – the Reynolds stress – results in the NS-equations to become unstable and thus in them to become ill-posed, meaning that, for small variations in either the initial or the boundary conditions, the solutions will diverge. Since one is not able to precisely determine all initial and boundary conditions, a certain variability will always be present within the solution of the NS-equations; there are thus several possible realisations for the same realistic boundary conditions. Therefore, one focuses on the statistics of the flow variables to describe turbulent flows. It is however not possible to reconstruct the turbulent flow field from the acquired statistics. This is called the closure problem (Nieuwstadt, Boersma, & Westerweel, 2016).

Other than the uncertainty in the outcomes related with the exact numerical modelling of turbulent flows, the computational process of the numerical simulation of these flows requires enormous computational effort since the calculations should be able to resolve the length and timescales of both the macro- and microstructure of the flow. This type of simulation – Direct Numerical Simulation (DNS) – is even with the availability of supercomputers still limited to flows with low Reynolds numbers (Nieuwstadt, Boersma, & Westerweel, 2016; Sodja & Podgornik, 2007).

Appendix IV: k-ε Closure Model

The three-dimensional eddy viscosity ν_{3D} can be calculated by means of the turbulent kinetic energy (k) contained within the turbulent motion and the mixing length (L), earlier described as the distance a particle travels until it loses its (turbulent energy) characteristics. Multiplied with the constant c'$_\mu$, these parameters represent the mean characteristics of the turbulent flows (Deltares, 2014).

$$\nu_{3D} = c'_\mu L\sqrt{k} \tag{22}$$

ν_{3D}	*Three-dimensional eddy viscosity [m²/s]*
c'_μ	*Coefficient derived from empirical constant, 0.09 [-]*
L	*Mixing Length [m]*
k	*Turbulent kinetic energy [m²/s²]*

Within the k-ε closure model, the turbulent kinetic energy and the mixing length are determined with the use of a transport equation for both the turbulent kinetic energy and the energy dissipation (ε), making it a second-order closure model. The mixing length (L) can be derived from the energy dissipation using (Deltares, 2014):

$$L = c_D \frac{k\sqrt{k}}{\varepsilon} \tag{23}$$

ε	*Energy dissipation [m²/(s²s)]*
c_D	*Constant of 0.1925 [-]*

As described in appendix II, the rate at which the kinetic energy is dissipated at the smallest turbulent scales is determined by the rate at which energy is supplied from the 'top' of the cascade (Nieuwstadt, Boersma, & Westerweel, 2016). The latter rate depends on the mixing length (L) which supports the implication of equation 23 to use the rate of dissipation to determine the mixing length.

The transport equation for the turbulent kinetic energy takes the following form (Deltares, 2014):

$$\frac{\partial k}{\partial t} + u\frac{\partial k}{\partial x} + v\frac{\partial k}{\partial y} + w\frac{\partial k}{\partial z} = \frac{\partial}{\partial z}\left(\left(\nu_{mol} + \frac{\nu_{3D}}{\sigma_k}\right)\frac{\partial k}{\partial z}\right) + P_k + B_k - \varepsilon \tag{24}$$

$u/v/w$	*Reynolds-Averaged velocity in x/y/z-direction [m/s]*
ν_{mol}	*Kinematic viscosity of water [m²/s]*
P_k	*Production of turbulent kinetic energy [m²/(s²s)]*
B_k	*Buoyancy flux of turbulent kinetic energy [m²/(s²s)]*

The transport equation of the kinetic energy assumes the production, dissipation and buoyancy to be dominant within the transport equation of the turbulent kinetic energy, conservation is thus less important and the driving forces of the transport of the turbulent kinetic energy can be found in the terms P_k, B_k and ε. Epsilon is defined through another transport equation, given by equation 27. The

production term 'P_k' describes the creation of turbulent kinetic energy due to differences in flow velocities between adjacent layers and the resulting shear stresses which, as described in section 2.2.2., lead to turbulence (Deltares, 2014). Only the vertical fluctuations of the horizontal velocities are taken into account. The buoyancy term B_k and production term P_k can be found using:

$$P_k = \nu_{3D}\left(\left(\frac{\partial u}{\partial z}\right)^2 + \left(\frac{\partial v}{\partial z}\right)^2\right) \tag{25}$$

$$B_k = \frac{\nu_{3D}}{\rho\sigma_p}\frac{g}{H}\frac{\partial \rho}{\partial z} \tag{26}$$

σ_p *Prandtl-Schmidt number [-]*

g *Gravitational acceleration [m/s²]*

H *Water depth [m]*

ρ *Density of fluid [kg/m³]*

The transport equation for the dissipation of energy is also described by a production, dissipation and buoyancy term:

$$\frac{\partial \varepsilon}{\partial t} + u\frac{\partial \varepsilon}{\partial x} + v\frac{\partial \varepsilon}{\partial y} + w\frac{\partial \varepsilon}{\partial z} = \frac{\partial}{\partial z}\left(\frac{\nu_{3D}}{\sigma_\varepsilon}\frac{\partial \varepsilon}{\partial z}\right) + P_\varepsilon + B_\varepsilon - c_{2\varepsilon}\frac{\varepsilon^2}{k} \tag{27}$$

P_ε *Production term of dissipation of turbulent kinetic energy [m²/(s³s)]*

B_ε *Buoyancy flux term of dissipation of turbulent kinetic energy [m²/(s³s)]*

$c_{2\varepsilon}$ *Constant of 1.92 [-]*

The production and buoyancy terms of the energy dissipation are given by:

$$P_\varepsilon = c_{1\varepsilon}\frac{\varepsilon}{k}P_k \tag{28}$$

$$B_\varepsilon = c_{1\varepsilon}\frac{\varepsilon}{k}B_k \tag{29}$$

$c_{1\varepsilon}$ *Constant of 1.44 [-]*

Appendix V: Sensitivity analysis HLES-parameters

Since a certain range of plausible values is present for the HLES-parameters and since the turbulent patterns are of high importance in the formation of groyne flames, a sensitivity analysis of the horizontal eddy viscosity to changes in HLES-parameters is performed within this section. No data is available on standard deviations and variances of the HLES-parameters in literature. The sensitivity analysis is therefore reduced to the evaluation of the variation of mean horizontal eddy viscosities as a result of the change of the HLES-parameters to values both slightly above and slightly below the values applied in this research.

The mean horizontal eddy viscosity is derived by taking the mean of the time-averaged horizontal eddy viscosity within the domain presented in Figure 44. Largest uncertainty is present in the chosen value of the spatial low-pass filter, on the one hand because no literature is found on the appropriate range of values of this parameter – the default value is used within other researches – and on the other hand because of its large impact on the values for the horizontal eddy viscosity (Table 5).

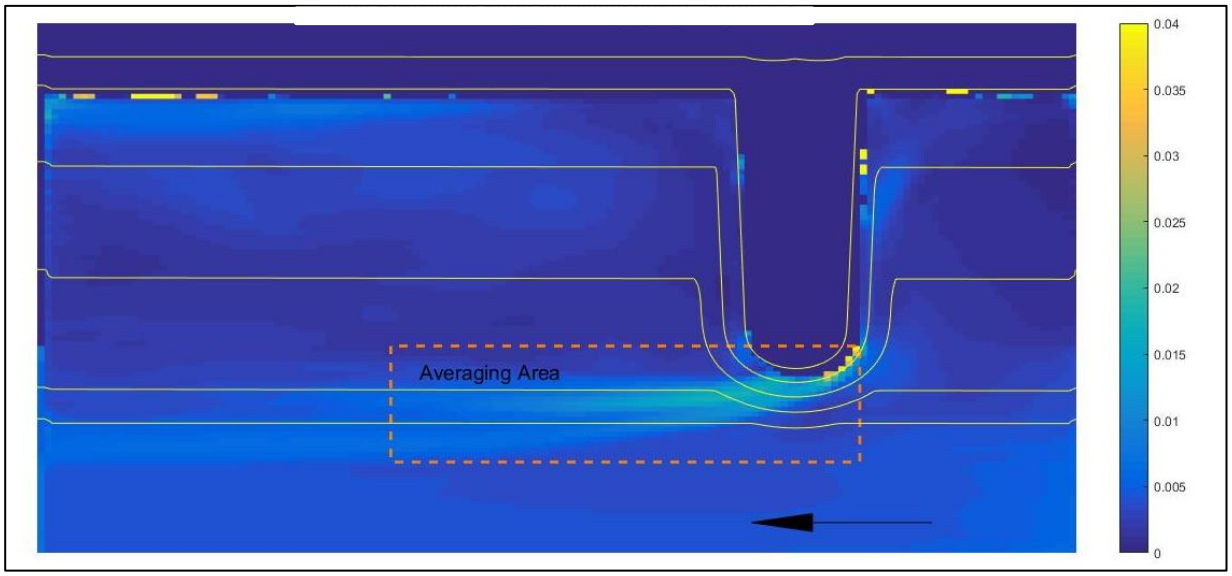

Figure 44: Mean Horizontal Eddy Viscosity using a slope in the log-log spectrum of 3 (1-by-1 m decomposed grid). Other HLES-parameters were assigned with the values used within this research (Table 5)

Table 5: Values of the HLES-parameters used in the sensitivity analysis

HLES-Parameters	Value used in research	Value used in sensitivity analysis	Mean horizontal eddy viscosity (m^2/s)
All on value used in research	-	-	0.0048
Slope in log-log spectrum (-)	5/3	3	0.0054
Chézy-coefficient ($m^{1/2}/s$)	50	45	0.0049
		55	0.0047

Spatial low-pass filter (-)	0.3	0.2	0.0101
		0.4667	0.0033
Dimensional number (-)	2	3	0.0042
Turbulence Prandtl-Schmidt number (-)	0.7	0.5	0.0038
		0.9	0.0058
Relaxation Time (minutes)	8.658	7.5	0.0047
		9.5	0.0054

Appendix VI: The effect of increasing the morphological factor

This appendix shortly addresses the impact of increasing the morphological factor on the results of the cumulative sedimentation and erosion patterns in the schematized Waal.

During each time-step, the pattern of flow and sediment transport is calculated at every grid cell. With the use of flow characteristics and resulting sediment concentrations, the bed load transport as well as the sink and source terms of the suspended sediment transport are calculated over the entire domain. The summation of the net inflow of bed load and suspended load at grid cells in the bottom layer of the flow results in a change of the bed level. The morphological factor simply multiplies this change by a certain factor (Deltares, 2014). Within a velocity field which shows temporal variation – e.g. the dynamic eddies migrate downstream and cause an alternating pattern of low and high bed shear stresses along the shear zone – a high morphological factor might induce different morphological patterns than lower morphological factors. It could for example occur that an area of artificially strong accretion changes the hydraulic pattern in the consecutive time-step in a way which would not have occurred if the morphological factor would not have been applied. The altered hydraulic pattern on its turn creates different morphological processes in this consecutive time-step.

In order to determine whether a morphological factor of 100 may be applied, the patterns of cumulative sedimentation and erosion for the morphological factors of 1, 10 and 100 are compared. The bed levels of two model runs corresponding to the same morphological time-step are compared (Figure 45 and Figure 46). The analysis shows that only minor differences are present between the results. These are furthermore only quantitative; similar erosion and sedimentation patterns are formed.

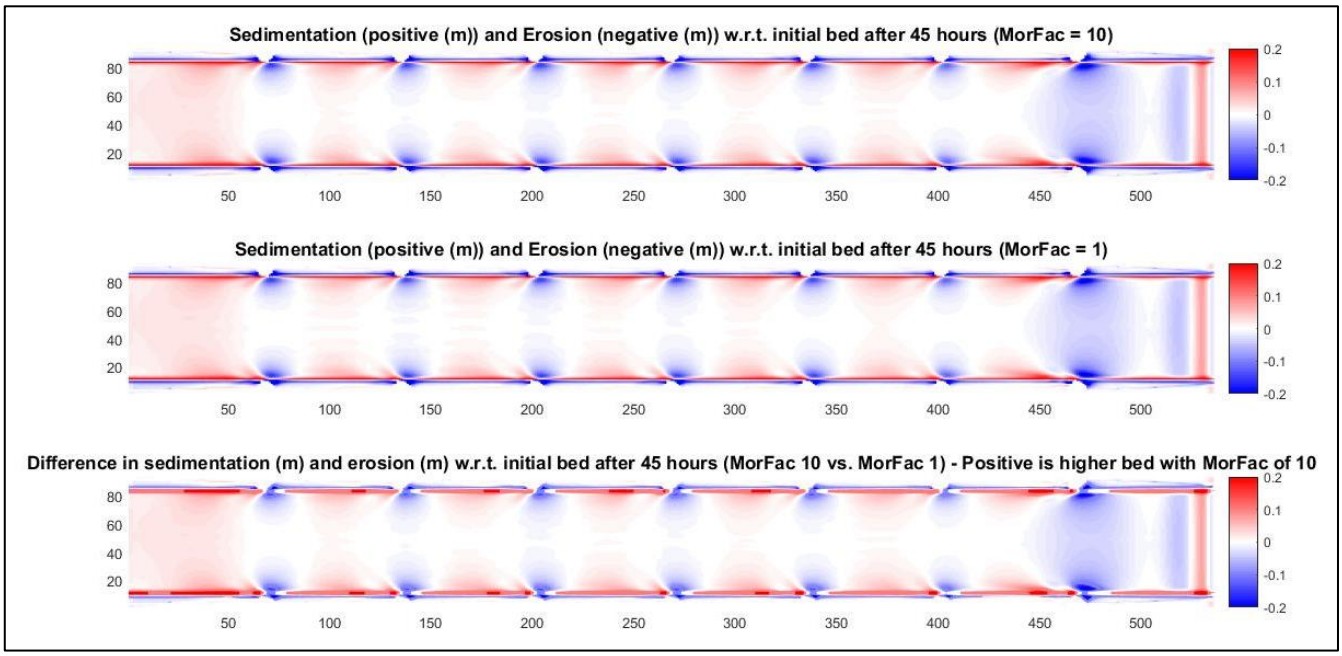

Figure 45: Comparison of bed level evolution for MorFac 1 vs. MorFac 10

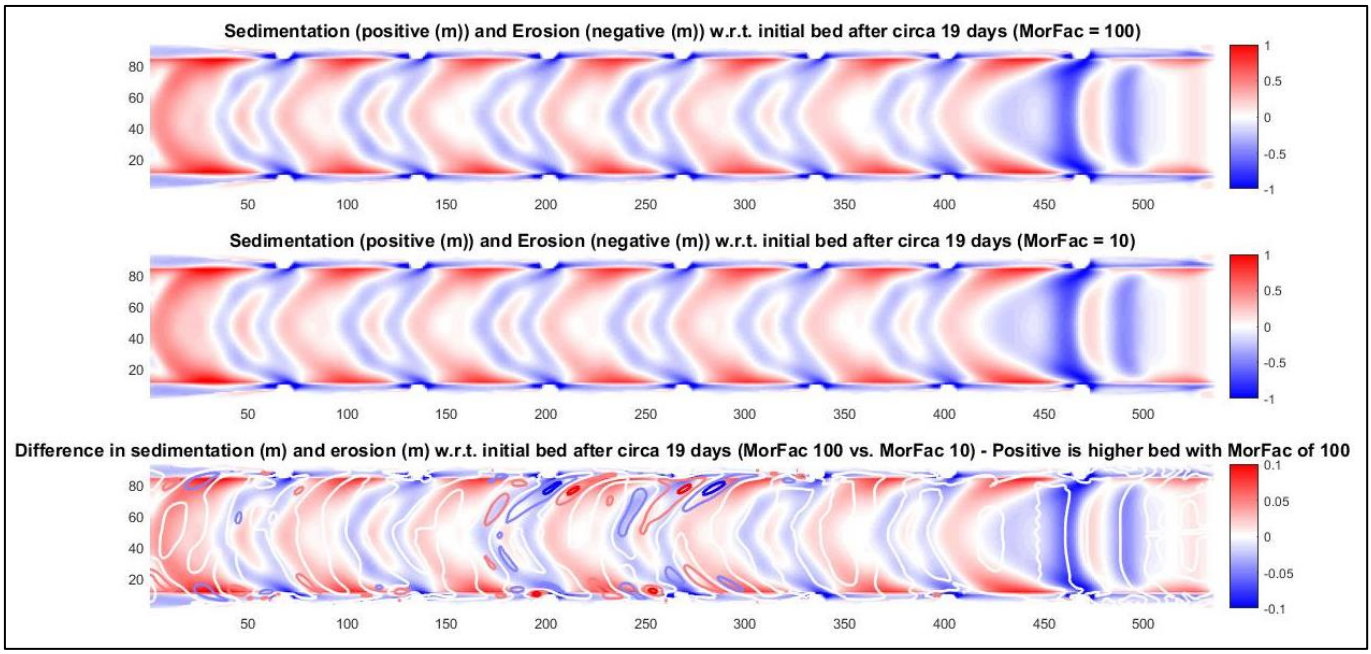

Figure 46: Comparison of bed level evolution for MorFac 10 vs. MorFac 100

Appendix VII: Waqua-analyses

The discharge along the upstream open boundary is calibrated as such that the average flow velocities in the main channel are similar to the average flow velocities in the Waal during discharge conditions corresponding to water levels of 5.0 metres above the bed. To determine these, the average flow velocities from the Delft3D-FLOW runs and those from a WAQUA-model are compared. WAQUA is the prescribed numerical model in the Netherlands for evaluation of the impact of measures within the main channel and floodplains of the river Waal (Kroekenstoel, 2017).

Water levels of circa 5.0 metres correspond to a discharge of 1600 m³/s near Lobith, of which approximately two-thirds is directed to the Waal (Havinga, Taal, Smedes, Klaassen, Douben, & Sloff, 2006). Unfortunately, no WAQUA-model results were available for these discharge conditions. For a discharge of 2000 m³/s at Lobith, the average flow velocities in the main channel of the Waal near Dodewaard fluctuate between 1.1 m/s and 1.3 m/s (Figure 47). Slightly lower flow velocities are expected for lower discharges. The average flow velocities of circa 1.05 m/s within the main channel (Figure 28) obtained from the Delft3D-FLOW runs using a discharge of 1200 m³/s in the Waal thus seem to be appropriate for this research.

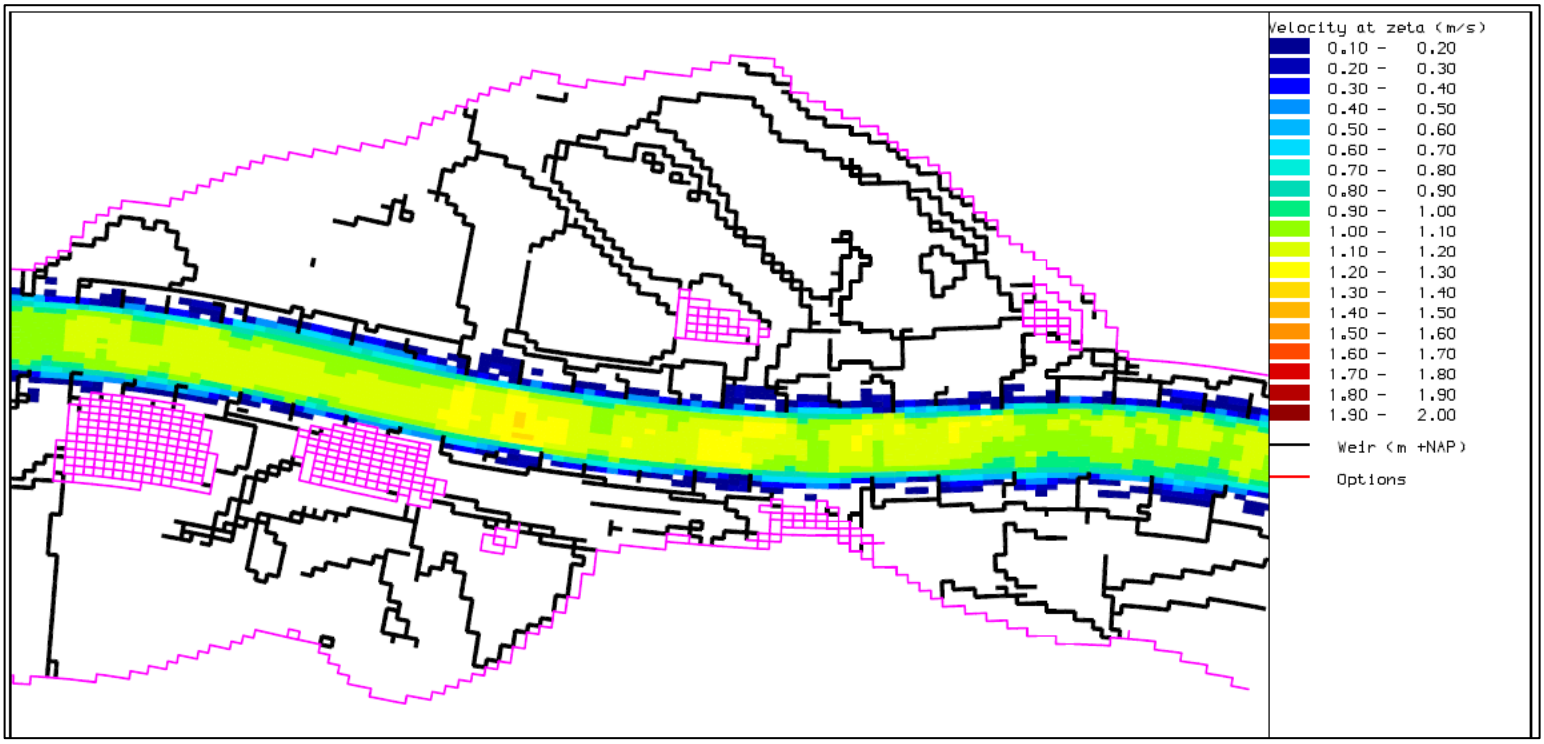

Figure 47: Flow velocities in the main channel of the Waal around Dodewaard calculated with the WAQUA-model for a discharge of 2000 m³/s at Lobith

Appendix IIX: Results on the morphology on left side of river

Chapter 6.2 presented the results on the differences in the evolution of groyne flames between the isle groyne and the current groyne. The analysis focused on the differences on the right-hand-side of the river. Qualitatively, the left-hand-side of the river showed similar effects for the implementation of the isle groyne. The results on the (maximum) average sedimentation along this side of the river are presented in this appendix.

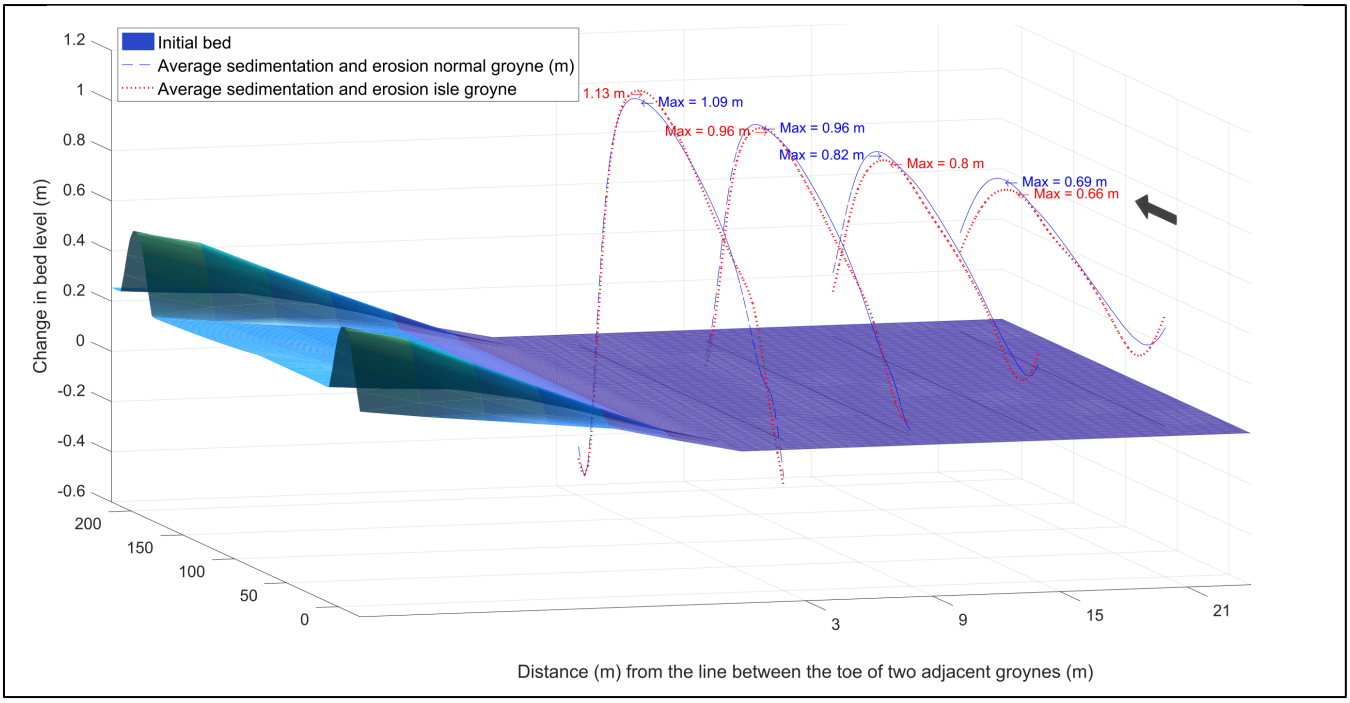

Figure 48: Average sedimentation and erosion with respect to the initial situation (m) along several longitudinal profiles parallel to the normal line between the isle groyne and current groyne (zoom 3) – left side of river

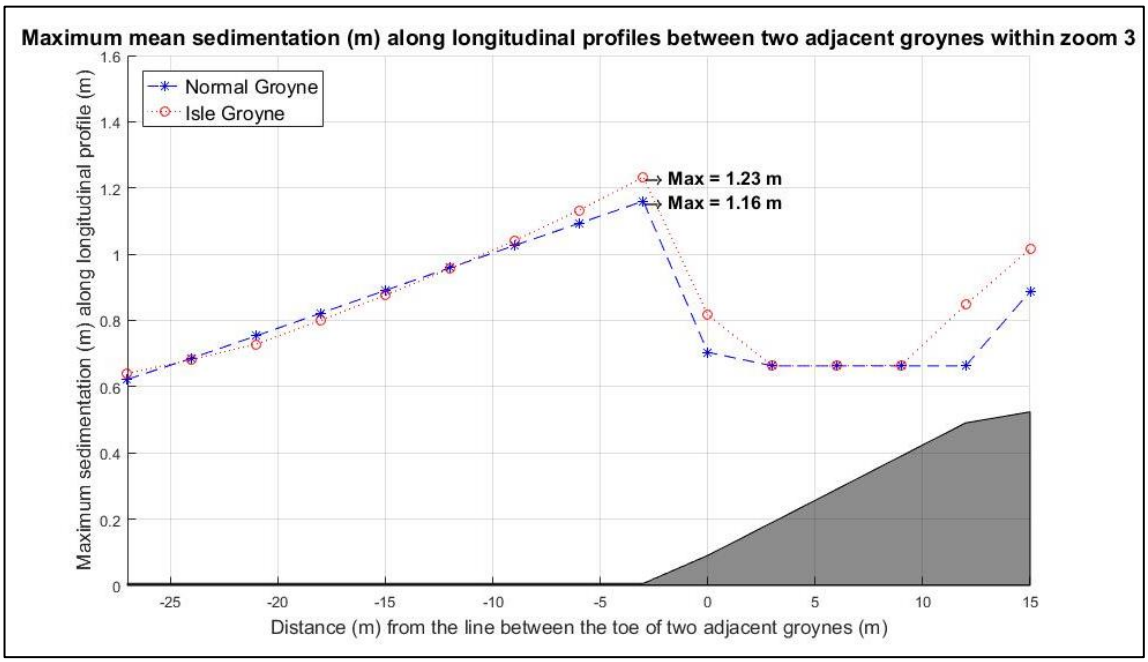

Figure 49: Maximum mean sedimentation along longitudinal profiles between two adjacent isle groynes and current groynes within zoom 3+4

Appendix IX: Different sediment transport formulae

Delft3D-FLOW allows for the use of different sediment transport formulae of which the total transport formula of Engelund-Hansen is used in this research. It has been investigated what the effect of using the formulae of Van Rijn (1984) and the formulae of Meyer-Peter-Muller would be on the model results.

Van Rijn

Despite its advantage of separating bed load and suspended sediment transport, the formulae of Van Rijn (1983) prove not to be applicable to this situation. The major reason for this is the strong accretion within the inlet, blocking the passage of any flow through the trapezoidal notch (Figure 50). The results further show a hand full of grid cells which show abnormally high accretion values (>10.000 m). It has been found in literature before that usage of suspended sediment transport formulae causes aberrant morphological behaviour in Delft3D-FLOW (Arailopoulos, 2014).

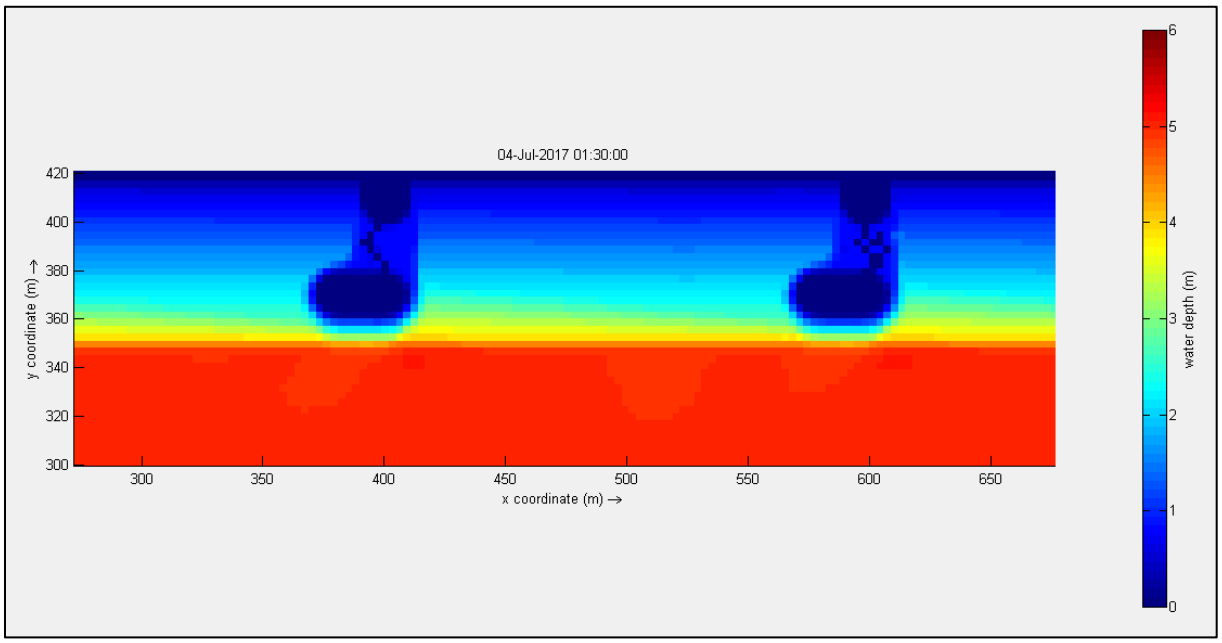

Figure 50: Water depth (m) after one morphological step using the sediment transport formulae of Van Rijn ('83)

Meyer-Peter-Muller

The calculations with the sediment transport formula of Meyer-Peter-Muller were carried out to conclude on the possible impact of the absence of a critical Shields parameter in the transport formulations of Engelund-Hansen on the formation of high-amplitude-bars in the main channel. However, also with the formula of Meyer-Peter-Muller – which includes a critical Shields parameter for the mobilization of sediment – the distinct pattern of bars is formed.